AN ABSTRACT OF THE DISSERTATION OF

Andrew R. Popchock for the degree of Doctor of Philosophy in Biochemistry and Biophysics presented on June 8, 2018.

Title: Mechanisms and Regulation of the Mitotic Kinesin-14 KlpA.

Abstract approved: _____
Weihong Qiu

Faithful segregation of genetic material during cell division is essential to all life on earth. In eukaryotes, the mitotic spindle – a bipolar array consisting of cytoskeletal filaments called microtubules – is the cellular machinery responsible for this function. The mitotic spindle requires both exquisite spatiotemporal organization and the generation of force to physically separate replicated chromosomes. Protein-based nanomachines called molecular motors are responsible for much of this activity within the mitotic spindle. Molecular motors interact directly with microtubules and convert the chemical energy in ATP into mechanical force and movement. One class of these molecular motors, termed kinesins, perform several essential processes within the mitotic spindle. Despite extensive study, the mechanisms that guide kinesin functions in the mitotic spindle remain an open question. Within this dissertation, the mechanisms and regulation of one such mitotic kinesin motor protein are investigated and discussed. These investigations include the development of a new technique that expands our ability to gain insight into kinesin mechanisms. Original work is presented in three chapters in the form of primary research reports. Chapter 2 describes the discovery and characterization of a novel mitotic kinesin-

14, KlpA, from the filamentous fungus, *Aspergillus nidulans*. KlpA is the first processive homodimeric kinesin-14 to be discovered. KlpA is also the first kinesin-14 to exhibit plus end-directed directionality on microtubules. Moreover, KlpA is the first kinesin-14 observed to be bidirectional, relying on its tail domain to maintain a context-dependent directionality. Both contexts that were explored are present within mitotic spindles, suggesting this functional regulation may be conserved in other mitotic kinesins. In chapter 3, the function and regulation of KlpA within the mitotic spindle is further explored. By using a conserved pair of mitotic proteins, TinA and AnWdr8, a regulatory pathway of KlpA was discovered. We found that TinA can cause KlpA to change its direction on microtubules and TinA and AnWdr8 can form a ternary complex with KlpA to anchor it on microtubules. This discovery enabled the proposal of a more complete model for KlpA function within the mitotic spindle. Furthermore, this work revealed that TinA is a microtubule binding protein whose affinity for microtubules is enhanced by AnWdr8. This information enabled the proposal of a potential mechanism for kinesin-14-dependent spindle microtubule anchoring at spindle pole bodies (SPBs) via TinA and AnWdr8. More importantly, this is the first proposed mechanism for kinesin-14-dependent anchoring, which is required for proper function of the mitotic spindle during chromosome segregation. In Chapter 4, an entirely new and powerful method for the generation of kinesin heterodimers is presented. This work was undertaken to expand our ability to probe the fundamental mechanisms of kinesin function and regulation. In order to overcome the shortcomings of existing techniques for kinesin heterodimer formation, genetic code expansion was used to introduce biorthogonal chemistries via noncanonical amino acid incorporation. These chemistries were then used to click together distinct monomeric

kinesin motors via a small-molecule linker. Importantly, this artificial tethering did not compromise kinesin motility and enabled formation of a novel heterodimer that was used to probe the mechanics of processive motility of the kinesin-8 protein, Kip3. Lastly, in chapter 5, I revisit the main points and themes of previous chapters in order to discuss the impacts and future directions of my work.

Mechanisms and Regulation of the Mitotic Kinesin-14 KlpA

by
Andrew R. Popchock

A DISSERTATION

submitted to

Oregon State University

in partial fulfillment of
the requirements for the
degree of

Doctor of Philosophy

Presented June 8, 2018
Commencement June 2019

Doctor of Philosophy dissertation of Andrew R. Popchock presented on June 8th, 2018

APPROVED:

_____

Major Professor, representing Biochemistry and Biophysics

_____

Chair of the Department of Biochemistry and Biophysics

_____

Dean of the Graduate School

I understand that my dissertation will become part of the permanent collection of Oregon State University libraries. My signature below authorizes release of my dissertation to any reader upon request.

_____

Andrew R. Popchock, Author

ACKNOWLEDGEMENTS

There are many people that helped me succeed during my graduate study. Without them I am sure I would not have made it here today. I will do my best to express my gratitude and appreciation.

First, I would like to thank my graduate advisor Dr. Weihong Qiu. Thank you Weihong for your encouragement and support you gave me to support my research and success in the lab. You always pushed me to do more and do better, and I believe that whatever success I have had is a testament to that. I know that I have learned a lot from you over the past four years and I hope that I have taught you something along the way too.

Secondly, I would like to thank my fellow lab members. I want to especially thank Kuo-Fu Tseng for acting as a mentor when I got to the lab. He always answered my many questions and was always willing to help and teach without hesitation. Your positive attitude and humble demeaner are things I strive for. I want to thank Allison Gicking, my peer and fellow graduate student in the lab. We have worked in close quarters the past three years and I want to thank you for putting up with me. I know I can be hard to work with sometimes and I thank you for your patience and willingness to talk kinesins and science and also help me with physics on the rare occasions that I tried understanding MATLAB. I want to also thank my undergraduate student, Youngmin Park, for remaining patient and determined enough to make a contribution to my research. It was an honor to have the opportunity mentor in whatever capacity that I could. I would also like to thank the rest of the members of our lab for all their help and advice over the years, good science often depends on those your peers, and I feel lucky to have them as such.

I want to thank all the members of my committee. Your guidance during my preliminary exam helped shape my projects into what they are today. I am thankful that all of you were willing to provide insight and guidance without hesitation when I sought it. I felt like you were personally invested in my own success and I am grateful for your time and consideration. I would also like to personally thank Dr. Ryan Mehl for his considerable investment of time and energy into me and my work. Without his unwavering support and guidance, I would not have been able to get GCE off the ground in our lab. At this point, I consider you a mentor, friend and colleague, and I hope you hold me in the same regard. I was fortunate enough to feel like a surrogate student of yours and I want to thank all the members of your lab for treating me as such. I would also like to thank Dr. Rick Cooley for all his assistance and overwhelming generosity of both his own time and resources. His willingness to provide me access to his research tools and expertise was more than I could ask for and I am forever indebted if I have success using them going forward. Rick, your attitude towards science and demeanor are things I hope to take with me. I would also like to thank the Biochemistry and Biophysics department at Oregon State University for providing funding and support as well as such a supportive and collaborative atmosphere which was integral to my success.

I want to thank all of my friends some old and many new from my time here in Corvallis. I am lucky to have such great people to share my time with and will always remember the adventures taken here in Oregon. I thank my family for their support and encouragement over the many years it has taken me to get here. Mom and Dad, I felt like you were always proud of me and that enabled me to pursue my dreams without fear or

hesitation. To Nile, who I know will always have my back through thick and thin. I love you all.

Lastly, and most importantly, I would like to thank Hailey. As my partner and best friend, I never could have finished what I set out to do without you. It hasn't always been easy, yet somehow, we found a way to make it work. Thank you for your patience and support and for pulling me back from the edge of the cliff so many times over the last few years. Your joy is infectious, and your talent is inspirational. I'm glad we made it through this adventure and look forward to many more.

CONTRIBUTION OF AUTHORS

Dr. Weihong Qiu conceived, designed and supervised the study presented in chapter 2. Dr. Kuo-Fu Tseng and myself performing the experiments presented. Dr. Kuo-Fu Tseng and Ms. Pan Wang contributed all KlpA constructs. Dr. Weihong Qiu, Dr. Kuo-Fu Tseng and Ms. Pan Wang assisted in discussing and interpreting the results. Dr. P Andrew Karplus, Dr. Xing Xang and Dr. Weihong Qiu assisted in writing of chapter 2 with input from Dr. Kuo-Fu Tseng and Ms. Pan Wang. Dr. Weihong Qiu was involved in conceiving, and supervised the study described in chapter 3. Youngmin Park assisted on construct design and purification as well as assisted in data collection in the study described in chapter 3. Dr. Ryan Mehl and Dr. Weihong Qiu conceived and supervised the study described in chapter 4. Dr. Subrahasis Jana provided reagents for the study presented in chapter 4. Dr. Ryan Mehl and Dr. Weihong Qiu assisted in the writing of chapter 4.

TABLE OF CONTENTS

TABLE OF CONTENTS (Continued)

TABLE OF CONTENTS (Continued)

Page

TABLE OF CONTENTS (Continued)

TABLE OF CONTENTS (Continued)

LIST OF FIGURES

LIST OF FIGURES (Continued)

Figure Page

LIST OF FIGURES (Continued)

Dedicated to:

To my family, Molly, Rich and Nile. To Gladys and Susan. To Jim and John.

Mechanisms and Regulation of the Mitotic Kinesin-14 KlpA

Chapter 1

Introduction

The Power of Molecular Motors

Molecular motors (or motor proteins) are biological molecules that transform chemical energy into mechanical work within cells. These nanometer-sized protein-based machines operate in highly crowded and dynamic cellular environments, strongly supporting fundamental cellular processes such as the transfer of genetic information, transport, and cytoskeletal organization and functioning. In the past four decades since their discovery, motor proteins have become the subject of intense research efforts aimed at uncovering the fundamental principles and mechanisms that compose the framework that governs their many functions.

Diversity of Kinesin Function Within Cells

Motor proteins are divided into three distinct families: myosins, which function on the cytoskeletal filament called actin, and dyneins and kinesins, which both function on microtubule cytoskeletal filaments[1]. While all three motor proteins rely on the energy released from the hydrolysis of ATP to produce force or generate movement within cells, they maintain distinct functional roles. Despite their difference in cytoskeletal filament preference, kinesins are more closely related to myosins, as the initial structural characterization of thier respective catalytic domains revealed they shared a common ancestor[2-7]. Interestingly, this was an unexpected finding due to a lack of notable sequence similarity between myosin and kinesin[4,7]. Like myosin, kinesin motors are typically homodimers, with each subunit consisting of a motor domains followed by a neck region, a stalk region and a tail region (Figure 1.1)[4,8]. Motor domains are responsible for microtubule binding and ATPase activity[9], while the neck undergoes a modulation of

conformation to generate forward motility (Figure 1.1)[10,11]. The stalk region acts to enable dimerization and the tail domains contain unique sequences that determine its cellular function and are required for processes like cargo binding, regulation, and localization (Figure 1.1)[12-14].

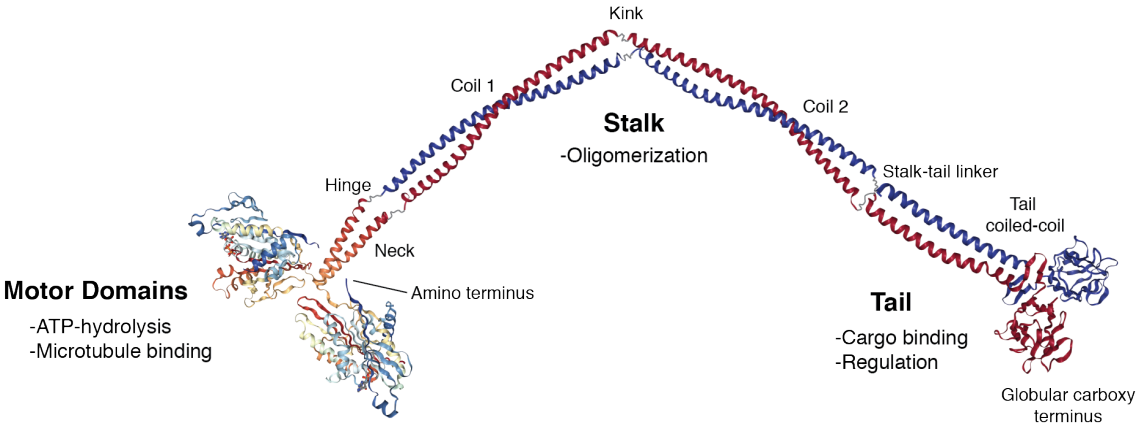

Figure 1.1: Model of conventional kinesin architecture.

Schematic diagram of structure and organization of kinesin-1 homodimer. Motor domain representations are derived from x-ray diffraction structure, PDB ID: 3KIN. Stalk coiled-coils are for illustration purposes and not to scale. Coiled-coil representations are derived from x-ray diffraction structure, PDB ID: 5D3A. Tail domain structure is for illustration purposes, representation derived from x-ray diffraction structure, PDB ID: 5DJO. Adapted from *Woehlke & Schliwa, Nat. Rev. Mol. Cell Biol. 2000.*

Functionally, kinesins are particularly diverse and are involved in a wide variety of cellular functions including the transport of various proteins, mRNAs and even organelles, the regulation of microtubule dynamics, the movement of flagella, and the segregation of genetic material during mitosis[8,15-19]. In plants, which maintain a larger assortment of kinesins thought to compensate for the role of cytoplasmic dynein (which they lack), kinesins are also responsible for further functions like vesicle transport, regulation of cell growth and membrane trafficking[9,16-23]. These kinesin-based processes are essential to cell function and in humans the misregulation of kinesin activity is associated with many pathologies including tumorigenesis, developmental defects and ciliopathies[15,20-22].

One to Fourteen - the Extended Kinesin Family

Upon its initial discovery in squid axonemes, kinesin was thought to be an entirely unique motor responsible for fast axonal transport of organelles[23]. Later studies revealed a wide variety of related proteins with diverse functions and properties, including the discovery of 45 different kinesin genes in humans and up to 75 in *Physcomitrella moss*[24-26]. Despite their functional diversity, all kinesins share a highly conserved catalytic motor domain responsible for ATPase activity and interaction with microtubules. Phylogenetic analysis of these motor domain sequences have been used to divide them into 14 distinct subfamilies, termed kinesin-1 through kinesin-14[8,15,24-26]. These fourteen subfamilies can be grouped into three broader categories based upon the position of the motor domain within their sequence: (1) N-terminal kinesins contain motor domains near the amino-terminus, (2) M-kinesins contain motor domains near the middle of their sequence, and (3) C-terminal kinesins contain motor domains near the carboxy-terminus. Generally, N-terminal kinesins generate microtubule plus end-directed movement (or movement towards

the microtubule fast-growing end). The founding member of the kinesin family, kinesin-1 or conventional kinesin, is one such example[27]. Conversely, C-terminal kinesins generate microtubule minus end-directed movement and are primarily members of the kinesin-14 subfamily[8]. M-kinesins belong to the kinesin-13 family and are primarily regulators of microtubule dynamics, commonly acting as microtubule depolymerases[28-31].

Mechanics of Kinesins

Since the initial discovery, the mechanisms that govern how kinesin converts chemical energy from ATP into mechanical work has been an area of intense interest and study. Once researchers determined that kinesin could move continuously on microtubules[32] and took distinct 8nm steps[33], the mechanism by which kinesin coordinated its two motor domains to take individual steps became a pressing question. Two possible mechanisms were proposed (Figure 1.4). The first, termed the "inchworm" stepping model (Figure 1.4a), proposed that within the kinesin homodimer, a general conformation was maintained where one motor domain remained in front dubbed the "leading head" while the other remained behind, dubbed the "lagging head." In the inchworm model, the leading head takes one 8nm step first followed by an 8nm step by the lagging head, in turn returning to the original conformation[34]. The second model, termed "hand over hand" (Figure 1.4c), was much closer to how we walk; where the leading and lagging heads trade places as one steps in front of the other[35]. While each model yields an 8nm displacement per step, the distinct stepping patterns lead to a critical difference between the two (Figure 1.4b): in the inchworm model each motor domain or "head" takes discrete 8nm steps. Whereas in the hand over hand model (Figure 1.4d), the lagging head moves 16nm per step. It was not until pioneering single molecule studies by the Selvin[36] and Block[37] groups that kinesin-1

was determined to move by a hand over hand mechanism. In the study by the Block group, a single motor domain of kinesin-1 was labeled with a fluorophore and single-molecule fluorescence microscopy was used to track the movement of the labeled motor domain as it stepped on microtubules (Figure 1.4). Clear 16nm steps were observed confirming that kinesin-1 coordinates its motor to move on microtubules via a hand over hand mechanism and not an inchworm mechanism or a mixture of the two stepping mechanisms[37]. Since its initial discovery, the structural elements and detailed mechanisms that guide the framework of kinesins hand over hand coordination have been an intense area of research.

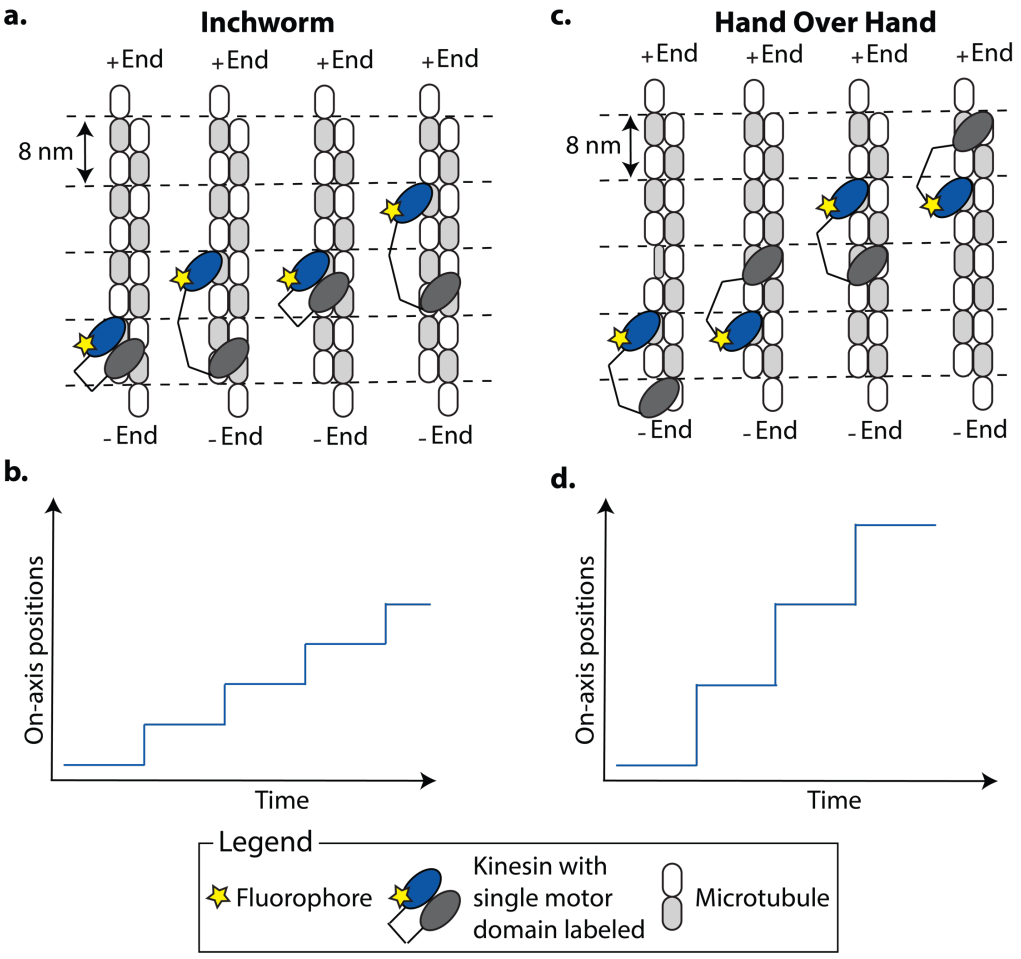

Figure 1.2: Kinesin stepping models

(a) Schematic diagram of kinesin movement via the inchworm stepping model. **(b)** Schematic of the resulting stepping trace of labeled kinesin motor domain that moves via the inchworm stepping model. **(c)** Schematic diagram of kinesin movement via the hand over hand stepping model. **(d)** Schematic of the resulting stepping trace of labeled kinesin motor domain that moves via the hand over hand stepping model.

Mechanochemical Coordination

Much of the research following the initial discovery of the kinesin-1 stepping mechanism has been focused on determining how conformational changes in the motor domain upon ATP binding and hydrolysis are coordinated with stepping. This process where each mechanical step is coordinated with the hydrolysis of a single ATP is termed the "mechanochemical cycle". Long before the stepping mechanism was known, it had been well established that kinsin-1 takes one 8 nm step for each ATP that it hydrolyzed[38-40]. Early structural analysis also revealed that ATP binding within kinesin-1s motor domain drives a major conformational change of the neck linker (the 14 amino acids adjacent to motor domain), going from undocked to docked upon ATP binding[35]. This structural change was proposed to drive kinesin-1 motility but the mechanism by which kinesin-1 prevented ATP binding to both motor domains, and thus preventing futile hydrolysis, remained unclear. Work by both the Block[41,42] and Vale[43] groups revealed that intramolecular strain generated by the neck linkers gated enzymatic activity and thus is the primary contributor to coordination (Figure 1.5).

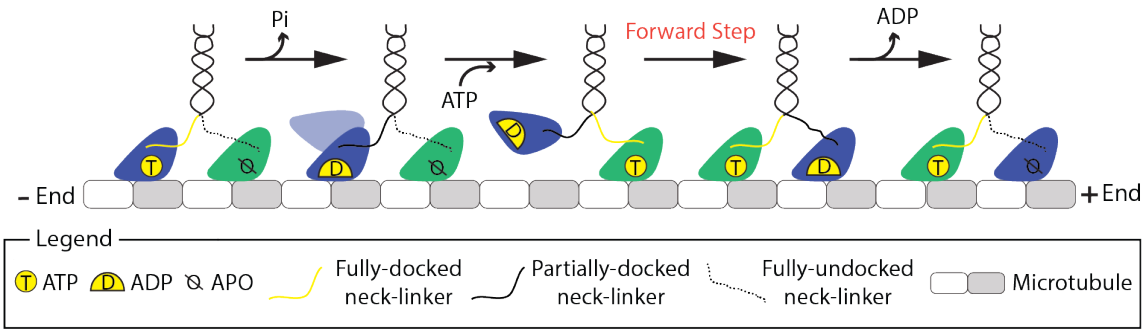

Figure 1.3: Schematic of Kinesin-1 stepping mechanism.

Schematic diagram of kinesin-1 mechanochemical cycle during forward stepping. ATP binding, hydrolysis, and subsequent dissociation, modulates each motor domains affinity for microtubules and neck-linker conformation. To ensure repeated forward steps, gating of ATP binding ensures this process happens asynchronously in each respective motor domain. Adapted from *Shang et al. eLife. 2014.*

When both kinesin-1 heads are bound to the microtubule, significant tension between the heads is generated via the neck linkers[44]. To explain how this tension gives rise to a gating mechanism, two different models have arisen: a front head-gated model that proposes that tension reduces ATP-binding affinity of the front head until the rear head releases from the microtubule[42,45,46], and a rear head-gated model, where tension generated by the docking of the neck linker in the front head accelerates detachment of the rear head[43,47,48]. While the mechanisms are not mutually exclusive, recent studies including structural work have provided evidence for the rear head-gated model; where the neck linker orientation provides tension necessary to promote detachment and movement of the rear head[9,49,50]. Despite these detailed findings, the contribution to kinesin coordination by different structural elements, such as neck-linker length and composition, remain an ongoing question[43,44,49,51-55]. Additional study is also needed to determine if these coordination mechanisms are universal among kinesins or adapted to distinct family members.

Processivity

Kinesin-1 must coordinate its two motor domains in order to take many consecutive steps on the microtubule without falling off. This is essential to long distant transport, one of the most critical kinesin functions[15,24,56]. This ability to take many consecutive steps without dissociation from the microtubule (in the case of kinesin-1 this can be >100 steps[57]), is referred to as processive motion. Initially, this processivity was determined in microtubule gliding assays: where the motor, kinesin-1, was fixed to a microtubule slide and fluorescently-labeled microtubules were then added and their resulting movement was observed using fluorescence-based microscopy[32]. Shortly thereafter, the movement of

individual kinesin-1 molecules that were fixed to beads was observed on microtubules confirming their ability to move processively[57].

As more kinesins from various subfamilies were characterized it became clear that processivity varied greatly and appeared to be tuned to specific function, as many kinesins outside of kinesin-1 were much more processive when analyzed in single molecule assays[15,58]. This processivity relies on one of the fundamental functions of kinesin motor domains; interacting with microtubules via microtubule-binding domains[8]. Many of these highly-processive kinesins rely on extra microtubule binding domains outside of their motors to achieve processive motion[59], or enhance processivity[60]. For those highly processive kinesins that did not contain extra microtubule-binding domains, the contribution of structural differences within the motor domain, or neck-linker length and composition became an intensive area of study. After work by the Vale group that determined intramolecular tension generated by the neck linkers coordinated stepping[43], Shastry and Hancock found that extended neck linkers reduced processivity in both kinesin-1 and kinesin-2 motors[52]. They proposed that kinesin-1s neck-linker length of 14 amino acids was optimized for kinesin processivity, but later work probing neck-linkers in kinesin-5 challenged this simple model, suggesting that different neck-linkers may be optimized for different kinesins[54]. Further exploration of neck-linkers effect on coordination and processivity, particularly among remaining unstudied subfamilies, is needed to expand our understanding of their role in kinesin motility.

Not all kinesins are processive, as several kinesins have been characterized as unable to move continuously on microtubules, termed non-processive. The majority of these non-processive motors belong to the distinct kinesin-14 subfamily[8,61]. Kinesin-14s

are characterized by their distinct C-terminal motor domain giving rise to their unique architecture. Because the motor domain maintains a conserved arrangement, a short amino acid stretch similar to kinesin-1s neck linker directly precedes the motor domain[5]. This distinct neck region acts as a directionality determinant[62,63] by enabling a unique "powerstroke" stepping mechanism that is conserved among kinesin-14s[64,65]. Despite this stepping mechanism, kinesin-14s were thought to be tuned to be non-processive as individual molecules on microtubules, but recent work from our group and others have revealed several processive kinesin-14s[59,66,67]. These findings were unexpected, but revealed a new paradigm where some kinesin-14s are tuned to be processive, either as a potential consequence of unique structural elements[66,68] or functional roles[67].

Directionality

Kinesins that remain coordinated, taking many unidirectional consecutive steps, exhibit a characteristic directionality on microtubules. This directionality is a consequence of the structure of microtubules. Microtubules are large protofilaments consisting of individual strands of α-tubulin and β-tubulin dimers which can be thought of as the "tracks" or a "roadway network" on which both kinesin and dynein move. However, unlike a traditional roadway network, microtubules are highly dynamic in cells, growing or rapidly disassembling in response to things like extracellular signals or cellular processes like cell division[17,69]. As these microtubules grow, α/β-tubulin dimers come together to form filaments that grow more rapidly from the β-end which is termed the microtubule plus end or "fast-growing end[69]." Conversely, these filaments grow more slowly from the α-end which is termed the microtubule minus end or "slow-growing end[17]." This inherent

polarity of microtubules gives rise to directional preference by interacting motor proteins. For example, dynein motors typically move towards microtubule minus ends, and are therefore termed "minus end-directed motors," while kinesins are typically plus end-directed or move towards microtubule plus-ends.

However, as discussed earlier, distinct architecture and coordination mechanisms give rise to minus end-directed kinesins[62-65]. Because upon discovery these motors were non-processive, their directionality had to be determined via fluorescent microscopy and microtubule-gliding assays[70], in which kinesin motors are fixed to a surface and fluorescently-labeled microtubules are added *in trans* in buffer that contains ATP. The fixed kinesin motors then work together to move or "glide" microtubules uniformly. By using polarity-marked microtubules that are polymerized in two steps, yielding a bright region at either the plus or minus end, the inherent directionality of the kinesin motors attached to the surface can be determined. After characterization of the first discovered minus end-directed motor Ncd from *Drosophila melanogaster*[70] (which is the founding member of kinesin-14s), subsequent analysis of kinesin-14s from different organisms yielded similar motility-based characteristics[71-74]. Kinesin-14s ability to glide microtubules with minus end-directed motility while remaining non-processive as individual molecules on microtubules was thought to be a consequence of their respective functions within mitotic spindles[74-77]. Recently, processive kinesin-14s have been discovered[59,66,67], one of which that we characterized maintains plus end-directed motility as individual molecules but still glides microtubules with minus end-directed motility[66]. These findings raise new questions as to how both processivity and directionality relate to these minus end-directed proteins functional roles.

Context-dependent Directionality

Following the discovery of both plus end-directed and minus end-directed kinesin proteins, it was widely assumed that kinesins were unidirectional due to the distinct motor architectures associated with each directionality. This was until pioneering work by the Schiebel and Surrey groups that uncovered the kinesin-5 protein, Cin8 from *Saccharomyces cerevisiae.* They showed that Cin8 was capable of being both a plus end-directed and minus end-directed motor[78]. They found that as individual tetramers on microtubules, Cin8 molecules moved with both diffusive and processive modes towards microtubule minus ends[78]. Even this initial finding was unexpected as this was contrary to canonical kinesin-5 behavior, which are typically are plus end-directed as individual motors[74,79]. Surprisingly, when Cin8 crosslinks and slides apart antiparallel microtubules (akin to its function within the mitotic spindle) it reverts to canonical plus end-directed motility[78]. More detailed analysis revealed that this directional switch was dependent upon the number of Cin8 molecules within this antiparallel microtubule overlap[78]. This phenomenon, termed "motor coupling" gives rise to a context-dependent directional preference of Cin8, the first characterization of such a mechanism for any kinesin motor. This behavior was thought at the time to be unique to Cin8, and was consistent with its functions *in vivo*: since kinesin-5s are transported to the spindle poles by a minus end-directed dynein[80], but dynein is not known to play this role in yeast[78]. Researchers proposed that Cin8s unique minus end-directed motility on single microtubules was compensatory for the lack of dynein function. Later work reinforced this hypothesis, as the kinesin-5 Cut7, from the another yeast *S. pombe,* was found to exhibit a similar context-dependent directionality[81]. Taken together, these findings constituted significant contributions to the

kinesin field, as they provided new evidence for both the complexity and ingenuity of kinesin motor design and how this translates to their potential functions *in vivo*.

This observed context-dependent directionality was limited to members of the kinesin-5 family until recent work from our group and our characterization of the kinesin-14 from *Aspergillus nidulans*, KlpA[66]. We discovered that KlpA was unexpectedly processive and plus end-directed; this is the opposite of the canonical non-processive minus end-directed motility of most kinesin-14s. This observed behavior of KlpA was akin to Cin8 and furthermore, we discovered that when sliding apart antiparallel or bundling parallel microtubules, KlpA reverted to minus end-directed motility. Unlike Cin8, we determined that this directional switch was dependent upon KlpAs tail domain which contained a nonmotor microtubule-binding domain. We proposed a model in which this tail domain acts as a context-dependent lever arm, or gear, that enables directional switching of KlpA. Despite the fact that this KlpA context-dependent directionality constitutes a separate directionality mechanism than Cin8, our work raised the possibility that this observed context-dependent directionality may be a unique feature of mitotic kinesins. Perhaps this autonomous context-dependent directionality is an ancestral trait that was lost in higher eukaryotes, which could rely on more complex regulation schemes to achieve the same functional output of these motors.

Kinesins Role in the Mitotic Spindle

A fundamental property of all cells is the ability to duplicate and divide their genetic material and divide with high fidelity in order to reproduce and proliferate. In eukaryotic cells, separation of replicated genetic material is accomplished by the mitotic spindle[82]. The mitotic spindle is primarily composed of microtubules, which are arranged into two

overlapping arrays to form a bipolar supramolecular structure (Figure 1.2)[83]. Within these arrays, microtubules are arranged such that microtubule minus-ends (or slow-growing ends) are clustered together and anchored to centrosomes (or spindle poles) while the microtubule plus-ends (fast-growing ends) extend outwards and overlap each other to form the microtubule midzone. Chromosomes attach to the spindle at the midzone by binding to microtubule plus-ends. This attachment is mediated by the kinetochore complex[84,85], which ensures that each chromosome is attached to both centrosomes and is responsible for the physical separation of chromosomes to each daughter cell. Force-generation is needed to physically separate duplicated chromosomes, and kinetochores include several motor proteins from both dynein and kinesin families[86-91] except in plants, which lack dynien[92]. Formation and organization of the mitotic spindle is highly regulated and requires the coordinated contributions of several kinesin motor proteins. Of these kinesins, the most well characterized contributions come from members of the kinesin-5 family and kinesin-14 family, which have been found to have conserved functions between species and in both plants and animals[77,93-103]. In these conserved functions, kinesin-5 and kinesin-14 are thought to work antagonistically to each other in order to establish and maintain spindle bipolarity.

Kinesin-5s are homotetrameric motors with a bipolar orientation, containing a pair of motor domains at each end of the molecule. Kinesin-5s have been shown to be weakly processive as individual molecules and in some organisms they have the ability to move towards either end of the microtubule depending upon context[81,104-106]. To function, kinesin-5s localize to spindle microtubules and mitotic organizing centers (MTOC) and mutations or deletions of kinesin-5 can block separation of opposite centrosomes (or

spindle poles) and thus prevent completion of mitosis[107,108]. Furthermore, kinesin-5 activity is required for mitotic spindle as the inhibition or deletion of kinesin-5s can cause cells to arrest before cell division as they fail to form bipolar microtubule arrays: instead, they form monoastral microtubule arrays with only one centrosome[109-114].

The overall structure of kinesin-5s is well suited for one of their primary functions, microtubule sliding or force generation[79,80,96,105,115]. Due to the inherent microtubule plus-end directionality of each motor domain pair within each tetramer, kinesin-5s can slide apart anti-parallel microtubules. This sliding activity is thought to provide an essential outward "pushing" force to balance forces and prevent the collapse of the mitotic spindle (Figure 1.2). To maintain mitotic spindle integrity, kinesin-5s form balanced antagonistic relationships with either other kinesin motors or dynein that provide opposing inward or "pulling" forces[74]. These relationships were established based upon the observation that cells containing kinesin-5 knockouts that displayed a collapsed spindle phenotype could be rescued by complementary dynein[116-119] or kinesin-14 knockouts[71,93,94,120,121]. Conversely, knockouts of the antagonistic partners of kinesin-5 alone yield elongated spindles that can result in arrest in cell division or errors in chromosome segregation[74,98,122-124]. To provide the necessary outward force, it has been proposed that kinesin-5s localize to spindle midzones, where there is enrichment of overlapping antiparallel microtubules and kinesin-5 can slide apart microtubules, effectively pushing apart each microtubule array that form the bipolar spindle.

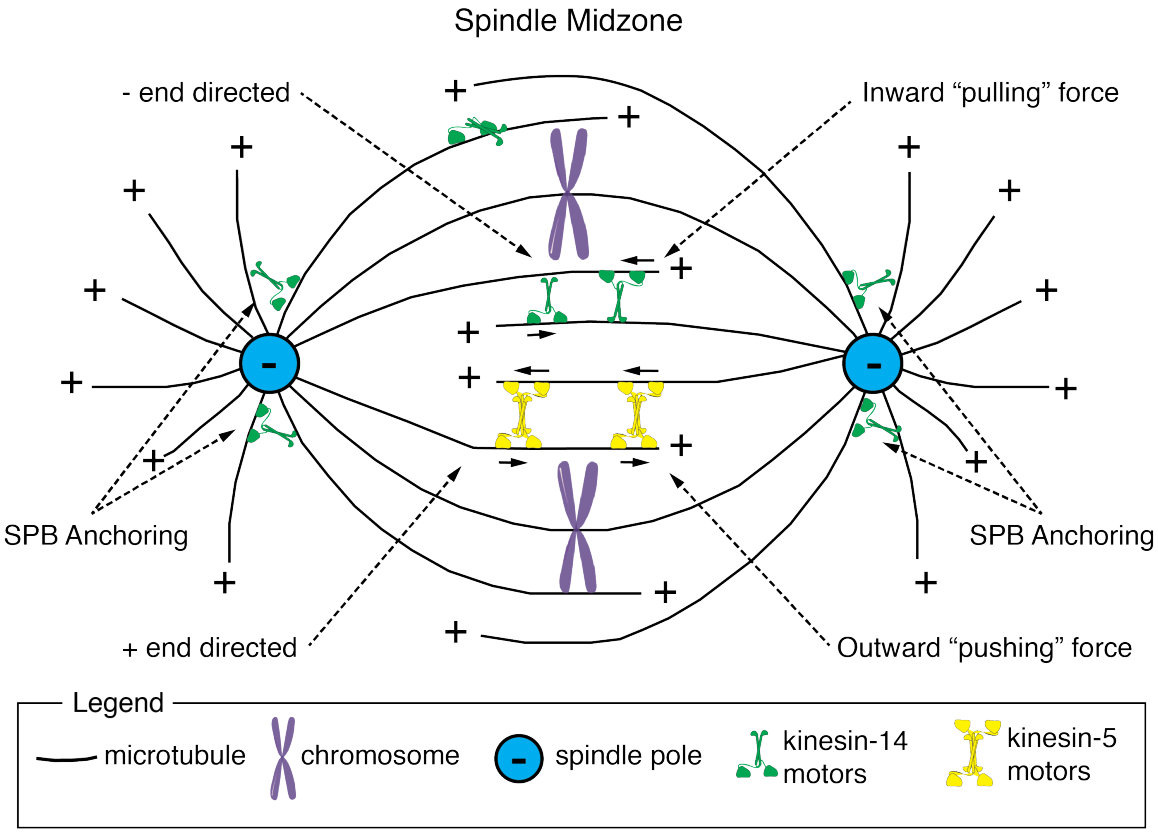

Figure 1.4: Model for kinesin-5 and kinesin-14 contributions within the mitotic spindle.

Schematic diagram of the fungal mitotic spindle illustrating the contributions of kinesin-5 and kinesin-14 proteins. Localization of kinesin-14 to both the spindle midzone and spindle pole bodies is shown. This distinct localization is required for proposed kinesin-14 functions within the mitotic spindle.

The primary antagonistic partner of Kinesin-5 within the mitotic spindle is kinesin-14. Kinesin-14s are typically homodimeric and maintain minus end-directed movement on microtubules (opposite to kinesin-5) and are normally non-processive, or lack the ability to move continuously on microtubules as individual molecules[72,125,126]. This minus-end directionality is thought to derive from kinesin-14s' unique arrangement of having thier motor domains at the C-terminus of their sequence, giving rise to novel structural properties[5,127]. This opposite directionality to kinesin-5 is essential to kinesin-14s' ability to counteract the activity of kinesin-5 within the mitotic spindle in a so called "tug of war" (Figure 1.2). Like kinesin-5s, kinesin-14s can crosslink and slide apart anti-parallel microtubules even though they are only dimeric. It has been shown that this activity is enabled by non-motor microtubule binding domains within their tail domains[66,70,77,94,128-130]. Kinesin-14s are known to strongly localize to MTOCs where they are proposed to provide an inward pulling force via microtubule sliding and bundling to counteract kinesin-5[71,103,131-133].

Besides counteracting the forces of kinesin-5 during mitosis, kinesin-14s' other primary role within the mitotic spindle is to organize and maintain the integrity of the bipolar array by crosslinking and focusing microtubule minus ends at spindle poles. Surprisingly, *in vitro* kinesin-14 can focus the minus ends of parallel microtubules to form asters[134,135]. Formation of microtubule asters with focused microtubule minus ends both in the presence and absence of MTOCs is required for spindle assembly and initiation of cell division[75,134-140]. The bundling and antiparallel sliding activity of kinesin-14s is proposed to be the primary mechanism for pole focusing in cells, where in animals, kinesin-14s work together with dynein (which is also minus end-directed) to establish the mitotic spindle. In

spindles that contain MTOCs, these focused minus ends of spindle microtubules must be anchored to the MTOCs to maintain spindle integrity[141]. Kinesin-14s are proposed to play a role in this anchoring of spindle microtubules to spindle poles, as loss of kinesin-14 can yield spindle pole fragmentation and spindle microtubules that extend far past spindle poles which lead to errors in subsequent chromosome separation[98,142-144].

While the mechanisms responsible for spindle microtubule anchoring by kinesin-14s remain largely uncharacterized, recent work has led to the conclusion that kinesin-14s coordinate with several other partner proteins at the MTOCs to anchor microtubules[103]. In fission yeast, the kinesin-14 Pkl1 was shown to directly interact with the conserved Msd1 (SSX2IP) protein *in vivo* for localizing to the spindle pole body (MTOC) and anchoring spindle microtubules[103]. At the MTOCs, the minus ends of spindle microtubules interact with the conserved γ-tubulin ring complex (γ-TuRC) component which stabilizes them (Figure 1.2a)[145]. Msd1 localizes to the spindle pole body[146] and both Msd1 and the fungi (TinA) and human (SSX2IP) orthologues have been shown to directly interact with the γ-TuRC component to anchor microtubules[133,146,147] indicating a conserved anchoring mechanism (Figure 1.3a).

Surprisingly, in an Msd1 deletion mutant, spindle microtubule minus ends do not anchor and protrude beyond spindle pole bodies[146], mimicking the phenotype of kinesin-14 knockouts[98,142-144]. This prompted researchers to investigate if both proteins acted together in the microtubule anchoring pathway. Yukawa et al. found that within fission yeast, Msd1 acts as an adapter protein for Pkl1 (kinesin-14) and the highly conserved WDR8 protein at the spindle poles[103]. All three proteins rely on each other for localization to the spindle pole body as well as the anchoring of spindle microtubules. In support of

these findings, this interaction between Msd1(SSX2IP) and WDR8 has been shown to be conserved in both fungal and human orthologues[103,147,148]. In their proposed mechanism, Pkl1 mediated the transport of Msd1 and Pkl1 to the spindle pole, where all three components then coordinated to tether spindle microtubules and the γ-TuRC component to spindle poles (Figure 1.3b). While this study provided significant contributions to developing a conserved mechanism of spindle microtubule anchoring within mitotic spindles, a detailed molecular mechanism for such anchoring remains a pressing question.

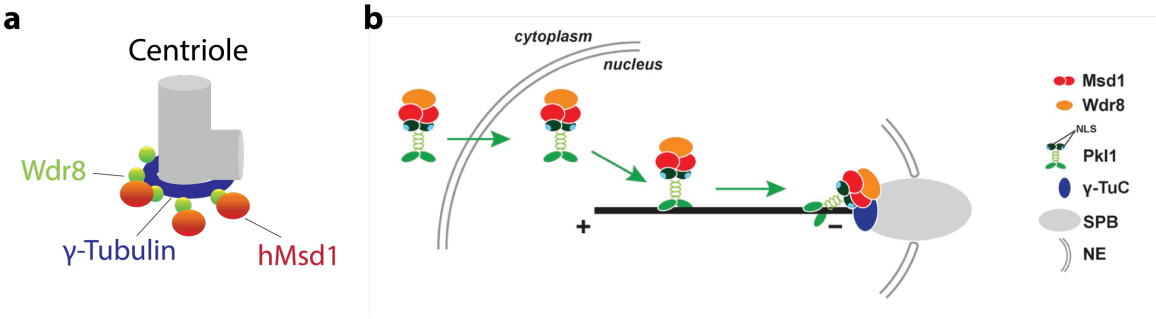

Figure 1.5: Localization of Msd1 and Wdr8 and anchoring mechanism in yeast.

(a) Schematic diagrams of Msd1 and Wdr8 localization to γ-tubulin ring complex (γ-TuC) at Centrioles (MTOCs). **(b)** Schematic of proposed anchoring mechanism of spindle microtubules at yeast spindle pole bodies (SPB). Adapted from *Yukawa et al. J. Cell Biol. 2015.*

Within the mitotic spindle, kinesin-5 and kinesin-14 have essential functional roles in both the initial formation and maintenance of the bipolar array to ensure proper division of genetic material. The interplay between kinesin-5 and kinesin-14 is finely coordinated through each motors' intrinsic biophysical properties yielding a perpetual stalemate in this cellular "tug of war." While clearly essential to cell viability, the detailed mechanisms of kinesin-5 and particularly kinesin-14 mitotic functions are largely uncharacterized and remain open questions within the field. Ongoing studies using a variety of model systems are aimed at uncovering these mechanisms of function and regulation.

Mitotic Kinesins and Disease

Due to their essential roles during cell division, both kinesin-5 and kinesin-14 have been implicated in errors of chromosome segregation (aneuploidy) which can lead to disease[98,149-152], but are more studied for their respective roles in cancer cells[20,122,131,153,154]. The human kinesin-5, Eg5, is the most well characterized cancer-implicated kinesin, as it has proven to be the most promising kinesin anti-cancer therapeutic target[155]. Eg5 is involved in formation of the mitotic spindle[79,109,156-158] and is expressed in actively dividing human cells (proliferative tissues) including the testis, thymus, tonsils and bone marrow[159,160]. As such, Eg5 is highly expressed or overexpressed in many different cancer cell types and tumors[161-165] and there is some evidence, based on findings in mice, that overexpression may be tumorigenic in and of itself[166]. This makes Eg5 an ideal therapeutic target, as it maintains inherent specificity (as non-mitotic cells don't express high levels of Eg5) and inhibition of its activity in cells induces mitotic arrest after formation of aberrant monoastral spindles (meaning both MTOCs move to the center of cell with chromosomes in a rosette-like conFigureuration)[167,168]. Mitotic arrest in turn leads to cell death through

the apoptotic pathway[109,169,170] and inhibition of Eg5 is an effective anti-cancer treatment in many cancer cell lines[171-176]. This high efficacy has led to the development of several clinical therapeutics, two of which (monastral and ispinesib) are currently used in anti-cancer treatments. Both these inhibitors bind selectively to Eg5's motor domain, locking it in an ADP-bound state and preventing Eg5 from undergoing its full mechano-chemical cycle[177-182].

The human kinesin-14, HSET, has recently become an attractive alternative to Eg5 as a kinesin anti-mitotic cancer therapeutic target. Unlike Eg5, HSET is non-essential in human cells despite it maintaining the canonical kinesin-14 antagonistic relationship to Eg5 (kinesin-5) and thus being involved in mitotic spindle formation[77,134]. HSET has been found to be overexpressed in several cancer cell types[154,183-185] and recent studies have revealed that levels of HSET overexpression are associated with overall malignancy and proliferation as well as certain drug resistance[154,183,184,186]. HSET's role in cancer progression was largely unknown until recent studies revealed that cancer cells employed a rather clever strategy to circumvent apoptotic pathways relying on HSET. The majority of invasive cancer cells contain excess genetic material or supernumerary centrosomes[187]. This extra centrosome material normally would lead to the formation of multiple centrosomes and the formation of a multipolar spindle[188]. This in turn activates cell cycle checkpoints, mitotic arrest, and eventual apoptosis[109,169,170]. To sidestep cell death, cancer cells containing extra centrosomes overexpress HSET in order to suppress multi-polar spindles and generate a pseudo-bipolar spindle that does not trigger apoptosis[20,131,151,153,154,185,188,189]. This makes HSET an attractive anti-cancer therapeutic target, as its inhibition can potentially trigger cancer cell apoptosis while leaving normal

cells unaffected. Development of specific inhibitors with clinical potential has been much more challenging than was the case for Eg5, as only three specific inhibitors have been identified[186,190,191]. This limited success has in part been due to significant cross reactivity with other kinesins, but recent structural characterization of HSETs motor domain have revealed a unique structural feature that may be used to improve drug-like properties of existing inhibitors or potentially develop new ones[192].

Targeting of both Eg5 and HSET is part of an overall general strategy of targeting the mitotic spindle as a way to target rapidly dividing cells. The most widely used drugs of this family are those that target microtubules to disrupt dynamics and interfere with normal cell division, termed microtubule poisons. During chemotherapy treatments with these microtubule poisons, cancer cells can develop resistance and HSET, along with several other mitotic kinesins have been implicated in this process. Overexpression of these kinesins results in increased resistance, suggesting that a combination of kinesin inhibitors and microtubule poisons could potentially be used to overcome resistance development in cancer cells. However, specific inhibitors for mitotic kinesins are at varying stages of drug development and there is limited validation and application to animal models. One key to identifying ideal kinesin drug targets, particularly in the case of specific cancer types, is expanding our knowledge of their mechanisms of function and cellular pathways. This includes fundamental studies of their functions within model systems and *in vitro*. These studies may be particularly powerful, as kinesins are particularly challenging targets for specific drug development as their high levels of homology lead to cross reactivity. Identification of interacting partner proteins and/or potential regulators may yield upstream targets that are much better suited to targeting for specific drug development.

My Work

My research on kinesin proteins began during my rotation in Dr. Weihong Qiu's lab. It was during this time that I got my first taste of single-molecule microscopy as well as more common biochemical and biophysical characterization techniques. During my rotation I aided with a project spearheaded by Dr. Kuo Fu Tseng, focused on characterizing a unique kinesin motor called FRA1 from the model plant *Arabidopsis thaliana*. That work is not included within this dissertation but will be included in a manuscript that is currently in preparation. Importantly, this work proved to be a springboard for my own research, providing me with the essential skills needed to develop the projects included within this dissertation.

In chapter 2, "The Mitotic Kinesin-14 KlpA Contains a Context-dependent Directionality Switch", I discuss my work on the discovery and characterization of a novel mitotic kinesin-14, KlpA, from the filamentous fungus, *A. nidulans*. KlpA proved to be an exceptionally unique member of the kinesin-14 subfamily. KlpA is the first processive homodimeric kinesin-14 to be discovered. KlpA is also the first kinesin-14 to exhibit plus end-directed directionality on microtubules. Moreover, KlpA is the first kinesin-14 observed to be bidirectional, relying on its tail domain to maintain a context-dependent directionality. Both contexts that were explored are present within mitotic spindles, providing a potential mechanism for KlpA function during cell division.

In chapter 3, "The Mitotic Kinesin-14 KlpA is Regulated by a Conserved Protein Pair", I further explore the function and regulation of KlpA within the mitotic spindle. By using a conserved pair of mitotic proteins, a complex regulation scheme of KlpA was discovered. These regulatory mechanisms enabled the proposal of a model for KlpA

function within the mitotic spindle. Furthermore, this work provided the molecular detail needed to propose a potential mechanism for kinesin-14-dependent spindle microtubule anchoring at SPBs. Importantly, this is the first proposed mechanism for kinesin-14-dependent anchoring, which is required for proper function of the mitotic spindle during chromosome segregation.

In chapter 4, "Engineering heterodimeric kinesins through genetic incorporation of noncanonical amino acids", I present my work to develop an entirely new and powerful method for generation of kinesin heterodimers. Kinesin heterodimers are essential tools for in-depth study of kinesin motility and regulatory mechanisms. Their use has enabled researchers to characterize several of the fundamental properties and design principles that are responsible for kinesin-1 motility on microtubules. However due to technical hurdles, generation of heterodimers outside of kinesin-1 are limited. In order to overcome the shortcomings of existing techniques for kinesin heterodimer formation, genetic code expansion was used to introduce biorthogonal chemistries via noncanonical amino acid incorporation. These chemistries were then used to click together distinct monomeric kinesin motors via a small-molecule linker. Importantly, this technique did not compromise kinesin motility and enabled the formation of a novel heterodimer that was used to probe coordination of the kinesin-8 protein, Kip3.

Lastly, in chapter 5 I revisit earlier chapters to emphasize the main points and themes of each. The impacts of the work presented in each chapter are also highlighted. Future directions of my work are presented as ongoing research projects that are a continuation of the work presented in each chapter as well as several research projects that are immediately approachable based on the findings of each chapter. I conclude my

dissertation with remarks on the current state of the kinesin field and potential direction moving forward as well as some closing remarks on scientific research in general.

Chapter 2

The Mitotic Kinesin-14 KlpA Contains a Context-dependent Directionality Switch

Andrew R. Popchock*, Kuo-Fu Tseng*, Pan Wang, P. Andrew Karplus, Xin Xiang & Weihong Qiu

*: Denotes equal contribution

Published in *Nature Communications*
8, Article number: 13999 (2017)
doi:10.1038/ncomms13999

Abstract

Kinesin-14s are commonly known as nonprocessive minus end-directed microtubule motors that function mainly for mitotic spindle assembly. Here we show using total internal reflection fluorescence microscopy that KlpA—a kinesin-14 from *Aspergillus nidulans*—is a context-dependent bidirectional motor. KlpA exhibits plus end-directed processive motility on single microtubules, but reverts to canonical minus end-directed motility when anchored on the surface in microtubule-gliding experiments or interacting with a pair of microtubules in microtubule-sliding experiments. Plus end-directed processive motility of KlpA on single microtubules depends on its N-terminal nonmotor microtubule-binding tail, as KlpA without the tail is nonprocessive and minus end-directed. We suggest that the tail is a de facto directionality switch for KlpA motility: when the tail binds to the same microtubule as the motor domain, KlpA is a plus end-directed processive motor; in contrast, when the tail detaches from the microtubule to which the motor domain binds, KlpA becomes minus end-directed.

Introduction

Kinesins are microtubule motor proteins that convert the energy of ATP hydrolysis into mechanical work for various essential cellular processes[107,120,185]. The mitotic spindle is a microtubule-based bipolar machine in eukaryotes that separates duplicated chromosomes to ensure that daughter cells each receive proper genetic material during cell division[193]. Several different kinesin motor proteins are orchestrated inside the mitotic spindle for its assembly and maintenance[76,82]. Of all mitotic kinesins, kinesin-14s (i.e. kinesins with a C-terminal motor domain) are commonly considered to be nonprocessive

minus end-directed microtubule motors[94,101,132,134,135,194-198]. Loss of kinesin-14s has been shown to cause erroneous chromosome segregation[98,122,135,142,199-201]. In cancer cells, the human kinesin-14 HSET/KIFC1 is needed for clustering multiple centrosomes, a process crucial for cancer cell proliferation and survival[185].

KlpA is a mitotic kinesin-14 from the filamentous fungus Aspergillus nidulans[120]. It is worth noting that *A. nidulans* is also the model organism for the discovery of BimC, the founding member of mitotic kinesin-5s[107]. Like mitotic kinesin-14s in other eukaryotic cells[93,97,134],KlpA counteracts the function of BimC[120]. Although KlpA is nonessential in wild-type cells[120], its loss becomes synthetically lethal with gamma tubulin mutations[202]. KlpA is an attractive model protein for dissecting the mechanism and function of kinesin-14s, as its loss-of-function mutations can be conveniently isolated as suppressors of the bimC4 mutation[102]. However, compared with other mitotic kinesin-14s such as Ncd from Drosophila melanogaster, Pkl1 and Klp2 from *S. pombe*, and Kar3 from *S. cerevisiae*, KlpA is much less well studied.

In this study, we report our in vitro characterization of KlpA motility in a variety of contexts using total internal reflection fluorescence (TIRF) microscopy. We find that, unlike all other kinesin-14s that have been studied to date, KlpA is a novel context-dependent bidirectional kinesin-14 motor: on single microtubules, KlpA unexpectedly moves towards the plus end in a processive manner, but when anchored on the coverslip (as in microtubule-gliding experiments) or interacting with a pair of microtubules (as in microtubule-sliding experiments), it reverts to exhibit canonical minus end-directed motility. We further show that KlpA requires its N-terminal nonmotor microtubule-binding tail (tail) for plus end-directed processive motility, as KlpA without this tail is minus end-

directed in microtubule-gliding experiments and fails to generate processive motility on single microtubules. Collectively, these results indicate that the tail of KlpA plays a novel function as a switch for controlling its direction of motion in different contexts. This study sheds new insight into KlpA motor mechanisms and also markedly expands our knowledge of the diversified design principles of kinesin-14s.

Results

KlpA glides microtubules with minus end-directed motility

We set out to determine the directionality of KlpA in vitro using TIRF microscopy. To that end, we purified the recombinant full-length KlpA tagged with an N-terminal green fluorescent protein (GFP-KlpA, Figure 2.1a,b). Because KlpA substitutes for Kar3 in *S. cerevisiae*[120] and Kar3 forms a heterodimer with the nonmotor proteins Cik1 or Vik1[59], we performed two different assays—hydrodynamic analysis and single-molecule photobleaching—to determine the oligomerization status of KlpA. The hydrodynamic analysis yielded a molecular weight that is close to the theoretical value of a GFP-KlpA homodimer (Supplementary Figure 2.1a,b). The photobleaching assay showed that the GFP fluorescence of GFP-KlpA was photobleached predominantly in a single step or two steps (Supplementary Figure 2.1c,d), similar to other dimeric kinesins[203]. Thus, KlpA formed a homodimer in our in vitro experiments.

We next performed a microtubule-gliding assay to determine the directionality of KlpA (Figure 2.1c). Briefly, GFP-KlpA molecules were immobilized on the coverslip via an N-terminal polyhistidine-tag, and KlpA directionality was deduced from the motion of polarity-marked microtubules. The assay showed that GFP-KlpA caused polarity-marked

microtubules to move with the bright plus ends leading (Figure 2.1d) and a mean velocity of 309±35 nm s−1 (mean±s.d., n=123, Figure 2.1e). In a control microtubule-gliding experiment using the plus end-directed human conventional kinesin hKHC[204], microtubules were driven to move with the bright plus ends trailing (Supplementary Figure 2.2). Taken together, these results demonstrate that KlpA, when anchored on the surface via its N terminus, is a minus end-directed motor protein, in agreement with a previous study using KlpA from clarified bacterial lysates[202].

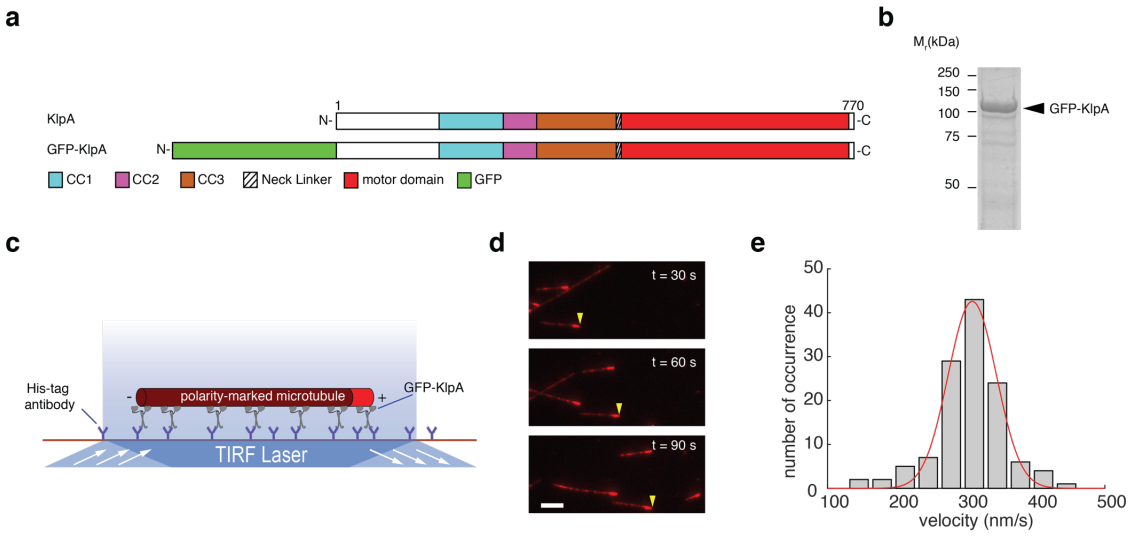

Figure 2.1: Surface-immobilized KlpA molecules exhibit minus end-directed motility to glide microtubules.

(a) Schematic diagrams of the full-length KlpA and the recombinant GFP-KlpA. The full-length KlpA consists of three consecutive coiled coils (CC1, aa 153–249; CC2, aa 250–297; and CC3, aa 298–416), a neck (aa 417–421) and a catalytic microtubule-binding motor domain (aa 422–756). GFP-KlpA contains an N-terminal polyhistidine-tag (not shown). **(b)** Coomassie-stained SDS–polyacrylamide gel electrophoresis (SDS–PAGE) of purified recombinant GFP-KlpA. **(c)** Schematic diagram of the microtubule-gliding assay. Movement of microtubules driven by surface-immobilized GFP-KlpA molecules was visualized by TIRF microscopy. Microtubules were fluorescently labelled with tetramethylrhodamine (TMR), and polarity-marked with a dim minus end and a bright plus end. (**d)** Representative TIRF microscopy images of polarity-marked microtubules moving on the coverslip surface with the bright plus ends leading (yellow arrowheads). **(e)** Histogram showing the microtubule-gliding velocity distribution of GFP-KlpA. Red line indicates a Gaussian fit to the velocity histogram. Scale bar, 5 μm.

KlpA is a plus end-directed processive kinesin-14 motor

With the lone exception of Kar3, which moves processively on single microtubules towards the minus end by forming a heterodimer with the nonmotor proteins Cik1 or Vik1[59,99], all other kinesin-14s that have been studied to date are exclusively nonprocessive minus end-directed motors. We thus wanted to determine whether KlpA is a typical kinesin-14 that lacks the ability to move processively on single microtubules as a homodimer. To address this, we performed an in vitro motility assay to visualize the movement of KlpA molecules on surface-immobilized polarity-marked microtubules (Figure 2.2a). The assay showed that, contrary to the notion of kinesin-14s as minus end-directed motors, GFP-KlpA molecules unexpectedly formed a steady flux of plus end-directed motion and accumulated at the microtubule plus end (yellow arrow, Figure 2.2b). Occasionally, there were GFP-KlpA particles moving towards the microtubule minus ends (white arrow, Figure 2.2b), but these minus end-directed particles were significantly brighter than the ones moving towards the plus end, implying that they were aggregates rather than simple homodimers.

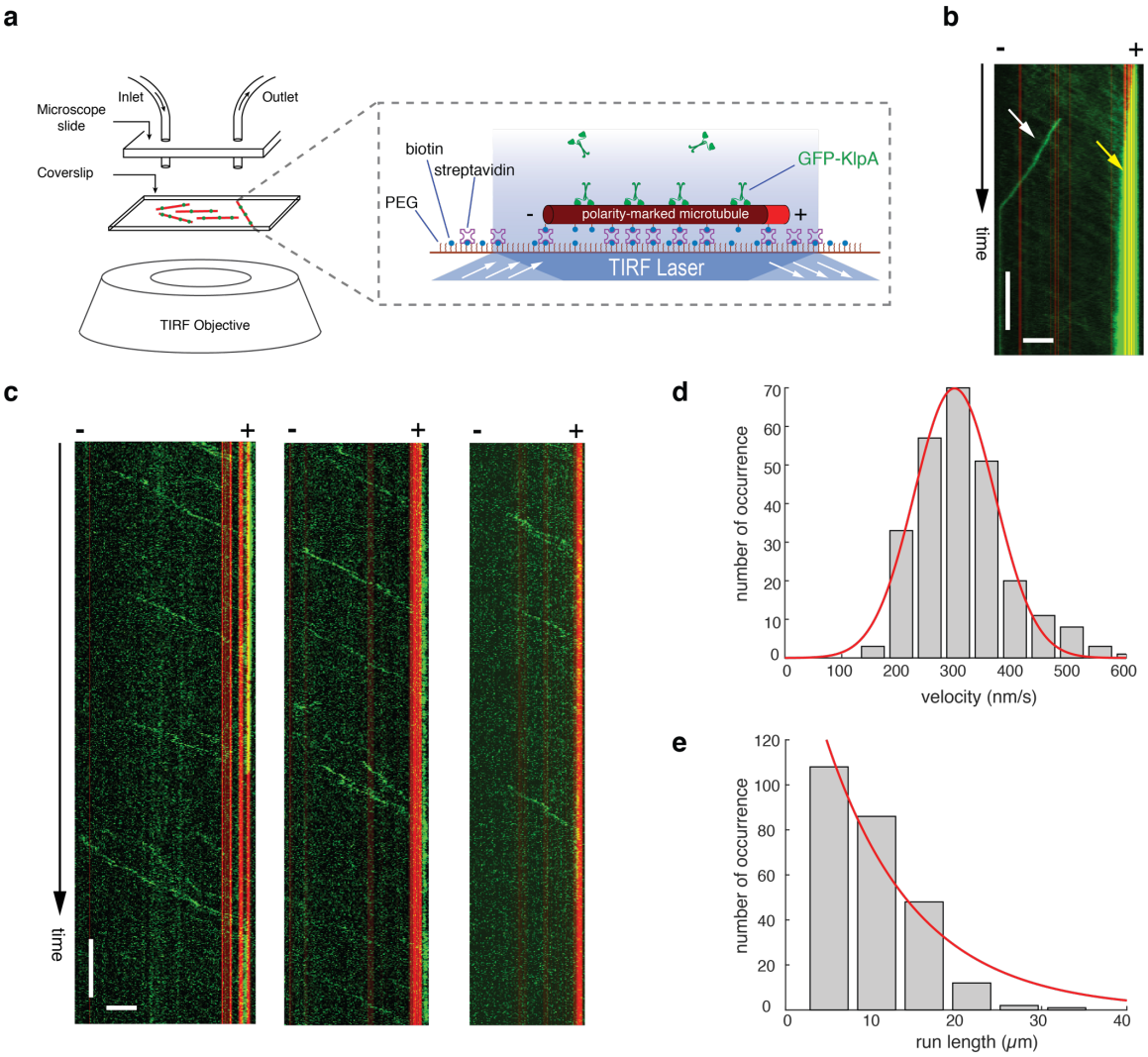

Figure 2.2: KlpA moves processively towards the plus end on single microtubules.

(**a**) Schematic diagram of the *in vitro* KlpA motility assay. Microtubules were fluorescently labelled with Hilyte 647, and polarity-marked with a dim minus end and a bright plus end. (**b**) Example kymograph showing GFP-KlpA molecules (green), at relatively high protein input levels, form a plus end-directed flux and accumulate there on a surface-immobilized polarity-marked microtubule (red). Yellow arrow indicates GFP-KlpA accumulation at the microtubule plus end, and white arrow indicates minus end-directed movement of a GFP-KlpA aggregate. (**c**) Example kymographs showing that individual GFP-KlpA molecules (green) move towards the plus end on single polarity-marked microtubules (red) in a processive manner. (**d**) Velocity histogram of individual GFP-KlpA molecules on single microtubules. Red line indicates a Gaussian fit to the velocity histogram. (**e**) Run-length histogram of individual GFP-KlpA molecules on single microtubules. Red line indicates a single exponential fit to the run-length histogram. Scale bars, 1 min (vertical) and 5 μm (horizontal).

Since the aforementioned motility experiments were performed at relatively high input levels of GFP-KlpA (≥4.5 nM; Figure 2.2b), we repeated the same motility assay at much lower protein input levels (≤0.2 nM) so that the motile behavior of individual GFP-KlpA molecules could be distinguished. The assay showed that individual GFP-KlpA molecules moved preferentially towards the microtubule plus end in a processive manner (Figure 2.2c) with a mean velocity of 300±70 nm s^{-1} (mean±s.d., *n*=257, Figure 2.2d) and a characteristic run-length of 10.5±2.2 μm (mean±s.e.m., *n*=257, Figure 2.2e). This run-length likely was an underestimate because most KlpA molecules reached the microtubule plus end. We also performed the mean square displacement (MSD) analysis, which showed that the motility of KlpA is dominated by directional movement (Supplementary Figure 2.3). Together, these results demonstrate that, in direct contrast to all other kinesin-14s that have been analyzed to date, KlpA is a novel kinesin-14 motor that uniquely exhibits plus end-directed processive motility on single microtubules. It is worth emphasizing that such novel processive motility is not due to coupling[203,205], but rather an intrinsic behavior of a single KlpA homodimer.

Plus end-directed KlpA motility requires its N-terminal tail

Like other kinesin-14s such as Klp2 in *S. pombe* and Ncd in *D. melanogaster*[130,206], KlpA was also able to slide apart antiparallel microtubules and to statically crosslink parallel microtubules via its N-terminal nonmotor microtubule-binding tail (Supplementary Figure 2.4a–g). As several other kinesins are known to rely on nonmotor microtubule-binding domains to either achieve processive motility[59] or enhance processivity[60], we sought to determine whether the microtubule-binding tail of KlpA plays

a similar role in enabling its unexpected plus end-directed processive motility on single microtubules.

To do this, we purified GFP-KlpA-Δtail (Figure 2.3a), a truncated construct lacking the N-terminal tail, for in vitro motility experiments. Like GFP-KlpA, GFP-KlpA-Δtail formed a homodimer (Supplementary Figure 2.5) and exhibited minus end-directed motility in the microtubule-gliding assay (Figure 2.3b) with a mean velocity of 287±10 nm s−1 (mean±s.d., n=138, Figure 2.3c). This latter observation implies that motor–neck core of KlpA is inherently minus end-directed, as would be expected based on its highly conserved neck[181,182,202,205]. However, the in vitro motility assay showed that GFP-KlpA-Δtail did not form a steady flux towards either end of the microtubule, nor did it accumulate at the microtubule ends (Figure 2.3d). Although some occasional brighter and presumably aggregated particles moved processively towards the microtubule minus ends (white arrow, Figure 2.3d), individual GFP-KlpA-Δtail molecules behaved like other nonprocessive kinesin-14s[188,201,204] and mostly interacted with the microtubules in a diffusive manner with no apparent directional preference (yellow arrow, Figure 2.3d). The MSD analysis showed that the motility of GFP-KlpA-Δtail on single microtubules is best described by one-dimensional diffusion (Supplementary Figure 2.6). Thus, besides allowing for microtubule-sliding and crosslinking, the tail of KlpA has an additional novel functionality of enabling the kinesin-14 motor to move on single microtubules towards the plus end in a processive manner.

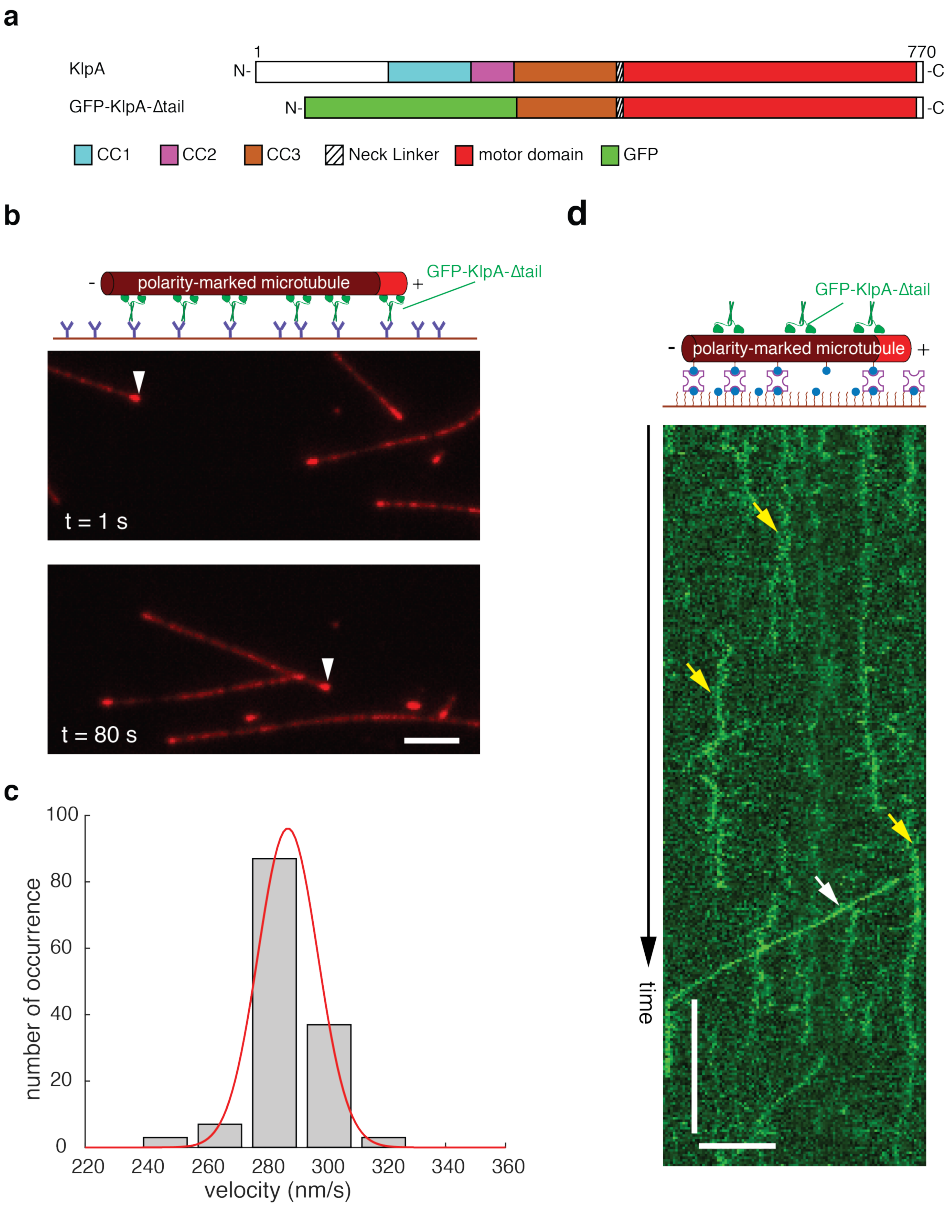

Figure 2.3: Plus end-directed processive motility of KlpA on single microtubules requires its N-terminal nonmotor microtubule-binding tail.

(**a**) Schematic diagrams of the full-length KlpA and the recombinant GFP-KlpA-Δtail. GFP-KlpA-Δtail contains a polyhistidine-tag (not shown) and a GFP at the N terminus, and residues 303–770 of KlpA. (**b**) Representative TIRF microscopy images of GFP-KlpA-Δtail driving polarity-marked microtubules (red) to glide with the bright plus ends leading (white arrowheads). (**c**) Velocity histogram of microtubule-gliding by GFP-KlpA-Δtail. Red line indicates a Gaussian fit to the velocity histogram. (**d**) Example kymograph showing that individual GFP-KlpA-Δtail molecules (yellow) exhibit nonprocessive movement on a single polarity-marked microtubule with a bright plus end. White arrow indicates minus end-directed movement of a rare GFP-KlpA-Δtail aggregate. Scale bars, 1 min (vertical) and 5 μm (horizontal).

KlpA exhibits context-dependent directional preferences

From the opposite directional preference exhibited by KlpA in the ensemble microtubule assays (Figure 1d and Supplementary Figure 2.4c) and the single-molecule motility experiments (Figure 2.2b,c), we inferred that KlpA contains a context-dependent mechanism to switch directions on the microtubule. We thus directly compared the motility of GFP-KlpA inside and outside the microtubule overlap on the same track microtubule using a microtubule-sliding assay (Figure 2.2.4a), as has been done previously for S. cerevisiae kinesin-5 Cin8[104]. Briefly, in this assay the track (blue) and cargo (red) microtubules were both polarity-marked but labelled with different dyes; track microtubules were first immobilized on a coverslip inside the motility chamber and bound with purified GFP-KlpA molecules; moreover, cargo microtubules were added into the chamber before three-colour time-lapse imaging was acquired to simultaneously visualize the motility of GFP-KlpA molecules and cargo microtubules on the same track microtubules. Like KlpA, GFP-KlpA was also able to slide antiparallel microtubules relative to each other (Figure 2.4b) and to statically crosslink parallel microtubules (Figure 2.4c). In both scenarios, when outside the microtubule overlap regions, GFP-KlpA molecules showed a plus end-directed flux and accumulated at the plus end on the track microtubule (yellow arrow, Figure 2.4b,c). This matched the behaviour of GFP-KlpA on single microtubules (Figure 2.2b). In contrast, inside the antiparallel microtubule overlap regions, GFP-KlpA molecules carried the cargo microtubule towards the minus end of the track microtubule (white arrow, Figure 2.4b). In the parallel orientation, the cargo microtubule remained stationary on the track microtubule, but GFP-KlpA molecules moved preferentially towards and gradually accumulated at the minus end inside the

parallel microtubule overlaps (white arrow, Figure 2.4c). This is similar to the observation that Ncd preferentially accumulates at the minus ends between statically crosslinked parallel microtubules[206]. Collectively, these results demonstrate that KlpA can, depending on its context, display opposite directional preferences on the same microtubule: it is plus end-directed outside the microtubule overlap regions and minus end-directed inside the microtubule overlap regions regardless of the relative microtubule polarity.

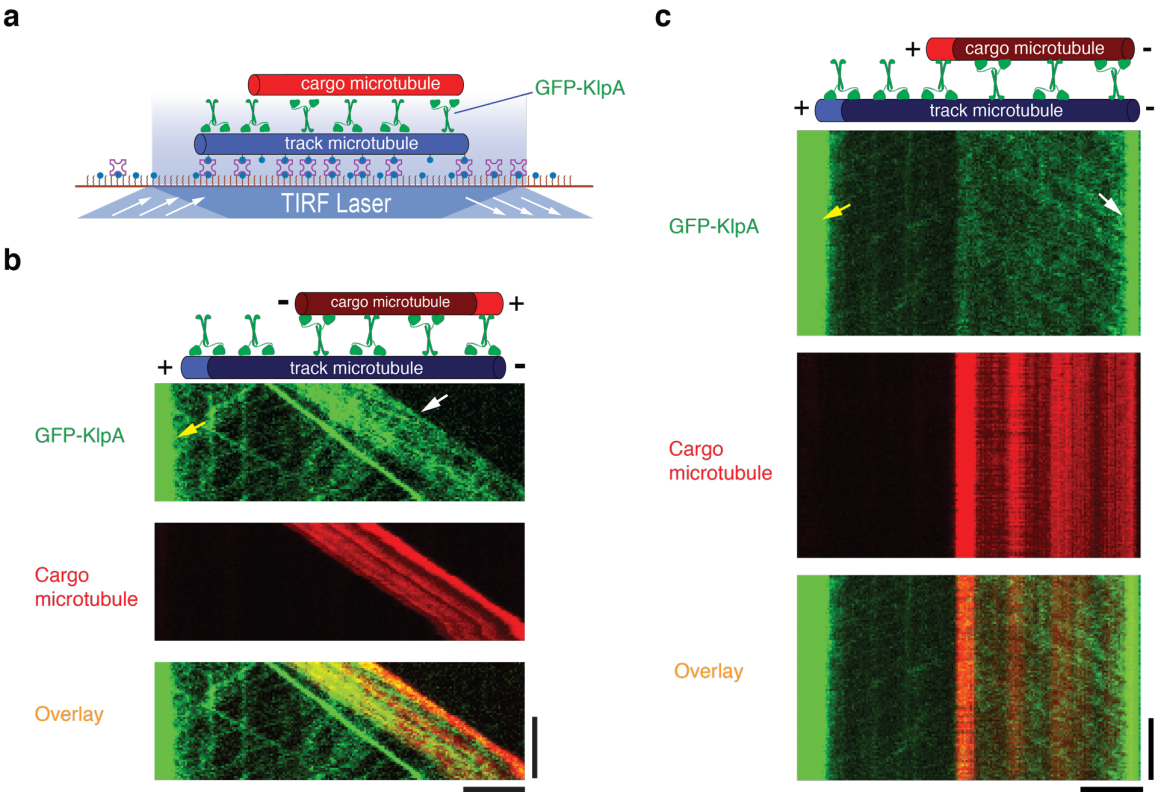

Figure 2.4: KlpA exhibits opposite directional preference inside and outside the microtubule overlaps.

(**a**) Schematic diagram of the microtubule-sliding assay showing that KlpA contains context-dependent opposite directional preference. Track and cargo microtubules were fluorescently labelled with Hilyte 647 and TMR, respectively, and polarity-marked with a dim minus end and a bright plus end. (**b**) Example kymographs of GFP-KlpA motility inside and outside the antiparallel microtubule overlap. Yellow arrow indicates GFP-KlpA accumulation at the microtubule plus end outside the antiparallel microtubule overlap. White arrow indicates minus end-directed movement of GFP-KlpA inside the antiparallel microtubule overlap. (**c**) Example kymographs of GFP-KlpA motility inside and outside the parallel microtubule overlap. Yellow arrow indicates GFP-KlpA accumulation at the microtubule plus end outside the parallel microtubule overlap. White arrow indicates GFP-KlpA accumulation at the microtubule minus end inside the parallel microtubule overlap. Scale bars, 30 s (vertical) and 5 μm (horizontal).

Discussion

Kinesin-14 has been an intriguing kinesin subfamily since the discovery of its founding member Ncd[207] because all kinesin-14s studied to date are exclusively minus end-directed based on the microtubule-gliding experiments[70,72,73,130,139,203,207-209]. In addition, no kinesin-14 has been shown to be able to generate processive motility on the microtubule as a single homodimer. Kar3 is the only kinesin-14 known to generate minus end-directed processive motility on single microtubules without clustering, and it does that by forming a heterodimer with its associated light chains Vik1 or Cik1[59,99]. To our knowledge, KlpA is the first kinesin-14 that exhibits both plus end-directed processive motility on single microtubules and context-dependent directional switching. Thus, our study markedly expands the diversity of kinesin-14s.

Our results show that while the full-length KlpA clearly moves towards the plus end on single microtubules in a processive manner (Figure 2.2b,c), a truncated KlpA lacking the N-terminal microtubule-binding tail glides microtubules with minus end-directed motility (Figure 2.3b) but becomes nonprocessive on single microtubules (Figure 3d). There are several important implications from these observations. First, without the tail, the motor–neck core of KlpA is inherently minus end-directed, which is consistent with the notion that all kinesin-14s share a highly conserved neck that serves as the minus end directionality determinant[62,63,204,210]. Second, on single microtubules, the tail enables KlpA to exhibit both processive motility and plus end directionality. We propose that on a single microtubule, KlpA assumes a cis conformation in which the catalytic microtubule-binding motor domain and the tail bind to the same microtubule. Binding of the tail to the

cis-microtubule subsequently prevents KlpA from premature dissociation, and this enables the kinesin to move processively on the microtubule, as has been observed previously for Kar3, which depends on the nonmotor microtubule-binding domain in Vik1 or Cik1 for processive motility on microtubules[59].

At present, it is unclear how exactly the tail enables the full-length KlpA to move preferentially towards the plus end on a single microtubule at the atomic level. Previous studies[64,211,212]suggest that kinesin-14 motors use a lever mechanism for minus end-directed motility, where the neck acts as an extended lever arm and undergoes rotation towards the microtubule minus end upon ATP binding. Building on this, we speculate that when KlpA adopts the cis conformation on a single microtubule, binding of the tail on the surface of the same microtubule as the motor domain induces a conformational strain through the stalk that causes the neck to rotate towards the microtubule plus end, thereby enabling the kinesin for plus end-directed motility. The precise underlying mechanism of plus end-directed KlpA processivity awaits future single-molecule studies of designed KlpA variants as well as cryo-electron microscopy (cryo-EM) studies of these variants on single microtubules.

Among all the experiments, KlpA exhibits plus end-directed motility only on single microtubules (Figure 2.2b,c); moreover, in this scenario, the tail of KlpA and its catalytic motor domain are expected to bind to the same microtubule. In contrast, KlpA exhibits canonical minus end-directed motility when it is either anchored on the coverslip via the N terminus in the ensemble microtubule-gliding experiments (Figure 2.1c,d) or between a pair of microtubules in the microtubule-sliding experiments (Figure 2.4b,c). In both scenarios, the N-terminal microtubule-binding tail of KlpA is not attached to the

microtubule to which its motor domain binds. These results suggest that the tail of KlpA is a de facto directionality switch: to achieve plus end-directed processive motility, the switch-like tail of KlpA must bind to the same microtubule as its catalytic motor domain; moreover, to achieve minus end-directed motility, the switch needs to be detached from the microtubule to which its motor domain binds.

Our results show that KlpA accumulates at the plus end on single microtubules (Figure 2.2b,c), and we suggest that this is enabled by its tail via a mechanism similar to that of the budding yeast kinesin-8 Kip3[213]. The tail likely binds strongly to the splayed protofilaments at the microtubule plus end to enhance the retention of KlpA there. It is worth noting that such accumulation requires the motor activity of KlpA to reach the microtubule plus end, as purified tail does not accumulate at either end of the microtubule and instead decorates the entire length of the microtubule rather uniformly (Supplementary Figure 2.4e).

It has long been established that KlpA counteracts the activity of BimC[120], but the underlying mechanism has been largely unknown. How could our results relate to the in vivo functions of KlpA? While KlpA localization inside the mitotic spindle has not yet been studied, one potential site of localization is the spindle pole, as several mitotic kinesin-14s, including HSET, CHO2, Kar3, Ncd, XCTK2 and Pkl1, are all known to localize to the spindle poles[103,131,214]. If KlpA does localize to the spindle poles, then how does it localize there? A recent study has shown that that Pkl1—a mitotic kinesin-14 from fission yeast—forms a complex with Msd1 and Wdr8 for translocating to and anchoring at the spindle poles[103]. As homologues of Msd1 and Wdr8 are both present in A. nidulans[147], it is plausible that binding of Msd1 and/or Wdr8-like proteins to KlpA dislodges its N-

terminal tail from the cis-microtubule surface, and this activates the kinesin for minus end-directed motility both on single microtubules and at the spindle poles. The spindle midzone is another potential site of localization. In this case, our results suggest that while other mitotic kinesin-14s appear to depend on partner proteins to localize to the microtubule plus end[18,125,139,197], KlpA can in principle autonomously localize to the spindle midzone via its inherent plus end-directed processive motility.

Several mitotic kinesin-5s were recently shown to be context-dependent bidirectional motor proteins[81,104-106], indicating that context-dependent directional switching is evolutionarily conserved among kinesin-5s. Our current work on KlpA provides the first evidence to suggest that context-dependent directional switching could also exist among some, if not all, mitotic kinesin-14s. Thus, the mechanism and regulation of bidirectional mitotic kinesins will be an important subject for future studies.

Methods

Molecular cloning of recombinant KlpA constructs

The full-length cDNA of KlpA was codon-optimized and synthesized for enhanced protein expression in bacteria. All recombinant KlpA constructs were integrated in a modified pET-17b vector (Novagen) using either isothermal assembly or the Q5 site-directed mutagenesis kit (NEB) and verified by DNA sequencing. All KlpA constructs contained an N-terminal 6 × His-tag for protein purification. Similarly, the recombinant human conventional kinesin hKHC(1–560) with a C-terminal HaloTag (Promega) and 6xHis-tag was derived from a gift plasmid from the Reck-Peterson laboratory at UCSD.

Protein expression and purification

All protein constructs were expressed in BL21(DE3) Rosetta cells (Novagen). Cells were grown at 37 °C in tryptone phosphate medium (TPM) supplemented with 50 μg ml−1 Ampicillin and 30 μg ml−1 chloramphenicol until OD600=0.8. Expression was induced with 0.1 mM isopropyl-β-D-thiogalactoside for 12–14 h at 20 °C. Cells were harvested by centrifugation, flash-frozen in liquid nitrogen and stored at −80 °C.

For protein purification, cell pellets were resuspended in 50 mM sodium phosphate (NaPi) buffer (pH 8.0) containing 250 mM NaCl, 1 mM MgCl2, 0.5 mM ATP, 10 mM β-mercaptoethanol, 5% glycerol and 20 mM imidazole in the presence of a protease inhibitor cocktail and then lysed via sonication. After centrifugation, soluble protein in the supernatant was purified by Talon resin (Clontech) and eluted into 50 mM NaPi buffer (pH 7.2) containing 250 mM NaCl, 1 mM MgCl2, 0.5 mM ATP, 10 mM β-mercaptoethanol, 5% glycerol and 250 mM imidazole. Protein was then flash-frozen in liquid nitrogen and stored at −80 °C.

Hydrodynamic analysis

To determine the size of a recombinant KlpA construct, a combination of gel filtration and sucrose gradient centrifugation was used as described previously[215]. For gel filtration, 500 μl of purified protein was applied to a Superdex 200 (GE Life Sciences) column pre-equilibrated with BRB50 (50 mM PIPES, pH 6.8, 1 mM EGTA and 1 mM MgCl2) supplemented with 100 mM KCl. A280 was monitored as 500-μl fractions were collected followed by SDS–PAGE analysis. Fraction intensity was calculated using ImageJ (NIH) and elution peak was determined with Origin 7.0 (OriginLab). For standard proteins,

300 µl of solution containing each standard at 3 mg ml−1 was applied to the column and analysed similarly. The Stokes radius of a given KlpA construct was determined using the plot of the Stokes radius of standard proteins (Thyroglobulin, 8.5 nm; β-amylase, 5.4 nm; BSA, 3.55 nm) versus peak elution volume.

For sucrose gradient centrifugation, 100 µl of purified protein was applied to an 11 ml 5–20% (w/v) sucrose gradient in BRB50 supplemented with 100 mM KCl buffer. The gradient was centrifuged in an SW41 rotor at 150,000 g for 18 h at 4 °C. Fractions (420 µl) were collected from the top of the gradient and analysed via SDS–PAGE. For standard proteins, 50 µl of solution containing each standard at 3 mg ml−1 was applied to the same gradient. Fraction intensity was calculated using ImageJ (NIH) and elution peak was determined with Origin 7.0 (OriginLab). The sedimentation coefficient was determined by plotting the peak elution fraction versus the sedimentation coefficient of standard proteins (alcohol dehydrogenase, 7.4 S; BSA, 4.4 S; carbonic anhydrase, 2.8 S).

Preparation of polarity-marked microtubules

All taxol-stabilized polarity-marked microtubules (tetramethylrhodamine (TMR), Alexa 488, and HiLyte 647) with bright plus ends were prepared as previously described [216]. To make the polarity-marked microtubules, a dim tubulin mix (containing 17 µM unlabelled tubulin and 0.8 µM fluorescently labelled tubulin) was first incubated in BRB80 (80 mM PIPES, pH 6.8, 1 mM EGTA and 1 mM MgCl2) with 0.5 mM guanosine-5′-[(α,β)-methyleno]triphosphate (GMPCPP) (Jena Bioscience) at 37 °C for 2 h to make dim microtubules, and then centrifuged at 250,000 g for 7 min at 37 °C in a TLA100 rotor (Beckman). The pellet was resuspended in a bright tubulin mix (containing 7.5 µM

unlabelled tubulin, 4 μM fluorescently labelled tubulin and 15 μM N-ethylmaleimide-tubulin) in BRB80 with 0.2 mM GMPCPP and incubated at 37 °C for additional 15 min to cap the plus ends. The resulting polarity-marked microtubules were pelleted at 20,000 g for 7 min at 37 °C in the TLA100 rotor and finally resuspended in BRB80 with 40 μM taxol. For making track microtubules used in single-molecule assays and microtubule-sliding assays, the dim tubulin mix also included additional 17 μM biotinylated tubulin.

TIRF microscopy

All time-lapse imaging experiments were performed at room temperature using the Axio Observer Z1 objective-type TIRF microscope (Zeiss) equipped with a × 100 1.46 numerical aperture oil-immersion objective and a back-thinned electron multiplier charge-coupled device camera (Photometrics). Except for the microtubule-gliding experiments, which used regular coverslips, all other experiments used microscope coverslips that were functionalized with biotinylated polyethylene glycol (biotin-PEG) as previously described[217] to reduce nonspecific surface absorption of molecules. All time-lapse imaging experiments in this study used flow chambers that were made by attaching a coverslip to a microscope glass slide by double-sided tape.

Single-molecule photobleaching assays

For the single-molecule photobleaching assays, GFP-tagged KlpA motors were diluted and bound to surface-immobilized HyLite 647 microtubules in a BRB50-based buffer supplemented with 25 mM KCl, 20 μM taxol and 1.3 mg ml−1 casein, and 1.5 mM AMPPNP. To remove GFP contamination for the assay, the full-length GFP-KlpA was additionally purified via gel filtration in 50 mM NaPi buffer (pH 7.2) containing 250 mM

NaCl, 1 mM MgCl2, 0.5 mM ATP and 10 mM β-mercaptoethanol. Time-lapse images were continuously recorded with 200-ms exposure until the field of view was bleached. The number of photobleaching steps of individual KlpA motors was obtained by tracking the fluorescence intensity in ImageJ (NIH).

In vitro motility assays

For all in vitro motility experiments, the motility chamber was perfused with 0.5 mg ml−1 streptavidin for immobilizing polarity-marked HyLite 647 microtubules. GFP-tagged kinesin molecules (GFP-KlpA and GFP-KlpA-Δtail) were then diluted in motility buffer (BRB50 supplemented with 25 mM KCl, 1 mM ATP, 25 μM taxol, 1.3 mg ml−1 casein and an oxygen scavenger system[218]) and added to the chamber. Time-lapse images were acquired at 1 frame per second. The setting was 100-ms exposure and 5-min duration for the high-concentration flux experiments and 200-ms exposure and 10 min for single-molecule experiments to determine the velocity and run-length of GFP-KlpA. Kymographs were generated and analysed in ImageJ (NIH) for determining directionality, velocity and run-length information of GFP-tagged kinesin motors. Velocity and run-length were determined by fitting the histograms to a Gaussian distribution and an exponential distribution, respectively, in MATLAB (MathWorks).

Microtubule-gliding assays

For microtubule-gliding assays, kinesin motors (diluted in BRB50 supplemented with 20 μM taxol and 1.3 mg ml−1 casein) were immobilized on the coverslip via the monoclonal Anti-His antibody (Fisher Scientific). Unbound kinesin molecules were removed with BRB50 supplemented with 20 μM taxol and 1.3 mg ml−1 casein. Polarity-

marked TMR microtubules diluted in the same buffer were then added to the chamber and incubated for 2 min. Unbound microtubules were removed by extensive wash with BRB50 supplemented with 20 μM taxol and 1.3 mg ml−1 casein. Finally, the chamber was perfused with a BRB50-based motility buffer supplemented with 100 mM KCl, 1 mM ATP, 25 μM taxol, 1.3 mg ml−1 casein and an oxygen scavenger system[218]. Time-lapse images were taken at 1 frame per second for 5 min.

Microtubule-sliding assays

For all microtubule-sliding assays, the motility chamber was first perfused with 0.5 mg ml−1 streptavidin for immobilizing polarity-marked track microtubules. After washing out free track microtubules, the kinesin motor was diluted into BRB50 supplemented with 20 μM taxol and 1.3 mg ml−1 casein and added to the chamber and incubated to allow for binding to the track microtubules. All unbound motors were washed away before the addition of polarity-marked cargo microtubules. After incubation all non-bundled cargo microtubules were washed away with BRB50 supplemented with 20 μM taxol and 1.3 mg ml−1 casein before the addition of motility buffer (BRB50 supplemented with 25 mM KCl, 1 mM ATP, 25 μM taxol, 1.3 mg ml−1 casein and an oxygen scavenger system[218]). Time-lapse images were taken at 1 frame per second.

MSD analysis

To perform the MSD analysis, single-molecule motility data of KlpA on polarity-marked microtubules were acquired with 100-ms exposure time and 130-ms interval for a total duration of 2 min. Sub-pixel xy coordinates of motile KlpA molecules were determined using TrackMate (http://fiji.sc/TrackMate). The MSD values were computed

from these xy coordinates using the formula as previously described[219]. The MSD-versus-time plots were analysed by fitting curves to data using nonlinear regression in Matlab (MathWorks).

Other microtubule-based assays

To confirm the microtubule-binding ability of KlpA-tail-GFP, HyLite 647 microtubules were immobilized on the surface of coverslip, and purified KlpA-tail-GFP diluted in BRB50 supplemented with 25 mM KCl, 25 μM taxol and 1.3 mg ml−1 casein was added in the flow chamber. Unbound KlpA-tail-GFP was washed away with BRB50 supplemented with 25 mM KCl, 25 μM taxol and 1.3 mg ml−1 casein after 2-min incubation, and TIRF microscopy images were taken for both HyLite 647 and GFP channels.

To confirm that the N-terminal tail is required for KlpA to crosslink microtubules, GFP-KlpA and GFP-KlpA-Δtail were each mixed with both HyLite 647 microtubules and TMR microtubules in BRB50 supplemented with 25 mM KCl, 25 μM taxol and 1.3 mg ml−1 casein, and added to the flow chamber after 2-min incubation for TIRF microscopy imaging in both HyLite 647 and TMR channels.

Acknowledgments

We thank Drs C. Mathews (Oregon State University), X. Su (UCSF) and B. Liu (UC Davis) for critical reading of the manuscript, and Mr Chun Liu (Pearl River Fisheries Research Institute, China) for initial plasmid construction. This work was supported in part by the National Science Foundation (MCB-1616462 to W.Q.).

Supplementary Materials

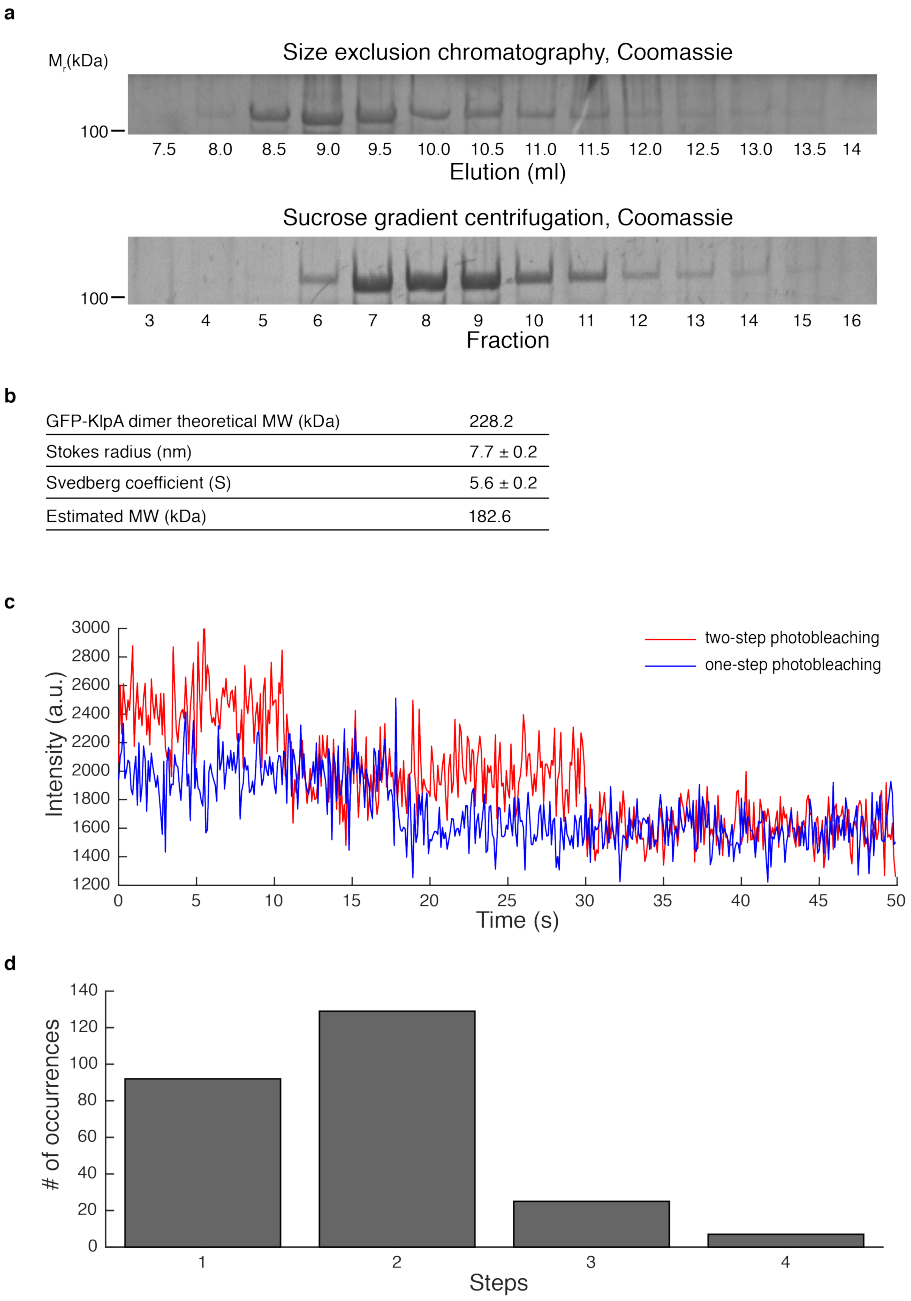

Figure 2.S1: Supplementary Figure 1: GFP-KlpA forms a homodimer.

(a) Hydrodynamic analysis of the purified full-length GFP-KlpA protein. Fractions from size exclusion chromatography and 5-20% (w v^{-1}) sucrose gradient centrifugation experiments. **(b)** Calculation of GFP-KlpA molecular weight based on the experimentally derived Stokes radius and Svedberg coefficient. **(c)** Representative photobleaching traces of GFP-KlpA fluorescence on surface-immobilized microtubules in the presence of 1.5 mM AMPPNP. **(d)** Histogram of fluorescence photobleaching steps of GFP-KlpA (n = 253).

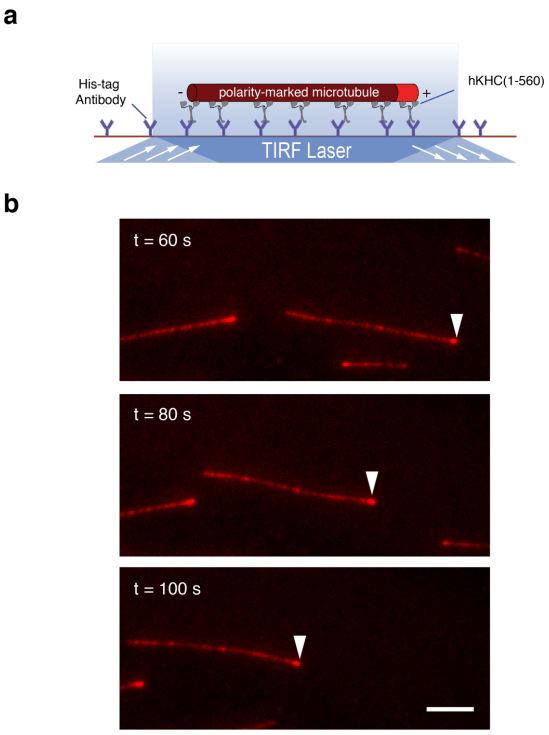

Figure 2.S2: Surface-immobilized human conventional kinesin hKHC(1-560) drives microtubule gliding with plus end-directed motility.

(a) Schematic diagram of the microtubule-gliding assay. **(b)** Representative TIRF microscopy images showing that surface-immoblized plus end-directed hKHC(1-560) molecules collectively drive microtubules to glide with the bright plus ends trailing. Microtubules are fluorescently labeled with TMR and polarity-marked with a dimly labeled fluorescent segment at the minus end and a more brightly labeled segment at the plus end. Arrowheads indicate the plus end of the microtubule. Scale bar: 5 μm.

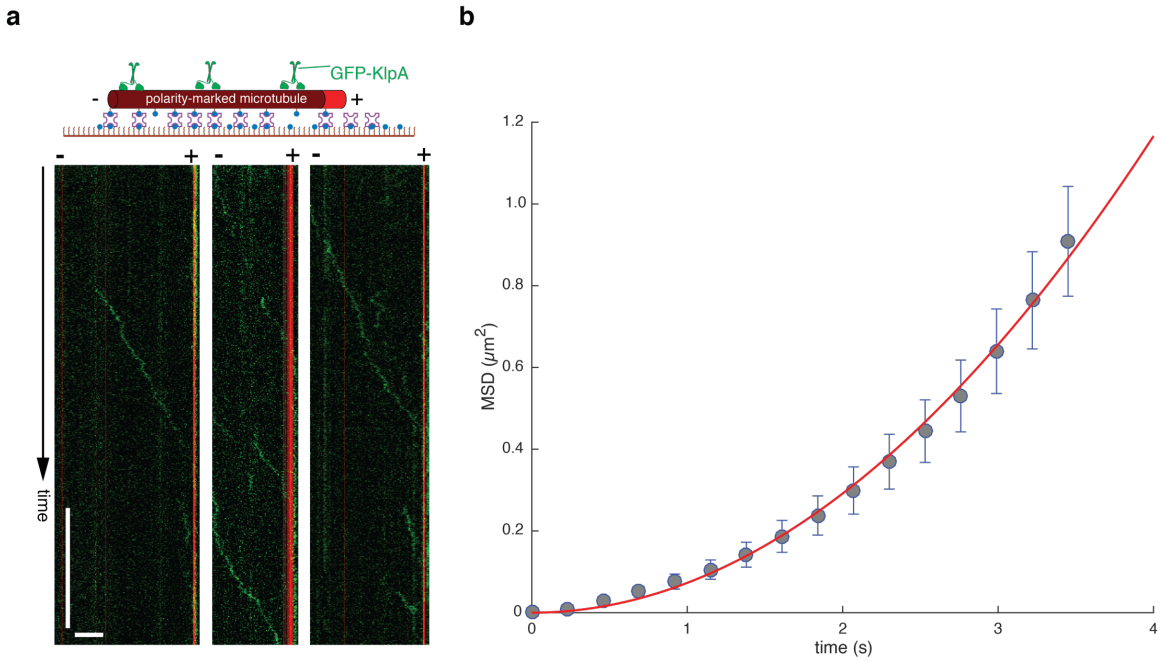

Figure 2.S3: GFP-KlpA motility is directional on individual microtubules.

(a) Example kymographs of GFP-KlpA molecules (green) moving in a directional manner on polarity-marked microtubules (red) with a bright plus end and a dim minus end. **(b)** MSD analysis of GFP-KlpA on polarity-marked microtubules. The MSD-versus-time plot was best fitted with a one-dimensional directional movement: $MSD = V^2t^2 + offset$. The mean velocity V was determined to be 270 ± 1 $nm^2\ s^{-1}$ (mean ± s.e.m., n = 79). Scale bars: 30 s (vertical) and 5 µm (horizontal).

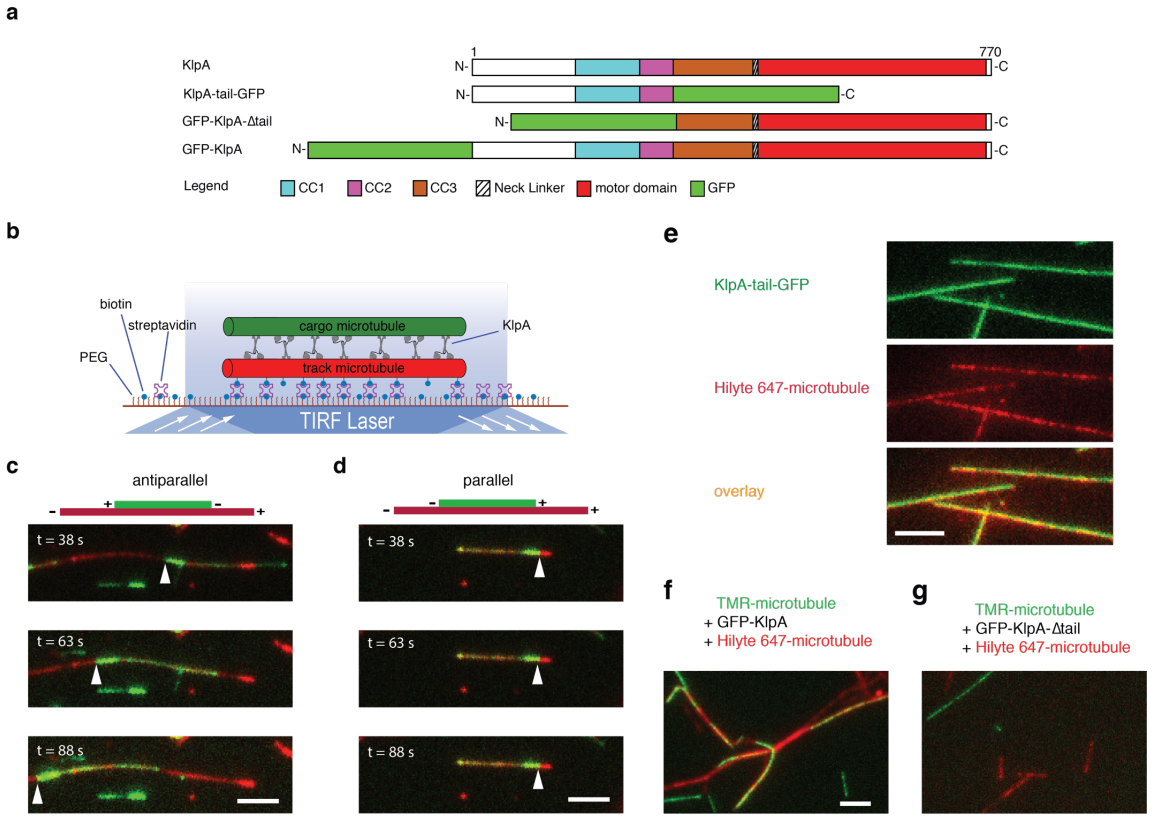

Figure 2.S4: KlpA slides antiparallel microtubules and statically crosslinks parallel microtubules using an N-terminal nonmotor microtubule-binding domain.

(a) Schematic diagram of the full-length KlpA, KlpA-tail-GFP, GFP-KlpA-Δtail and GFP-KlpA. KlpA-tail-GFP and GFP-KlpA-Δtail containing residues 1-302 and 303-770 of the full-length KlpA respectively. **(b)** Schematic diagram of the microtubule-transport assay. Polarity-marked track microtubules (red) are immobilized on the coverslip via the biotin/streptavidin/biotin chemistry, and then incubated with KlpA (gray) and polarity-marked cargo microtubules (green). **(c, d)** Representative diagrams and image sequences of KlpA dynamically sliding antiparallel microtubules in **(c)** and statically crosslinking parallel microtubules in **(d)**. Track and cargo microtubules are both polarity-marked with bright plus ends but fluorescently labeled with different dyes. Arrowheads indicate the plus end of the cargo microtubule. **(e)** Microscopy images showing that GFP-KlpA-tail (green) binds to surface-immobilized HyLite 647 microtubules (red). **(f, g)** Microscopy images showing that TMR microtubules (green) readily bundle with HyLite 647 microtubules (red) in the presence of GFP-KlpA **(f)** but not GFP-KlpA-Δtail **(g)**. Scale bar: 5 µm.

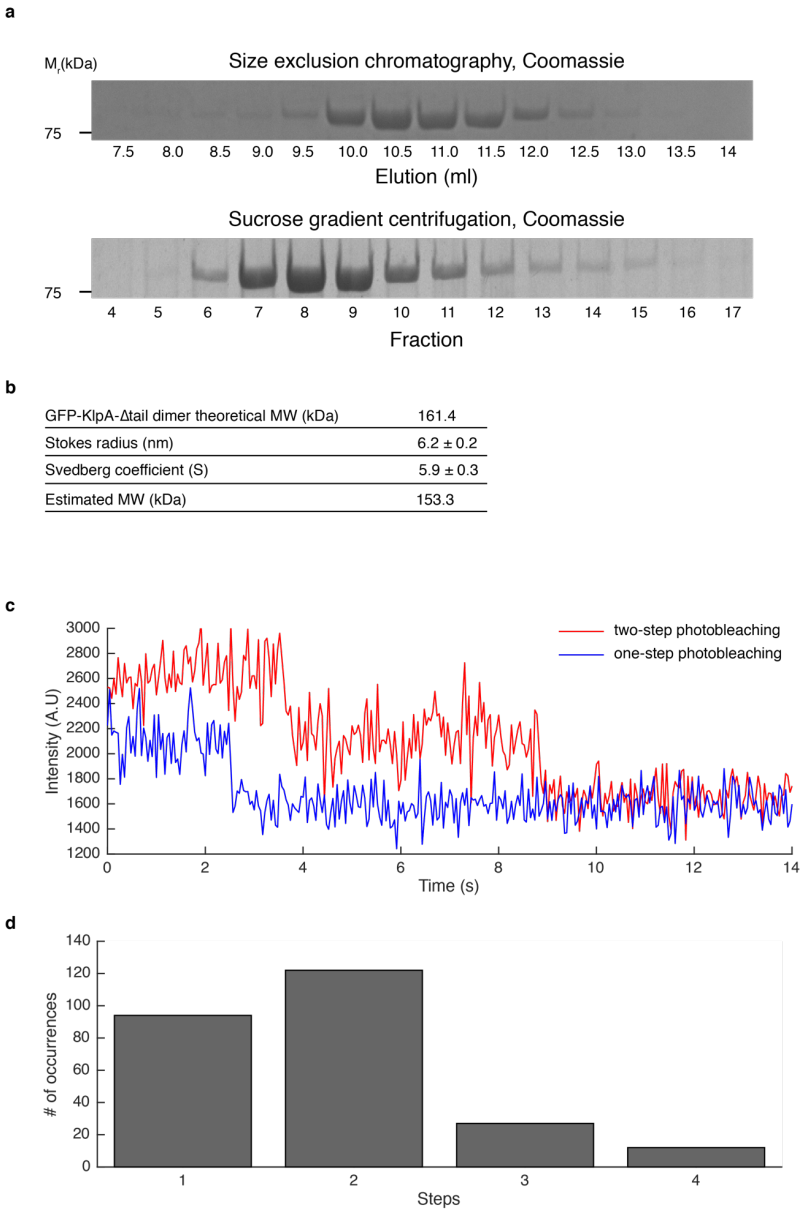

Figure 2.S5: GFP-KlpA-Δtail forms a homodimer.

(a) Hydrodynamic analysis of purified GFP-KlpA-Δtail protein. Fractions from size exclusion chromatography and 5-20% (w v^{-1}) sucrose gradient centrifugation experiments. **(b)** Calculation of GFP-KlpA-Δtail molecular weight based on the experimentally derived Stokes radius and Svedberg coefficient. **(c)** Representative photobleaching traces of GFP-KlpA-Δtail fluorescence on surface-immobilized microtubules in the presence of 1.5 mM AMPPNP. **(d)** Histogram of fluorescence photobleaching steps of GFP-KlpA-Δtail (n = 255).

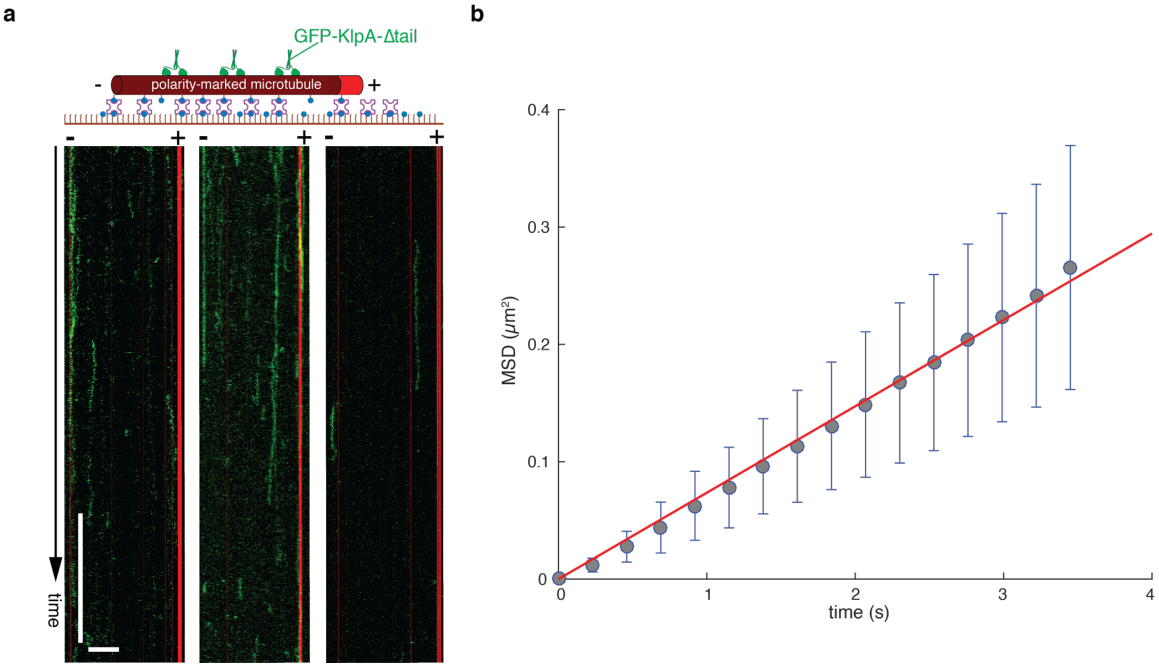

Figure 2.S6: GFP-KlpA-Δtail is diffusive on individual microtubules with no apparent directional preference.

(a) Example kymographs of GFP-KlpA-Δtail molecules (green) showing diffusive motility on polarity-marked microtubules (red) with a bright plus end and a dim minus end. **(b)** MSD analysis of GFP-KlpA-Δtail on polarity-marked microtubules. The diffusion constant *D* was derived by fitting the MSD-versus-time plot with a one-dimensional diffusion: $MSD = 2Dt$. The mean diffusion constant *D* was determined to be 0.0368 ± 0.0003 $\mu m^2 s^{-1}$ (mean ± s.e.m., n = 40). Scale bars: 30 s (vertical) and 5 μm (horizontal).

Chapter 3

The Mitotic Kinesin-14 KlpA is Regulated by a Conserved Mitotic Protein Pair

Andrew R. Popchock, Youngmin Park, & Weihong Qiu

Abstract

Kinesin-14s motor proteins are important components of the microtubule-based mitotic spindle assembly that is responsible for chromosome segregation during cellular division. Disruption of kinesin-14 activity within the mitotic spindle often leads to protrusion of spindle microtubules past mitotic organizing centers resulting in errors in chromosome segregation which in turn can cause cellular aneuploidy. As many tumors show some degree of aneuploidy, mechanistic understanding of these pathways has been an intense area of research, yet mechanisms responsible for this kinesin-14-based anchoring of spindle microtubules have yet to be explored in depth. Here we show using total internal reflection fluorescence microscopy that a conserved pair of mitotic proteins can regulate the activity of KlpA, a kinesin-14 from *Aspergillus nidulans* that is a context-dependent bidirectional motor. These mitotic proteins are able to interact with KlpA to cause it to switch directionality on microtubules and coordinate to form a stable anchored complex on microtubules. Based on these findings, we propose a model for KlpA function within the mitotic spindle and a potential mechanism for spindle microtubule anchoring at spindle poles.

Introduction

Proper assembly and maintenance of the microtubule-based bipolar mitotic spindle is required for accurate chromosome segregation during mitosis[82,140,193]. Errors in this process can lead to cellular aneuploidy, a hallmark of cancer[149-151]. Within the mitotic spindle the centrosomes (or spindle pole bodies (SPB) in fungi) are the primary microtubule-organizing centers (MTOCs). Localizing to the MTOCs are the γ-tubulin ring

complexes (γ-TuRC) which are responsible for spindle microtubule nucleation[145]. MTOCs are responsible for the anchoring of these spindle microtubules at their minus ends in coordination with the γ-TuRC[133], which is required for maintenance of the bipolar spindle and capture of kinetochores[141,220].

The anchoring of spindle microtubules at the MTOCs relies on a highly-conserved protein pair, Msd1/SSx2IP and Wdr8[221]. The coiled-coil protein Msd1/SSX2IP has been shown to localize to the MTOCs and interact with the γ-TuRC both in yeast[146] and humans[133,221]. Wdr8 interacts directly with Masd1/SSX2IP through its conserved WD40 domain[74,129,134] and the localization of both Msd1/SSX2IP and Wdr8 to the MTOCs has been shown to be interdependent[66]. This interaction between Msd1/SSX2IP and Wdr8 is known to be required for spindle microtubule anchoring and has been shown to be a conserved function from fungi to yeast and humans. It was recently reported that in fission yeast, the anchoring of spindle microtubules by the Msd1-Wdr8 complex required a third protein partner, the kinesin-14, Pkl1. Kinesin-14s are known to contribute to spindle assembly and organization[147] by functioning antagonistically to its kinesin-5 counterpart[74,129,134]. While these findings expanded the mechanism of anchoring of spindle microtubules at the MTOC (SPB) in yeast, it remains unclear if this interaction with kinesin-14 is conserved in other organisms. Mechanistic details of how all three proteins could potentially coordinate to anchor spindle microtubules remain unknown.

We previously found that the homolog of Pkl1 from *Aspergillus nidulans,* KlpA, was a processive kinesin-14 with context-dependent directionality[74,103]. In this study, we report our characterization of the interactions between KlpA and the Msd1/SSX2IP homolog, TinA, and the Wdr8 homolog AnWdr8. In *A. nidulans, An*-Wdr8 has been

proposed to regulate the levels of TinA,[147] but its role in the anchoring of spindle microtubules remains unclear. Here we report that the interaction between kinesin-14, Msd1 and Wdr8 appears to be conserved in *A. nidulans*. Specifically, we find that TinA can interact directly with KlpA to modulate its motility and directionality on individual microtubules. We further show that TinA and AnWdr8 coordinate with KlpA to form an anchored complex on microtubules. Taken together, these findings provide mechanistic detail of how this conserved interaction between KlpA, TinA and AnWdr8 could potentially coordinate to anchor spindle microtubules at the SPB in *A. nidulans.*

Results

Conserved TinA protein is required for KlpA localization to the SPB.

To determine if the relationship between kinesin-14 and Msd1/SSX2IP is potentially conserved in the fungi *A. nidulans,* we sought to investigate the relationship between KlpA (kinesin-14) and TinA (Msd1/SSX2IP) within the mitotic spindle. Like other mitotic kinesin-14s[66], KlpA localizes strongly to mitotic SPBs (Figure 3.1a). In a background lacking TinA, KlpA localization became disperse in mitotic spindles (Figure 3.1b). These results show that like its fission yeast counterpart, KlpA relies on the conserved TinA protein for strong localization to the SPBs. Moreover, because it has been shown that TinA is required for localization of AnWdr8 to SPBs[103], it appears that the interdependence of all three components (KlpA, TinA, AndWdr8) for localization is conserved from *S. pombe* to *A. nidulans.*

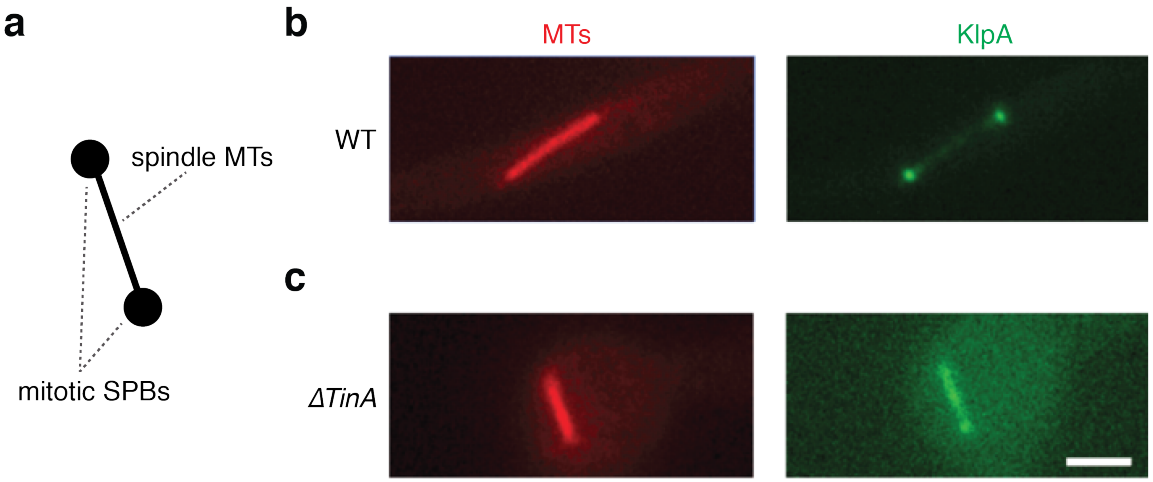

Figure 3.1: Conserved partner protein TinA is required for KlpA localization to spindle poles.

(a) Schematic representation of the mitotic nucleus including spindles and SBPs. **(b)** Localization of KlpA in WT background. Confocal images of WT cells during mitosis were taken to visualize localization of KlpA. Spindle microtubules labeled with TubA antibody are shown in red (left). GFP-KlpA molecules were visualized simultaneously (right). **(c)** Localization of KlpA in ΔTinA background. Confocal images of ΔTinA cells during mitosis were taken to visualize localization of KlpA. Spindle microtubules labeled with TubA antibody are shown in red (left). GFP-KlpA molecules were visualized simultaneously (right). Scale bar, 5 μm.

Presence of TinA activates KlpA for minus end-directed motility on individual microtubules.

We previously reported that KlpA is a plus end-directed processive kinesin-14 on individual microtubules that can become minus end-directed under certain contexts[66]. Because TinA is required for KlpA localization to SPBs and the equivalent protein pair had been shown to directly interact in fission yeast[66], we sought to investigate the KlpA and TinA interaction. To that end, we fused TinA with the fluorescent protein mCherry (Figure 3.2a) to enable visualization in Total Internal Reflection Microscopy (TIRF) single-molecule motility assays (Figure 3.2b). To investigate interaction between TinA and KlpA, we mixed purified GFP-KlpA with purified TinA-mCherry in excess prior to introduction into single-molecule motility assays. Alone, KlpA moves towards and accumulates at microtubule plus ends (Figure 3.2c), but upon the addition of TinA-mCherry many KlpA molecules were observed to be minus end-directed on microtubules (Figure 3.2d Top). TinA-mCherry was visualized simultaneously within these single-molecule motility assays and those particles containing TinA-mCherry particles were observed to be exclusively minus end-directed (Figure 3.2d Middle). Minus end-directed TinA-mCherry molecules contained KlpA particles (Figure 3.2d Bottom) presumably responsible for the observed motivity, as TinA is not a motor protein and therefore not capable of autonomous movement on microtubules. These assays indicated that TinA was potentially interacting with KlpA to form a complex that enables KlpA for minus end-directed motility on microtubules. While these results were surprising, this context-dependent directionality was consistent with the behavior of KlpA that we had previously observed within microtubule bundles[66].

Analysis of these minus end-directed particles revealed a velocity distribution that was consistent with the convolution of two distinct velocities centered at 50 nm s^{-1} and 350 nm s^{-1} which we termed a "slow" minus end-directed motility and a "fast" minus end-directed motility (Figure 3.2e). Because we had previously shown that the tail domain of KlpA enabled both processivity and directional switching under differing contexts[66], we hypothesized that TinA interacted directly with this tail domain resulting in the observed minus end-directed motility of these observed complexes. We have previously shown the tail domain of KlpA to contain a nonmotor microtubule binding domain[66], and hypothesized that displacement of KlpA tail binding to microtubules by TinA binding could be supplemented by TinA interaction with microtubules. TinA interaction with microtubules in turn could regulate the velocity of KlpA-TinA complexes on microtubules. To determine if this could be the case, we tested whether or not TinA was a microtubule binding protein. Microtubule co-sedimentation assays revealed that TinA was able to bind to microtubules under similar conditions to those used in our single-molecule motility assays (Figure 3.2f).

To further investigate the role of this microtubule-binding activity of TinA as a potential velocity regulator of the KlpA-TinA complex, we sought to decouple the microtubule-binding activity and KlpA interaction functions of TinA. To that end, we made a truncated TinA which lacked its predicted C-terminal coiled-coil domain (TinA(1-369)-mCherry, Supplementary Figure 3.1a) whose microtubule binding was dramatically reduced when compared to full-length TinA-mCherry in sedimentation assays (Supplementary Figure 3.1d). To ensure that that removal of this coiled-coil did not disrupt dimerization on TinA(1-369)-mCherry, single molecule photobleaching experiments were

used to confirm that similar to full-length TinA-mCherry (Supplementary Figure 3.2), TinA(1-369)-mCherry formed a stable dimer under single-molecule motility assay conditions (Supplementary Figure 3.3). We then introduced TinA(1-369)-mCherry to our single molecule assays in place of full-length TinA-mCherry, and analyzed the resulting motility behavior of both GFP-KlpA and TinA(1-369)-mCherry. In these assays, GFP-KlpA was activated for minus end-directed motility much like we observed with full-length TinA-mCherry (Supplementary Figure 3.1b). However, unlike full-length TinA-mCherry, these colocalized particles appeared to move with only a single velocity, and analysis of these velocities revealed a single distribution with an average velocity of 290±90 nm s^{-1} (mean±s.d., n=161, Supplementary Figure 3.1c). This velocity was similar to the "fast" velocity observed in the presence of full-length TinA-mCherry.

Taken together, these results indicate that TinA can enable KlpA for minus end-directed motility by potentially forming a stable complex. Once formed, the velocity of this complex can then potentially be regulated through the microtubule binding domain present within TinA.

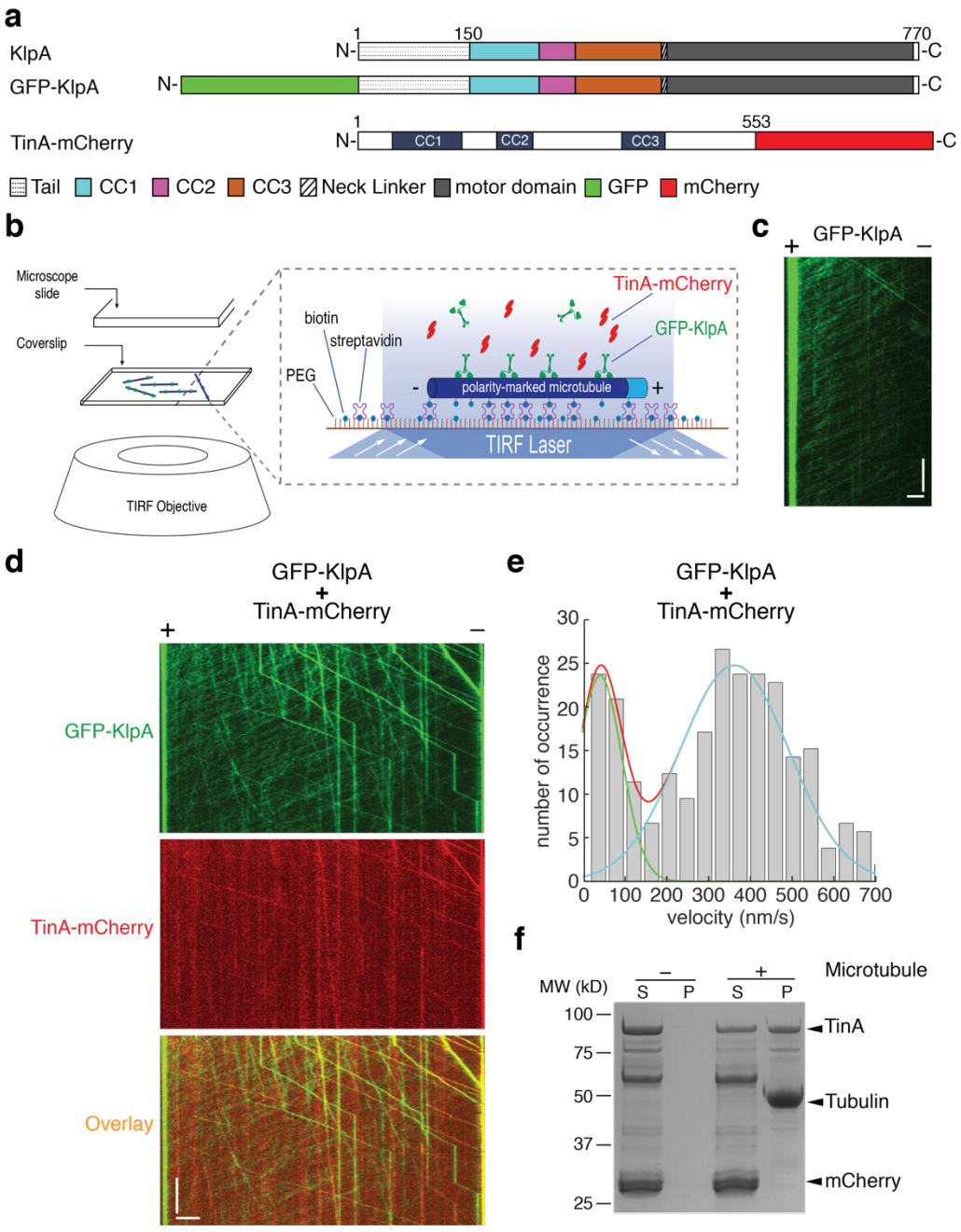

Figure 3.2: Presence of TinA activates KlpA for minus end-directed motility on single microtubules with two distinct velocities.

Figure 3.2: Presence of TinA activates KlpA for minus end-directed motility on single microtubules with two distinct velocities.

(a) Schematic diagram of full-length KlpA, GFP-KlpA and TinA-mCherry constructs. **(b)** Schematic diagram of the *in vitro* GFP-KlpA/TinA-mCherry motility assay. Microtubules were fluorescently labelled with Hilyte 647, and polarity-marked with a dim minus end and a bright plus end. **(c)** Representative kymograph of GFP-KlpA alone on single microtubules. **(d)** Representative kymographs of GFP-KlpA and TinA-mCherry movement on individual microtubules in single-molecule motility assays with GFP-KlpA (Top) and TinA-mCherry (Middle) channels separated as well as overlaid on each other (Bottom). **(e)** Velocity histogram of colocalized GFP-KlpA and TinA-mCherry molecules on single microtubules with two distinct mean velocities of 50±10 nm s^{-1} and 350±90 nm s^{-1} (mean±s.d., n=251). Green and blue lines indicate single Gaussian fits to the velocity histogram and red line indicates the sum of both Gaussian fits to the velocity histogram. **(f)** Microtubule co-sedimentation assay of TinA-mCherry. Scale bars, 1 min (vertical) and 5 μm (horizontal).

The tail domain acts as a directional determinant of KlpA that is required for interaction with TinA.

To further investigate if interaction with TinA was localized to the tail domain of KlpA, we sought to disrupt KlpA/TinA complex formation through the removal of this tail domain. Our previous work had revealed that removal of an extended tail domain (residues 1-302) yielded a non-processive KlpA motor[66], so we determined a minimal tail domain consisting of the first 150 residues of KlpA immediately upstream of predicted coiled-coil domains (Figure 3.3a). Single molecule photobleaching experiments confirmed that homodimerization of this shortened KlpA tail-less construct (GFP-KlpA-Δtail) was not disrupted, as GFP-KlpA-ΔTail exhibited a photobleaching pattern typical of a homodimer[66] (Supplementary Figure 3.4a,b). Single molecule microtubule gliding assays (Supplementary Figure 3.4c) were then used to confirm that GFP-KlpA-Δtail was an active motor and maintained minus end-directed directionality (Supplementary Figure 3.4d) consistent to what we had previously observed to both full-length KlpA as well as an further truncated tailless KlpA motor[66].

To determine if processive motility of GFP-KlpA-Δtail was disrupted, single-molecule motility assays were then used to characterize its motility on single microtubules. Surprisingly, we observed that GFP-KlpA-Δtail remained processive on individual microtubules but became a minus end-directed motor (Figure 3.3b). Analysis of the motility of GFP-KlpA-Δtail revealed an average velocity of 340 ± 90 nm s^{-1} (mean +/- s.d. n = 268, Figure 3c) and a characteristic run-length of 5.3 ± 0.9 μm (mean ± s.e.m., n = 268, Figure 3.3d). While the velocity of GFP-KlpA-Δtail was similar to that of full-length GFP-KlpA, GFP-KlpA-Δtail exhibited approximately a 50% reduction in run-length when

compared to full-length GFP-KlpA[103]. These findings are consistent with our hypothesis that the tail domain of KlpA acts as a tether to ehance processive motility of KlpA via its interaction with microtubules. It is likely that removal of this minimal tail domain does not completely abolish the microtubule binding activity of the N-terminus of KlpA and therefor yields a reduction in processivity and not complete elimination, as we observed previously with an extended KlpA tail domain deletion[148]. It is clear that that this minimal tail domain (a.a. 1-150) is a directionality determinant of KlpA, as upon its removal GFP-KlpA-Δtail reverts to canonical minus end-directed motility.

To investigate if TinA could potentially bind to this KlpA tail domain and in turn displace it from microtubules to activate this observed directionality switch, we tested whether TinA-mCherry was able to colocalize with GFP-KlpA-Δtail in our single-molecule motility assays. Subsequent analysis revealed that under the same conditions used as full-length GFP-KlpA, TinA-mCherry did not colocalize with GFP-KlpA-Δtail (Figure 3.3e). Analysis of the sequence of this KlpA-tail domain revealed that it was predicted to be highly disordered which we confirmed using NMR spectroscopy (Supplementary Figure 3.5). These results indicate that the intrinsically disordered N-terminus of KlpA is required for interaction with TinA-mCherry and subsequent directional switching to minus end-directed motility.

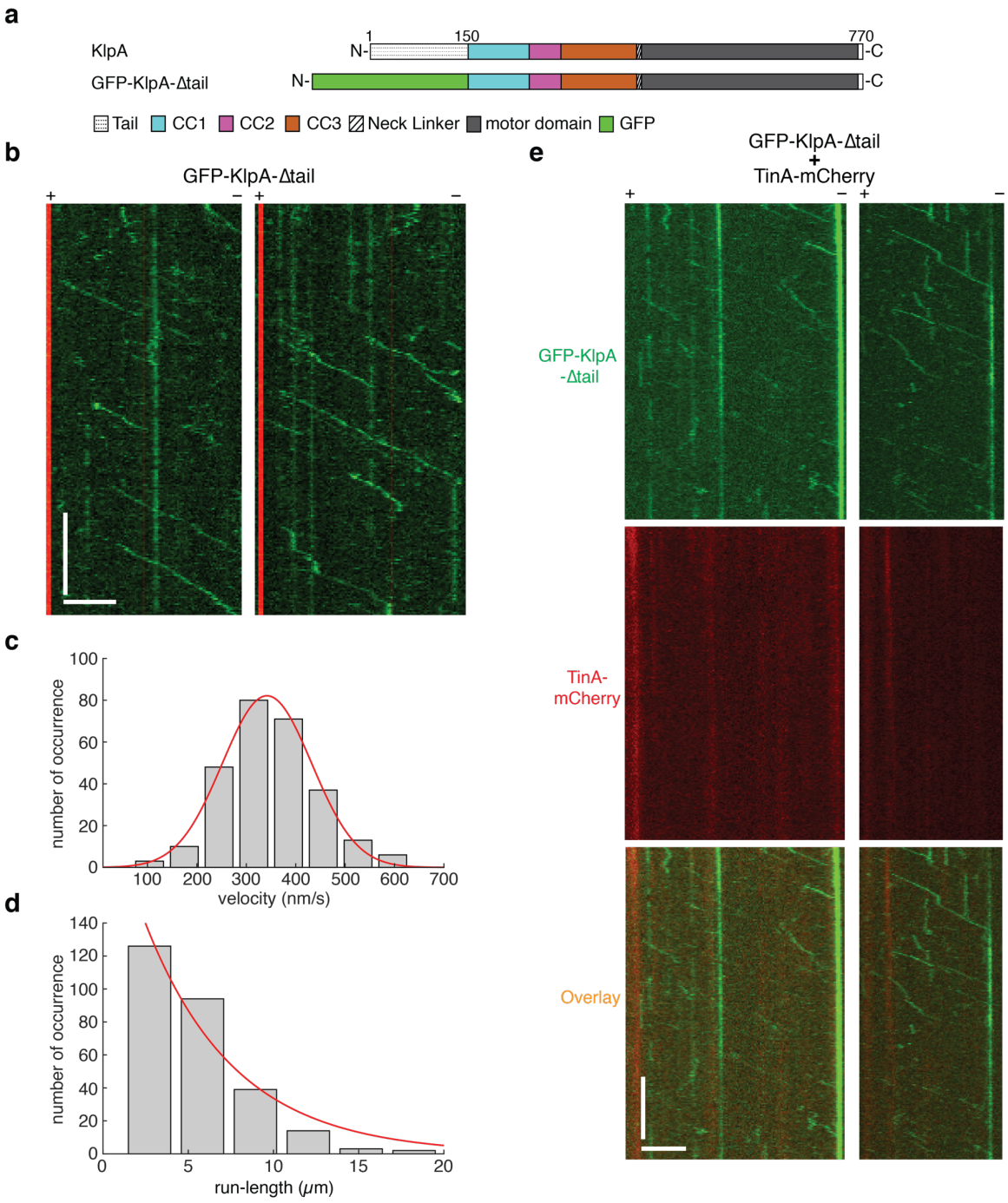

Figure 3.3: The N-terminal tail of KlpA acts as a directionality determinant and is required for interaction with TinA.

Figure 3.3: The N-terminal tail of KlpA acts as a directionality determinant and is required for interaction with TinA.

(a) Schematic diagram of full-length KlpA and GFP-KlpA-Δtail constructs. **(b)** Representative kymographs of GFP-KlpA-Δtail minus end-directed motility on single microtubules. **(c)** Velocity histogram of GFP-KlpA-Δtail molecules on single microtubules with an average velocity of 340±90 nm s^{-1} (mean±s.d., n=268). Red line indicates the Gaussian fit to the velocity histogram. **(d)** Run-length histogram of individual GFP-KlpA-Δtail molecules on single microtubules with a characteristic run-length of 5.3±0.9 μm (mean±s.e.m., n=268). Red line indicates a single exponential fit to the run-length histogram. **(e)** Representative kymographs of GFP-KlpA-Δtail and TinA-mCherry movement on individual microtubule under single-molecule motility assays with GFP-KlpA-Δtail (Top) and TinA-mCherry (Middle) channels separated as well as overlaid on each other (Bottom). Scale bars, 1 min (vertical) and 5 μm (horizontal).

TinA and AnWDR8 coordinate with KlpA to become anchored on microtubules.

In fission yeast, the TinA homolog (Msd1) was proposed to be an adapter for the AnWDR8 homolog (Wdr8) in complex formation with the KlpA homolog (Pkl1) [66]. TinA has been shown to interact with AnWdr8 *in vivo*[103,133,146,221], and we sought to explore if the interaction scheme proposed in fission yeast was potentially conserved in the *A. nidulans* system. To that end, full-length AnWdr8 (Figure 3.4a) was purified for introduction into our single-molecule motility assays alongside GFP-KlpA and TinA-mCherry (Figure 3.4b). Consistent with TinA acting as an adapter protein, AnWdr8 alone did not have any observed effect on GFP-KlpA motility in single-molecule assays (Figure 3.4c). However, when AnWdr8 was introduced to GFP-KlpA and TinA-mCherry in single-molecule assays, GFP-KlpA and TinA-mCherry strongly colocalized on individual microtubules with an extremely slow minus end-directed motility which we termed "anchored" motility on microtubules (Figure 3.4d). While some colocalized fast moving minus end-directed particles were observed (Figure 3.4d, white arrows), the majority of both GFP-KlpA and TinA-mCherry particles were observed to be locked in this "anchored" state on microtubules.

To see if the intrinsically disordered tail domain of KlpA was sufficient for the KlpA interactions with TinA and AnWdr8, we tested if adding the KlpA tail to another kinesin 14 would be recapitulate their observed effects. We decided to use the founding member of the kinesin-14 family, Ncd, from *Drosophila melanogaster* for our model kinesin-14. TinA-mCherry, AnWdr8, or TinA-mCherry in the presence of AnWdr8 was not observed to have any effect on the motility of Ncd (Supplementary Figure 3.6). We proceeded to remove the native tail domain of Ncd (a.a. 1-236) and replace it with the

disordered KlpA-tail domain that was previously characterized along with an N-terminal GFP to generate a GFP-KlpA$_{tail}$-Ncd chimera (Supplementary Figure 3.7a). While this GFP-KlpA$_{tail}$-Ncd chimera maintained diffusive motility on individual microtubules in single-molecule motility assays (Supplementary Figure 3.7b) similar to the wild-type Ncd equivalent (Supplementary Figure 3.6a), in the presence of TinA-mCherry, colocalized GFP-KlpA$_{tail}$-Ncd and TinA-mCherry particles were observed (Supplementary Figure 3.7c). Furthermore, upon the addition of AnWdr8 to single-molecule motility assays, the slow "anchored" motility previously observed with GFP-KlpA/TinA-mCherry/AnWdr8 (Figure 3.4d) was successfully recapitulated (Supplementary Figure 3.7d). Together, these data show that TinA and AnWdr8 coordinate with KlpA via its N-terminal disordered tail domain to form a stable complex that is anchored on microtubules.

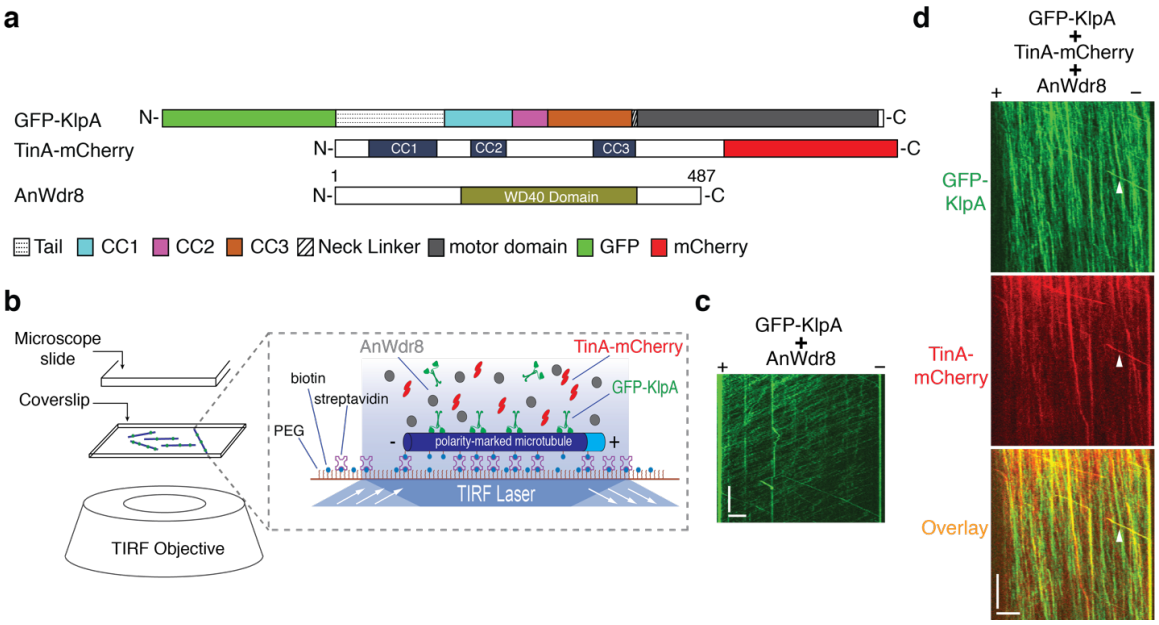

Figure 3.4: In the presence of AnWdr8, KlpA and TinA strongly colocalize and bind to microtubules.

(a) Schematic diagram of GFP-KlpA, TinA-mCherry and AnWdr8 constructs. **(b)** Schematic diagram of the *in vitro* GFP-KlpA/TinA-mCherry/AnWdr8 motility assay. Microtubules were fluorescently labelled with Hilyte 647, and polarity-marked with a dim minus end and a bright plus end. **(c)** Representative kymograph of GFP-KlpA motility on single microtubules in the presence of AnWdr8 alone. **(d)** Representative kymographs of GFP-KlpA and TinA-mCherry movement on individual microtubule in the presence of AnWdr8 in single-molecule motility assays with GFP-KlpA (Top) and TinA-mCherry (Middle) channels separated as well as overlaid on each other (Bottom). White arrows indicate occasional observed fast colocalized motility. Scale bars, 1 min (vertical) and 5 μm (horizontal).

AnWdr8 anchors the KlpA/TinA/AnWdr8 complex by enhancing TinA binding to microtubules.

After observation of the anchored KlpA/TinA/AnWdr8 complex on microtubules, we were intrigued as to how AnWdr8 could generate such a dramatic change in behavior on microtubules in single-molecule motility assays. Because we had previously determined that TinA was a microtubule binding protein (Figure 3.2f) and that this microtubule binding activity could potentially regulate the velocity of GFP-KlpA/TinA-mCherry molecules on microtubules (Supplementary Figure 3.1), we wondered if AnWdr8 could potentially affect the microtubule binding activity of TinA. To more closely match the context under which this anchored complex was observed we decided to remove GFP-KlpA from our single-molecule motility assays to isolate the behavior of TinA-mCherry in the presence and absence of AnWdr8. Consistent with what was observed in microtubule co-sedimentation assays (Figure 3.2f), moderate microtubule binding of TinA-mCherry under single-molecule assays was observed (Figure 3.5a). Upon the addition of AnWdr8, TinA-mCherry was observed to bind much more strongly to microtubules (Figure 3.5b), with a near order of magnitude increase in observed intensity at equivalent concentrations (Figure 3.5c). This indicated that AnWdr8 was indeed regulating the microtubule binding activity of TinA, dramatically increasing the strength of TinA binding to microtubules. With this information we are able to propose an expanded model for the context-dependent directionality of KlpA that we previously characterized[71,103,132,133,222]. Like our previous model, the directionality of KlpA is dependent upon the context of its N-terminal tail domain, although we have now narrowed this directional switch to the first 150 amino acids of KlpA. In our expanded model KlpA can be activated for minus end-directed motility

with two distinct velocities in the presence of TinA dependent upon the microtubule binding of TinA (Figure 3.5d). Upon the addition of AnWdr8, TinA is then locked into a strong-binding state to microtubules which in turn forms a stable ternary complex that is anchored to microtubules (Figure 3.5d).

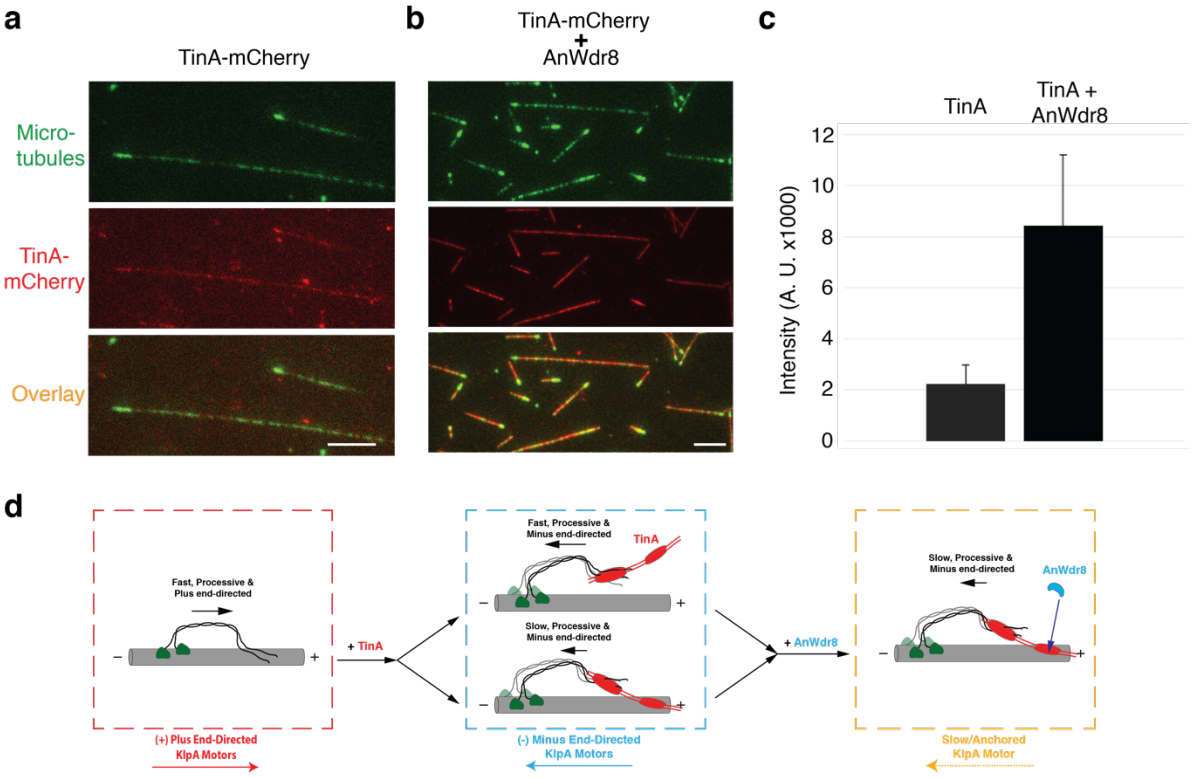

Figure 3.5: In the presence of AnWdr8, TinA has a much higher affinity for microtubules.

(a) Representative TIRF images of TinA-mCherry localization to microtubules with microtubule (Top) and TinA-mCherry (Middle) channels separated as well as overlaid on each other (Bottom). **(b)** Representative TIRF images of TinA-mCherry localization to microtubules in the presence of AnWdr8 with microtubule (Top) and TinA-mCherry (Middle) channels separated as well as overlaid on each other (Bottom). **(c)** Quantification of TinA-mCherry localization to microtubules alone, 2.1± .8 A.U. (mean±s.d., n=51) and in the presence of AnWdr8, 8.3± 3.5 A.U. (mean±s.d., n=56). **(d)** Schematic model of KlpA context-dependent directionality. KlpA is activated for minus end-directed motility in the presence of TinA-mCherry and becomes anchored when in complex with both TinA-mCherry and AnWdr8. Scale bars, 5 µm.

Discussion

We have revealed that the kinesin-14-containing spindle microtubule anchoring complex in *S. pombe* is potentially conserved in *A. nidulans*. We find that these conserved mitotic proteins TinA and AnWdr8 can interact with the kinesin-14 KlpA *in vitro* to cause it to switch direction on microtubules and form a ternary complex that is anchored on microtubules. We found that TinA regulates the velocity of this minus end-directed KlpA/TinA complex via its microtube binding activity (Figure 2) that is enhanced in the presence of AnWdr8 to anchor KlpA/TinA/AnWdr8 on microtubules (Figure 4, 5). Additionally, we revealed that this interaction with KlpA required its intrinsically disordered N-terminal tail which has can act autonomously as a directional switch (Figure 3, Supplementary Figure 5, 7) To our knowledge, this is the first example of an interacting or potential cargo protein (TinA) causing a directional switch of a kinesin motor protein. Additionally, to our knowledge this is the first example of ternary complex formation that locks a kinesin motor protein in a "rigor" type-like state on microtubules. These findings markedly expand our knowledge of kinesin-14 regulation and mechanisms for directional switching in context-dependent directional kinesin motors. Importantly, these findings provide the framework to propose a potential mechanism for kinesin-14-based anchoring of spindle microtubules at spindle poles (MTOCs) that may be conserved in higher eukaryotes[98,142-144].

Kinesin-14s play critical roles in mitotic cell division as they are proposed to counteract the activity of kinesin-5s at the spindle midzone[223] as well as anchor spindle microtubules at the MTOCs[72,125,126]. While there has been some evidence of microtubule plus-end tracking in human kinesin-14[59,66,67], the mechanisms responsible for kinesin-14

localization within the mitotic spindle remain largely uncharacterized, due in part because of their diffusive motility on microtubules[71,103,147,148]. However, recent findings from us and others have revealed several processive kinesin-14s[146], allowing us to expand the diversity of this kinesin subfamily. Using one such processive kinesin-14, KlpA, as a model, we then studied its motility behavior *in vitro* and by using a conserved mitotic protein pair, we were able to reveal a complex regulation scheme of KlpA. These findings have significant implications as the equivalent complex was shown to be required for anchoring of spindle microtubules at spindle poles in *S. pombe*, and all three proteins are conserved in humans[98,142-144]. Moreover, disruption of this anchoring complex in *S. pombe* yielded spindle microtubule minus ends that did not anchor and protruded beyond spindle pole bodies[98], mimicking the phenotype of kinesin-14 knockouts in several cell types[98,149-152]. Importantly, failure of spindle microtubules to anchor leads to chromosome cutting and resulting cellular aneuploidy[20,122,153,154,222], a hallmark of disease[66] and present in almost all cancerous cells[146].

Despite this critical function of kinesin-14-dependent spindle microtubule anchoring, a mechanism for anchoring at spindle pole bodies has yet to be proposed. Our findings reveal potential KlpA function and regulation within the mitotic spindle and enable the proposal of such an anchoring mechanism. Within the mitotic spindle, KlpA can act as a plus end-directed motor individually to autonomously localize to the spindle midzone where it can switch to a minus end-directed motor to slide apart antiparallel microtubules and oppose the activity of the kinesin-5 BimC to maintain spindle bipolarity[146] (Supplementary Figure 3.8a, blue box). To localize to microtubule minus ends at spindle poles, KlpA can potentially interact with TinA to become activated for minus

end-directed motility (Supplementary Figure 3.8a, blue arrows). Once this KlpA/TinA complex reaches the spindle poles, it can then associate with AnWdr8 to become anchored on microtubules (Supplementary Figure 3.8a, red boxes). Because the TinA homolog Msd1 has been shown to directly interact with γ-TuRC and this interaction was required for anchoring of spindle microtubules to SPBs through the γ-TuRC[224,225], we propose TinA maintains a similar functional role. In this case, the simple model of Msd1(TinA)-γ-TuRC mediated spindle microtubule anchoring[147] is expanded to include contributions from AnWdr8 and KlpA. We propose that at the SPBs, AnWdr8 locks TinA in a high affinity state for γ-tubulin, due to its structural similarities to α and β tubulin in microtubules[148]. Because AnWdr8 and TinA are in complex with KlpA, KlpA remains bound to spindle microtubules – providing a secondary physical linkage between the γ-TuRC (which is directly bound to SPBs) and spindle microtubules that strengthens this association – which anchors these spindle microtubules to the SPBs through the γ-TuRC (Supplemental Figure 8b). There is evidence to support this model *in vivo*: as TinA has been show to interact directly with AnWdr8[202] and be involved in regulation of microtubule nucleation via interaction with NIMA kinase[146]. KlpA was shown to have an overlapping role with γ-tubulin in establishment of spindle bipolarity[98,142-144].

This model is the first to propose a potential mechanism for Kinesin-14s role in spindle microtubule anchoring at MTOCs. This model can also potentially account for spindle microtubules that protrude past spindle pole bodies in kinesin-14 knockouts[226,218]: whereby removal of kinesin-14 from the anchoring complex weakens the attachment of the spindle microtubule minus end to the γ-TuRC, so that pushing forces generated at the midzone during chromosome segregation can cause it to uncouple from the γ-TuRC and

protrude past spindle poles (Supplementary Figure 3.9). Because all three components of this proposed model represent highly conserved proteins with conserved functions, future studies are planned to explore if this mechanism is potentially conserved in higher eukaryotes.

Methods

Molecular cloning of recombinant KlpA constructs

The full-length cDNA of KlpA, Ncd, TinA and AnWDR8 were codon-optimized and synthesized for enhanced protein expression in bacteria. All recombinant KlpA, Ncd, TinA and AnWDR8 constructs were integrated in a modified pET-17b vector (Novagen) using either isothermal assembly or the Q5 site-directed mutagenesis kit (NEB) and verified by DNA sequencing. All KlpA, Ncd, TinA and AnWDR8 constructs contained an N-terminal 6 × His-tag for protein purification.

Protein expression and purification

All protein constructs were expressed in BL21(DE3) Rosetta cells (Novagen). Cells were grown at 37 °C in tryptone phosphate medium (TPM) supplemented with 50 μg ml−1 Ampicillin and 30 μg ml−1 chloramphenicol until OD600=0.8. Expression was induced with 0.1 mM isopropyl-β-D-thiogalactoside for 12–14 h at 20 °C. Cells were harvested by centrifugation, flash-frozen in liquid nitrogen and stored at −80 °C.

For protein purification, cell pellets were resuspended in 50 mM sodium phosphate (NaPi) buffer (pH 8.0) containing 250 mM NaCl, 1 mM MgCl2, 0.5 mM ATP, 10 mM β-mercaptoethanol, 5% glycerol and 20 mM imidazole in the presence of a protease inhibitor cocktail and then lysed via sonication. After centrifugation, soluble protein in the

supernatant was purified by Talon resin (Clontech) and eluted into 50 mM NaPi buffer (pH 7.2) containing 250 mM NaCl, 1 mM MgCl2, 0.5 mM ATP, 10 mM β-mercaptoethanol, 5% glycerol and 250 mM imidazole. Protein was then flash-frozen in liquid nitrogen and stored at −80 °C.

Preparation of polarity-marked microtubules

All taxol-stabilized polarity-marked microtubules (tetramethylrhodamine (TMR), Alexa 488, and HiLyte 647) with bright plus ends were prepared as previously described 218. To make the polarity-marked microtubules, a dim tubulin mix (containing 17 μM unlabelled tubulin and 0.8 μM fluorescently labelled tubulin) was first incubated in BRB80 (80 mM PIPES, pH 6.8, 1 mM EGTA and 1 mM MgCl2) with 0.5 mM guanosine-5′-[(α,β)-methyleno]triphosphate (GMPCPP) (Jena Bioscience) at 37 °C for 2 h to make dim microtubules, and then centrifuged at 250,000 g for 7 min at 37 °C in a TLA100 rotor (Beckman). The pellet was resuspended in a bright tubulin mix (containing 7.5 μM unlabelled tubulin, 4 μM fluorescently labelled tubulin and 15 μM N-ethylmaleimide-tubulin) in BRB80 with 0.2 mM GMPCPP and incubated at 37 °C for additional 15 min to cap the plus ends. The resulting polarity-marked microtubules were pelleted at 20,000 g for 7 min at 37 °C in the TLA100 rotor and finally resuspended in BRB80 with 40 μM taxol. For making track microtubules used in single-molecule assays and microtubule-sliding assays, the dim tubulin mix also included additional 17 μM biotinylated tubulin.

Microtubule co-sedimentation assays

Microtubule co-sedimentation assays were performed as previously described[218]. Briefly, taxol-stabilized microtubules were polymerized from unlabeled tubulin (200 μM)

using the aforementioned protocol. Purified TinA-mCherry constructs were each mixed with microtubules in a BRB50 buffer supplemented with 40 μM taxol and 25 mM KCl, incubated at room temperature for 30 min, and centrifuged at 100,000 × g using a TLA100 rotor (Beckman Coulter) for 20 min at 37 °C. Coomassie-stained SDS-PAGE gels were analyzed to compare the protein amount in the supernatant and pellet fractions.

TIRF microscopy

All time-lapse imaging experiments were performed at room temperature using the Axio Observer Z1 objective-type TIRF microscope (Zeiss) equipped with a × 100 1.46 numerical aperture oil-immersion objective and a back-thinned electron multiplier charge-coupled device camera (Photometrics). Except for the microtubule-gliding experiments, which used regular coverslips, all other experiments used microscope coverslips that were functionalized with biotinylated polyethylene glycol (biotin-PEG) as previously described[227] to reduce nonspecific surface absorption of molecules. All time-lapse imaging experiments in this study used flow chambers that were made by attaching a coverslip to a microscope glass slide by double-sided tape.

Single-molecule photobleaching assays

For the single-molecule photobleaching assays, mCherry-tagged TinA molecules were diluted and bound to surface-immobilized HyLite 647 microtubules in a BRB50-based buffer supplemented with 25 mM KCl, 20 μM taxol and 1.3 mg ml−1 casein. Time-lapse images were continuously recorded with 200-ms exposure until the field of view was bleached. The number of photobleaching steps of individual TinA molecules was obtained by tracking the fluorescence intensity in ImageJ (NIH).

Microtubule-gliding assays

For microtubule-gliding assays, GFP-KlpA-Δtail (diluted in BRB50 supplemented with 20 μM taxol and 1.3 mg ml−1 casein) was immobilized on the coverslip via the monoclonal Anti-His antibody (Fisher Scientific). Unbound GFP-KlpA-Δtail molecules were removed with BRB50 supplemented with 20 μM taxol and 1.3 mg ml−1 casein. Polarity-marked polarity-marked HyLite 647 microtubules diluted in the same buffer were then added to the chamber and incubated for 2 min. Unbound microtubules were removed by extensive wash with BRB50 supplemented with 20 μM taxol and 1.3 mg ml−1 casein. Finally, the chamber was perfused with a BRB50-based motility buffer supplemented with 100 mM KCl, 1 mM ATP, 25 μM taxol, 1.3 mg ml−1 casein and an oxygen scavenger system[228]. Time-lapse images were taken at 1 frame per second for 5 min.

In vitro motility assays

For all in vitro motility experiments, the motility chamber was perfused with 0.5 mg ml−1 streptavidin for immobilizing polarity-marked HyLite 647 microtubules. GFP-tagged KlpA molecules (GFP-KlpA and GFP-KlpA-Δtail) or GFP-Ncd molecules were then mixed with mCherry-tagged TinA constructs and/or AnWDR8 and diluted in motility buffer (BRB50 supplemented with 25 mM KCl, 1 mM ATP, 25 μM taxol, 1.3 mg ml−1 casein and an oxygen scavenger system220) and added to the chamber. Time-lapse images were acquired at 1 frame per second. The setting was 200-ms exposure and 5-min duration for single-molecule experiments to determine the velocity of GFP-KlpA-Δtail and of colocalized GFP-KlpA and TinA-mCherry particles in the absence and presence of AnWDR8. Kymographs were generated and analyzed in ImageJ

(NIH) for determining directionality, run-length (for GFP-KlpA-Δtail) and velocity information of GFP-KlpA-Δtail and colocalized GFP-tagged kinesin motors. Velocity and run-length were determined by fitting the histograms to a Gaussian distribution and an exponential distribution, respectively, in MATLAB (MathWorks)

Other microtubule-based assays

To confirm the microtubule-binding ability of TinA-mCherry in the presence and absence of AnWDR8, HyLite 647 microtubules were immobilized on the surface of coverslip, and purified TinA-mCherry (or purified TinA-mCherry mixed with AnWDR8) was diluted in BRB50 supplemented with 25 mM KCl, 25 μM taxol and 1.3 mg ml−1 casein was added in the flow chamber. Unbound TinA-mCherry was washed away with BRB50 supplemented with 25 mM KCl, 25 μM taxol and 1.3 mg ml−1 casein after 2-min incubation, and TIRF microscopy images were taken for both HyLite 647 and mCherry channels. Intensity of TinA-mCherry alone and in the presence of AnWDR8 was analyzed analyzed in ImageJ (NIH).

NMR Spectroscopy

NMR samples of purified KlpA-tail were prepared as described previously[228] in shape tubes. Samples were approximately 200 μM in NMR buffer (10% D_2O, 20 mM MES, pH 6.5, 100 mM NaCl) supplemented with a protease inhibitor mixture (Roche Applied Science), and 2,2-dimethylsilapentene-5-sulfonic acid for ^{1}H chemical shifts referencing. NMR data were acquired on a Bruker Avance 800 spectrometer equipped with a cryoprobe. Two-dimensional ^{1}H-^{15}N HSQC experiments using echo-antiecho phase discrimination of 200 increments and 1024 points were collected at 298 K. Indole hydrogen–deuterium

exchange rates were measured for the KlpA-tail using CLEANEX-PM experiments recorded at 800 MHz at a temperature of 298 K[228]. Mixing periods of 0 and 40 ms were used with an interscan delay of 2 s. The collected data were fitted to the previously described equation and compared relatively[15,214,229-232]. NMR spectra were processed and analyzed with TopSpin (Bruker).

Acknowledgments

We thank the Qiu lab members for critical reading of this manuscript. This work was supported in part by the National Science Foundation (MCB-1616462 to W.Q.).

Supplementary Materials

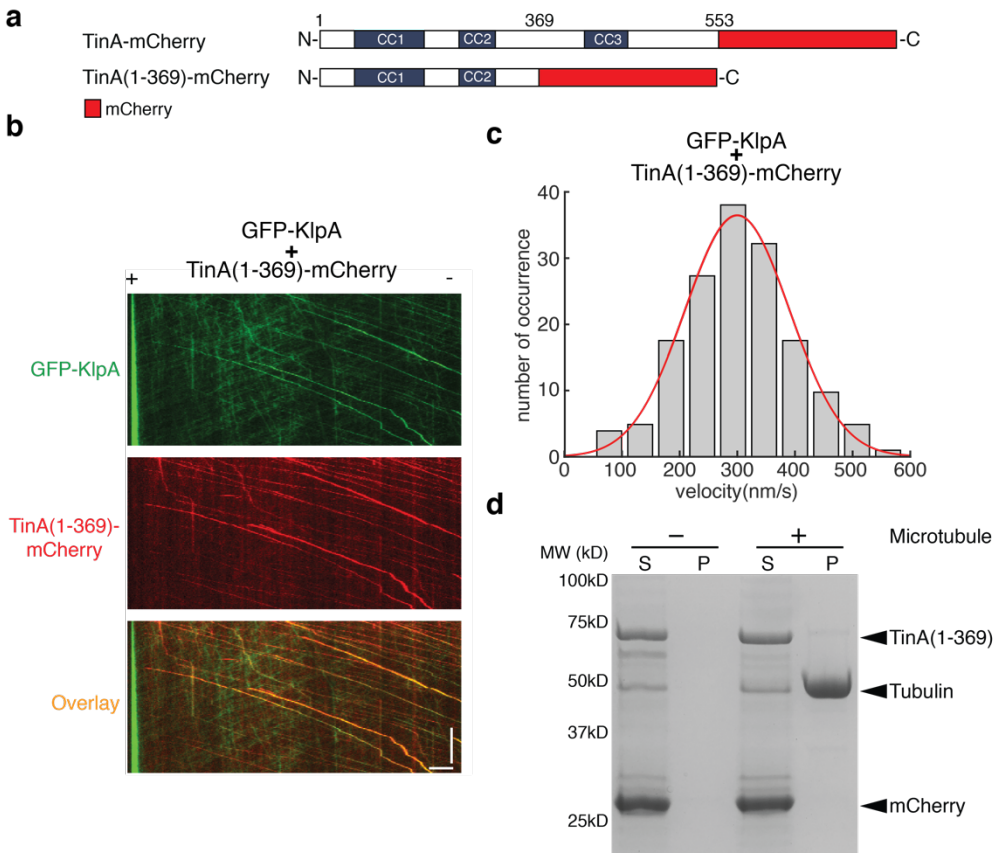

Figure 3.S1: Velocity of KlpA and TinA colocalized particles is regulated by the microtubule binding activity of TinA.

(a) Schematic diagram of full-length TinA-mCherry and TinA(1-369)-mCherry constructs. **(b)** Representative kymographs of GFP-KlpA and TinA(1-369)-mCherry movement on individual microtubules in single-molecule motility assays with GFP-KlpA (Top) and TinA-mCherry (Middle) channels separated as well as overlaid on each other (Bottom). **(c)** Velocity histogram of colocalized GFP-KlpA and TinA(1-369)-mCherry molecules on single microtubules with a mean velocity of 286±86 nm s^{-1} (mean±s.d., n=161). Red line indicates a Gaussian fit to the velocity histogram. **(d)** Microtubule co-sedimentation assay of TinA(1-369)-mCherry. Scale bars, 1 min (vertical) and 5 µm (horizontal).

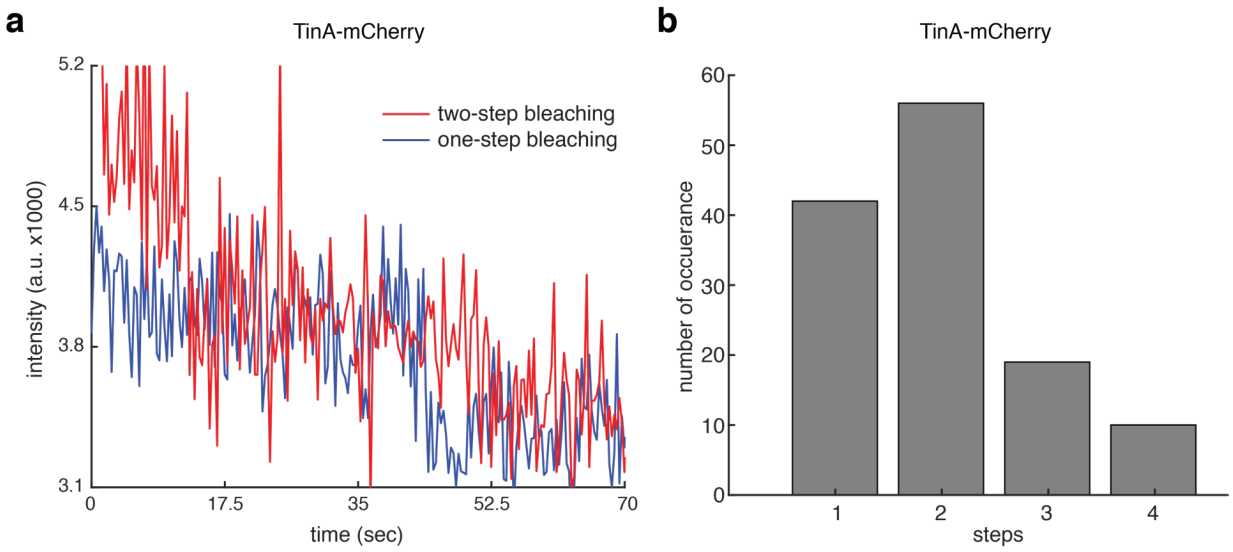

Figure 3.S2: TinA-mCherry exhibits photobleaching behavior typical of a dimer.

(a) Representative photobleaching traces of TinA-mCherry on surface-immobilized microtubules. **(b)** Photobleaching histogram of TinA-mCherry (n = 127).

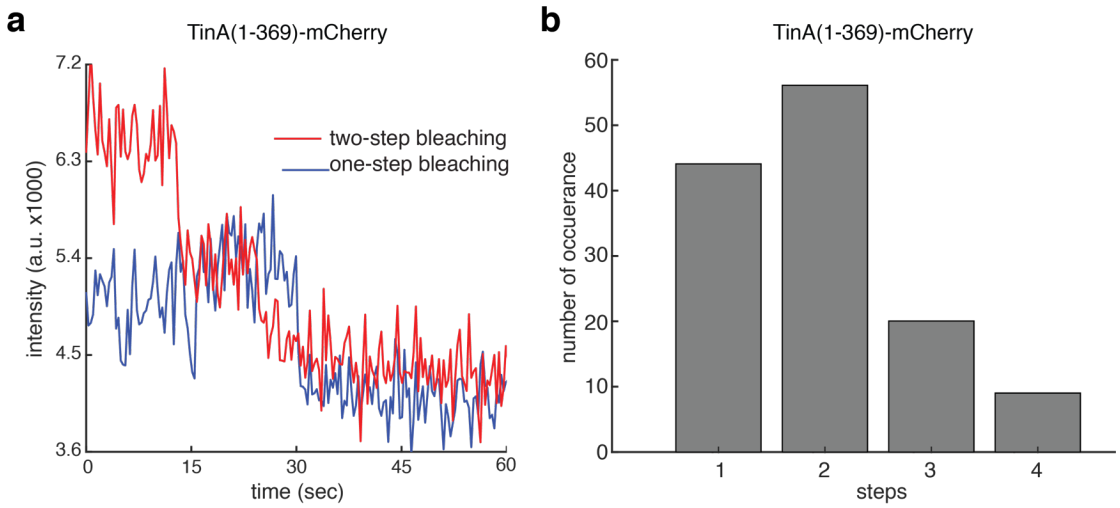

Figure 3.S3: TinA(1-369)-mCherry exhibits photobleaching behavior typical of a dimer.

(a) Representative photobleaching traces of TinA(1-369)-mCherry on surface-immobilized microtubules. **(b)** Photobleaching histogram of TinA(1-369)-mCherry (n = 129).

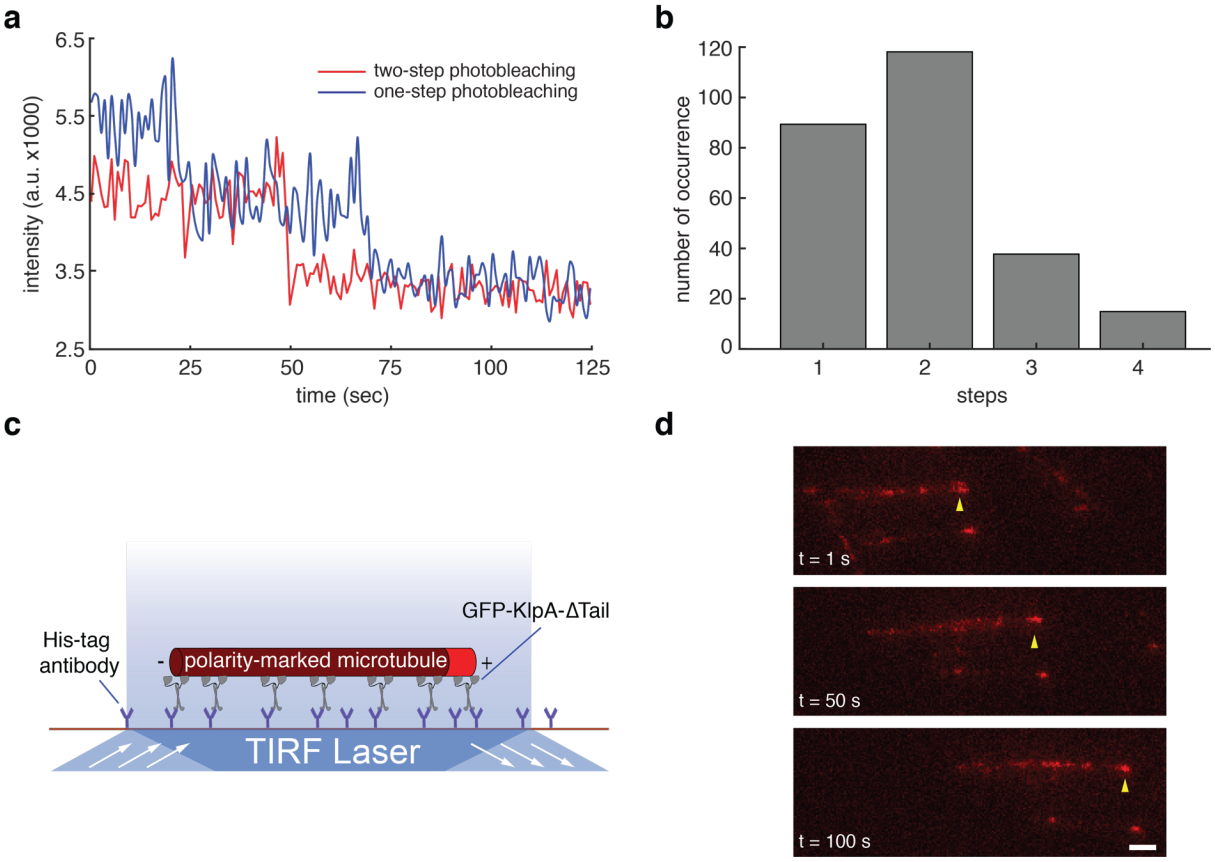

Figure 3.S4: GFP-KlpA-Δtail exhibits photobleaching behavior typical of a dimer and glides microtubules with minus end-directionality.

(a) Representative photobleaching traces of GFP-KlpA-Δtail on surface-immobilized microtubules. **(b)** Photobleaching histogram of GFP-KlpA-Δtail (n = 262). **(c)** Schematic of microtubule gliding assays. **(d)** Representative TIRF microscopy images of GFP-KlpA-Δtail driving polarity-marked microtubules (red) to glide with the bright plus ends leading (yellow arrowheads). Scale bar, 5 µm.

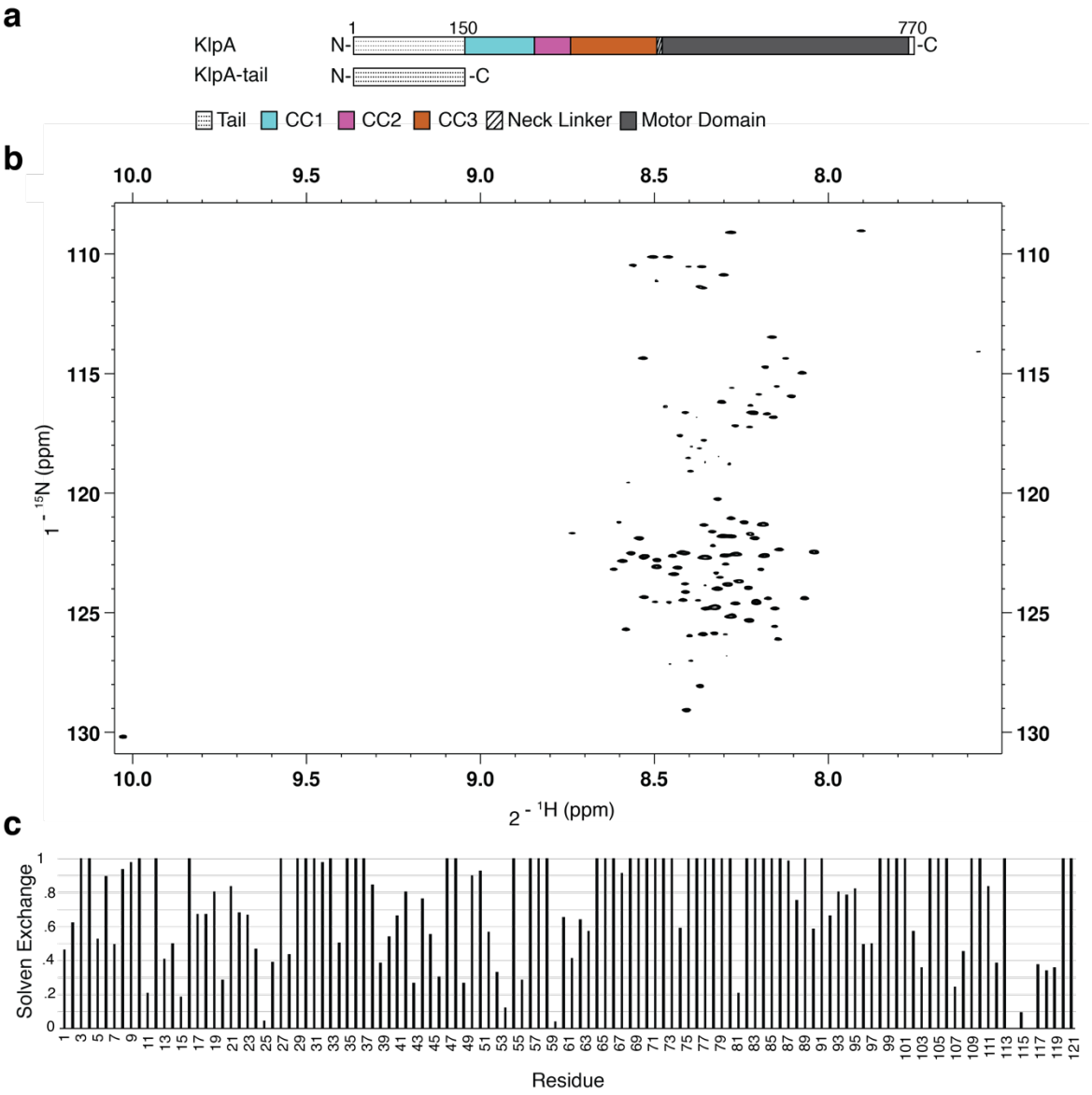

Figure 3.S5: The N-terminal tail of KlpA is an intrinsically disordered protein.

(a) Schematic diagram of full-length KlpA and KlpA-tail constructs. **(b)** 2D TROSY HSQC spectra of KlpA-tail. **(c)** CLEANEX-based experiments to measure solvent exchange of KlpA-tail.

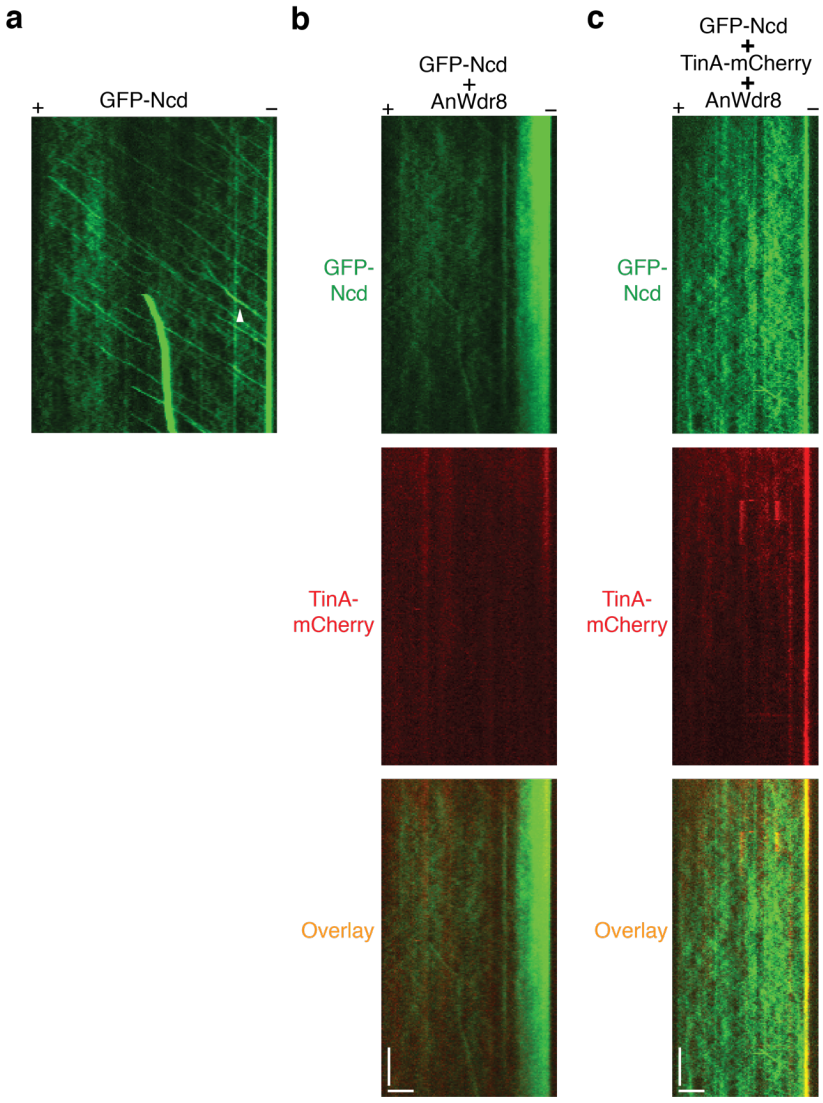

Figure 3.S6: Ncd does not colocalize with TinA-mCherry alone or in the presence of AnWdr8.

(a) Representative kymograph of diffusive GFP-Ncd movement on individual microtubules under single-molecule motility assays. Higher order aggregates were observed to move processively towards microtubule minus ends (white arrow). **(b)** Representative kymographs of GFP-Ncd and TinA-mCherry movement on individual microtubules in single-molecule motility assays with GFP-KlpA (Top) and TinA-mCherry (Middle) channels separated as well as overlaid on each other (Bottom). **(c)** Representative kymographs of GFP-Ncd and TinA-mCherry movement in the presence of AnWdr8 on individual microtubules in single-molecule motility assays with GFP-KlpA (Top) and TinA-mCherry (Middle) channels separated as well as overlaid on each other (Bottom). Scale bars, 1 min (vertical) and 5 µm (horizontal).

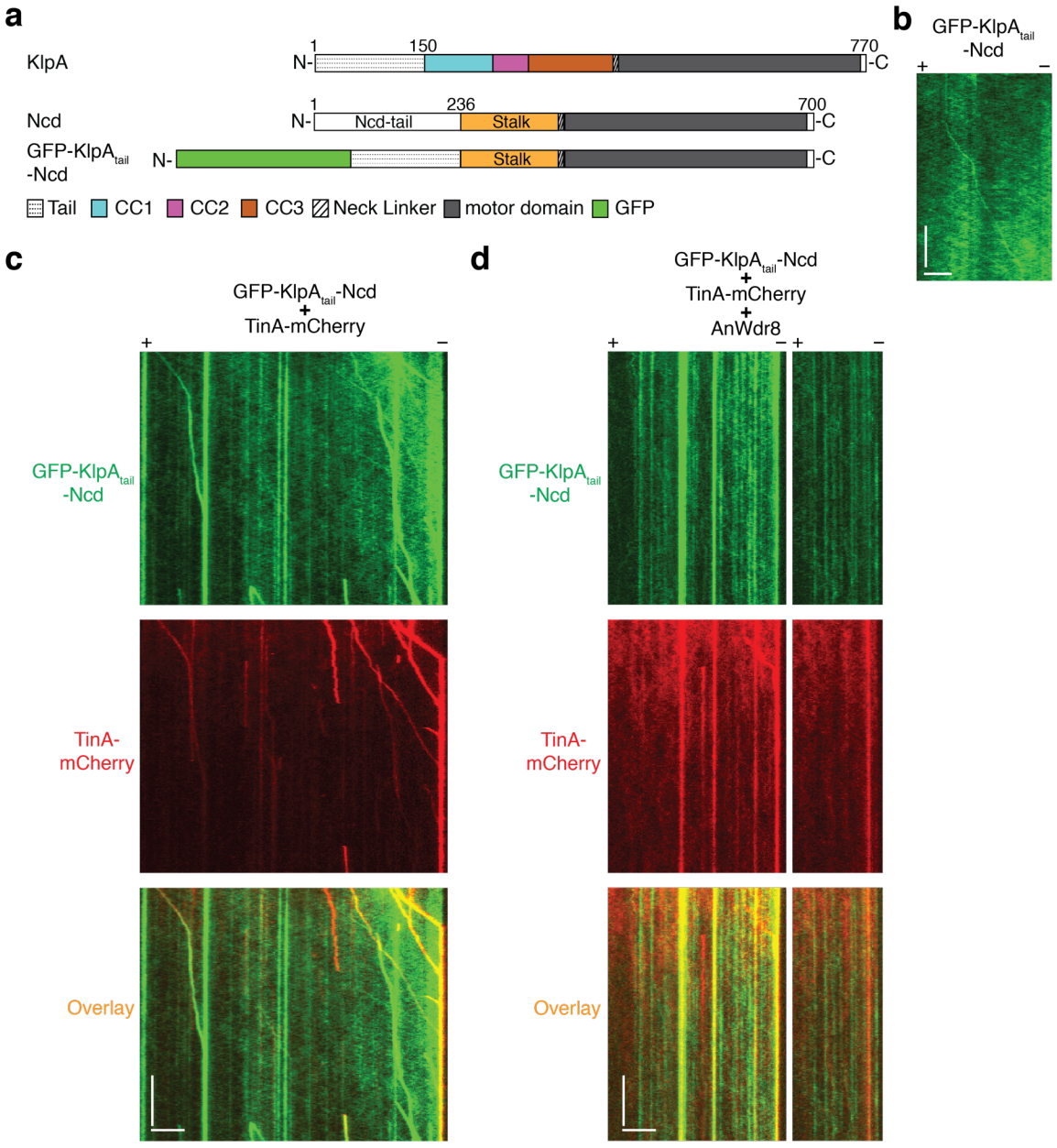

Figure 3.S7: KlpA tail domain enables Ncd to colocalize with TinA-mCherry and TinA-mCherry in the presence of AnWdr8 on microtubules.

Figure 3.S7: KlpA tail domain enables Ncd to colocalize with TinA-mCherry and TinA-mCherry in the presence of AnWdr8 on microtubules.

(a) Schematic diagram of full-length KlpA, Ncd and GFP-$KlpA_{tail}$-Ncd chimera constructs. **(b)** Representative kymograph of diffusive GFP-$KlpA_{tail}$-Ncd movement on individual microtubules under single-molecule motility assays. **(c)** Representative kymographs of GFP-$KlpA_{tail}$-Ncd and TinA-mCherry movement on individual microtubules in single-molecule motility assays with GFP-KlpA (Top) and TinA-mCherry (Middle) channels separated as well as overlaid on each other (Bottom). **(d)** Representative kymographs of GFP-$KlpA_{tail}$-Ncd and TinA-mCherry movement in the presence of AnWdr8 on individual microtubules in single-molecule motility assays with GFP-$KlpA_{tail}$-Ncd (Top) and TinA-mCherry (Middle) channels separated as well as overlaid on each other (Bottom). Scale bars, 1 min (vertical) and 5 μm (horizontal).

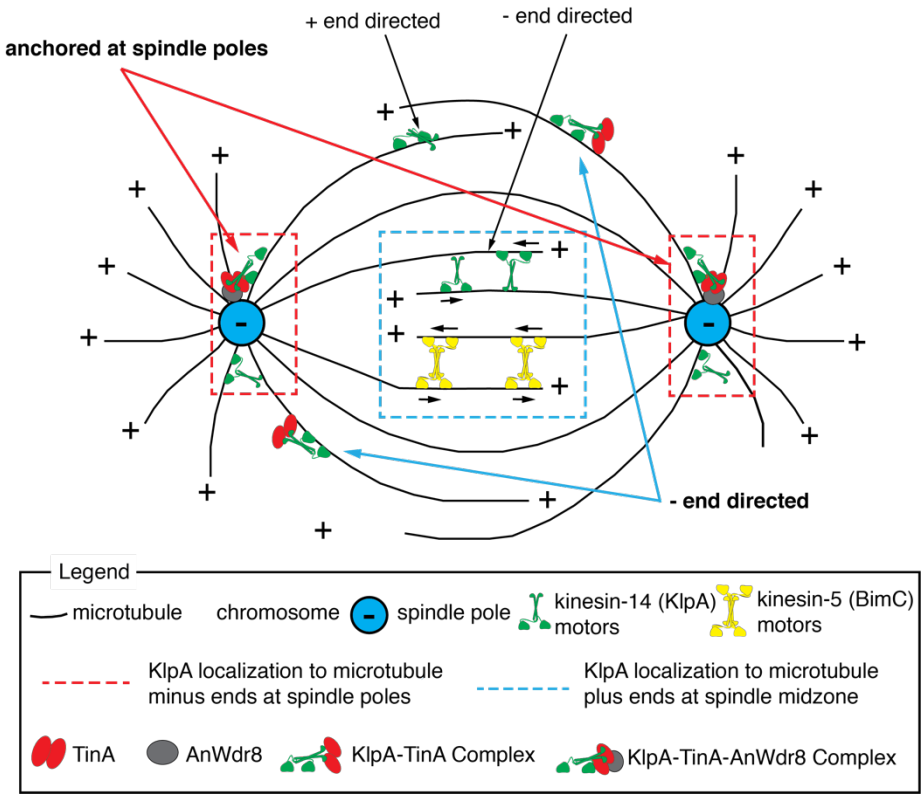

Figure 3.S8: Model for KlpA function within the mitotic spindle of *A. nidulans*.

Schematic diagram highlighting the localization, directionality and functions of KlpA as well as interaction with the mitotic proteins TinA and AnWdr8.

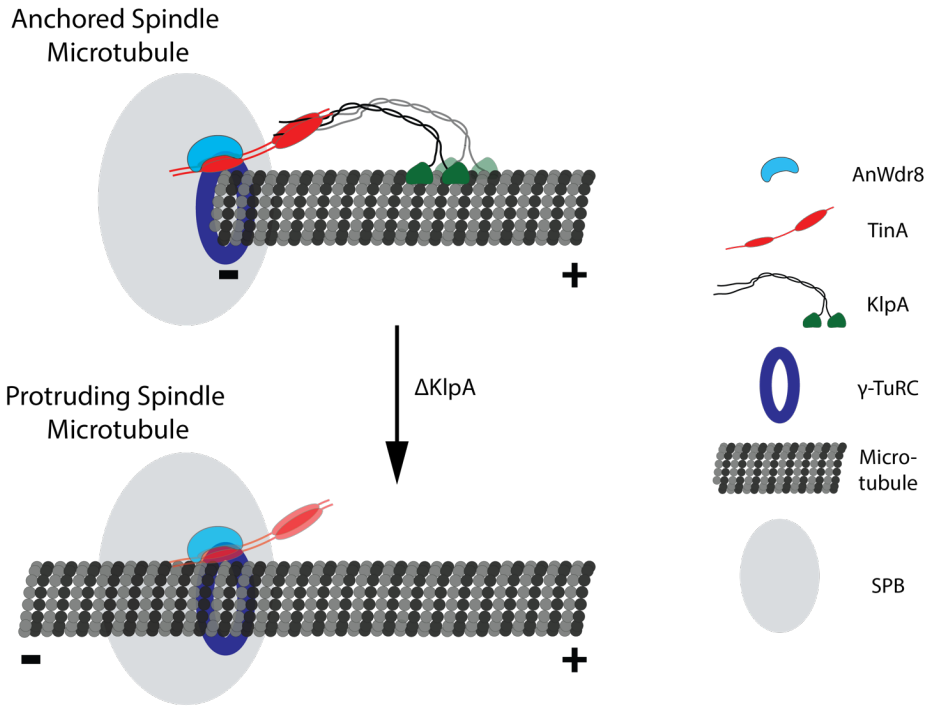

Figure 3.S9: Model for mechanism of Kinesin-14-dependent anchoring of spindle microtubules in *A. nidulans.*

Schematic diagram of KlpA in complex with TinA and AnWdr8 to anchor spindle microtubules at spindle poles. In the absence of KlpA, spindle microtubules become unattached and protrude past the SPB.

Chapter 4

Engineering heterodimeric kinesins through genetic incorporation of noncanonical amino acids

Andrew R. Popchock, Subhashis Jana, Ryan A. Mehl, and Weihong Qiu

Accepted for publication in *ACS Chemical Biology,* (2018)

Abstract

Kinesins are commonly homodimers with two identical heavy chains (protomers) and play indispensable roles in many intracellular processes. Engineered heterodimeric kinesins with two distinct protomers are important tools for dissecting coordination and regulation of naturally-occurring kinesin homodimers. Here, we report a chemical biology-based approach that generates kinesin heterodimers by combining genetic incorporation of reactive noncanonical amino acids and small molecule-based crosslinking. We verified using yeast kinesin-8/Kip3 as a model system that our method yields kinesin heterodimers of desired properties without introducing unintended motility disruption. To demonstrate the utility of our method, we engineered a crippled Kip3 heterodimer that contains both a wildtype-like protomer and a catalytically inactive one; and our results revealed that the resulting heterodimer moves on the microtubule with significant reduction in velocity but not processivity. Due to its versatility, we expect that our method can be broadly adopted to create novel heterodimers for other kinesins and will thus greatly expand the studies on kinesin mechanisms.

Introduction

Kinesins are microtubule-based motor proteins that transform chemical energy into mechanical work for a wide range of essential intracellular processes, such as organelle transport, organization of the microtubule cytoskeleton, regulation of micro-tubule dynamics, and chromosome segregation[36,37]. Kinesin motors are typically homodimers composed of two identical heavy chains (protomers), each of which contains a conserved motor domain that not only hydrolyzes ATP but also interacts with the

microtubule[11,35,43,50,52,233-238]. Homodimeric kinesins commonly need to coordinate their two motors domains in order to function with high efficacy. For example, single-molecule studies revealed that to achieve processive motility on single microtubules as an individual homodimer, kinesin-1 uses a coordinated "hand-over-hand" mechanism to alternately advance its two motor domains with 16-nm steps[43,49,51,53-55]. Further studies showed that the mechanical process of kinesin-1 motor domain binding to and release from micro-tubules is tightly coupled to the biochemical events of ATP hydrolysis on individual motor domains[239]. Despite these detailed findings, the contribution to kinesin coordination by different structural elements, such as neck-linker length and composition, remain an ongoing question[237]. Furthermore, effects of post-translational modifications on kinesin coordination, which often occur within their motor do-mains[68,236,237,240,241], are largely unknown. Further study is needed to determine these coordination mechanisms and whether they are universal among kinesins or adapted to distinct family members.

Engineered kinesin heterodimers that contain two distinct protomers are important reagents for dissecting the mechanism and regulation of naturally-occurring kinesin homodimers. For example, an engineered heterodimeric kinesin-1 construct enabled researchers to obtain direct evidence for the hand-over-hand stepping model[68,236,237]. Currently, only two published methods are available for generating heterodimeric kinesins[241], and neither is without limitations. The first method requires coexpression of two different kinesin protomers followed by enrichment of the desired heterodimer product via tandem affinity purification[235,241]. However, complete removal of kinesin homodimers can be difficult to achieve, which can lead to contamination that complicates further studies. In the second method, two kinesin protomers are differentially labeled with two

complementary single stranded DNA (ssDNA) oligos and then coupled to form a heterodimer via the hybridization between these two ssDNA oligos[235]. The latter method has a rather stringent requirement that multiple endogenous cysteines must be simultaneously mutated to generate cysteine-light protomers that contain a single cysteine for site-specifically attaching a ssDNA oligo[235]. However, recent work from the Block group showed that cysteine-light kinesin-1 mutants do not produce the motility of the wildtype kinesin-1 under load[242,243], implying that complete elimination of native cysteine residues likely compromises kinesin motility and the resulting DNA-based kinesin heterodimers may not be suitable for many mechanistic studies[213].

To enable studies on the kinesin coordination mechanisms and the influence of neck compositions on function, a method to engineer kinesin heterodimers would benefit from four attributes: (1) no contamination from residual homodimers that complicate functional analysis, (2) no reliance on cysteine ligation chemistries since altering native cysteines can compromise motility, (3) use of a crosslinker between protomers that does not compromise motor function, and (4) site-specific attachment of functionality on protomers using mild biorthogonal chemistry as to not compromise motor function.

To develop a suitable heterodimerization method, we used a model Kip3 system that could be manipulated to verify that it contained all four de-sired attributes. Kip3 is a kinesin-8 protein that regulates microtubule dynamics in budding yeast[244,245]. Like other homodimeric kinesins, a monomeric Kip3 protomer generated by removal of its coil-coil domain can be artificially dimerized via addition of a leu-cine zipper domain. This leucine zipper dimerized Kip3 results in a fully functional homodimer with a defined velocity and run-length that can be easily compared to engineered heterodimers[213].

Using this monomeric Kip3 protomer, cysteine ligation sites were replaced by a non-canonical amino acid (ncAA), p-azido-phenylalanine (AzF) using genetic code expansion methods[246]. To replace the leucine zipper dimerization motif, azide-reactive DNA oligonucleotides were explored as a linker. To our surprise, total internal reflection fluorescence (TIRF) microscopy analyses reveal this DNA-based homodimer exhibits significantly impeded motility when compared to the leucine zipper-based Kip3[240]. In order to restore native-like function, it was necessary to remove the DNA linker. Simple polyethylene glycol (PEG) linkers did not compromise Kip3 function. In order to generate engineered Kip3 heterodimers using a PEG-based heterolinker, it was necessary to generate two orthogonal Kip3 protomers – one containing the ncAA tetrazine derivative (Tet-v2.0) [68] and the other containing AzF. Using the Kip3 model, we verified that these non-canonical amino acids (ncAAs), the linker and the biorthogonal labeling conditions do not compromise Kip3 function.

To demonstrate the function of our method for evaluating heterodimeric kinesins, a Kip3 hetero-dimer containing an inactivating (rigor) mutation in one of its motor domains was generated and evaluated. Previous work revealed that a kinesin-1 heterodimer containing a rigor-type mutation in one motor domain retained processive motility on single microtubules but moved at a significantly reduced velocity[213]. While this finding was unexpected, later studies revealed natural kinesin heterodimers that remained processive with one motor domain lacking catalytic activity[244]. We find that crosslinking a wildtype-like Kip3 protomer with a protomer containing a rigor-type mutation yields a processive Kip3 heterodimer that moves at approximately half the speed of the wildtype-

like Kip3 homodimer while retaining the ability to move long distances on single microtubules.

To our knowledge, this work is the first demonstration of creating kinesin dimers of desired properties using ncAA incorporation. In addition, it is the first demonstration of dimerizing two different proteins using tetrazine and azide derivative ncAAs.

Results and Discussion

DNA oligos interfere with kinesin motility.

We set out to improve the DNA-based heterodimer method by eliminating its reliance on cysteine-based chemistry. To that end, we chose Kip3 – a kinesin-8 motor from the yeast – as the model system. Previous work showed that Kip3 without its C-terminus (a.a. 481-805) forms a diffusive monomer (Kip3ΔT-GFP$^{\boldsymbol{M}}$), which can be artificially coupled via a leucine zipper (LZ) to form a homodimer (Kip3ΔT-LZ-GFP$^{\boldsymbol{D}}$) that exhibits wildtype-like motility on single microtubules (Figure 1a)[244,245]. We reasoned that a Kip3ΔT-LZ-GFP$^{\boldsymbol{D}}$ equivalent could be obtained without invoking cysteine mutations by: (*1*) generating a dimerization-deficient Kip3 promoter that replaces LZ with a genetically incorporated ncAA azido-phenylalanine (AzF) to produce a reactive Kip3ΔT-AzF-GFP$^{\boldsymbol{M}}$ protomer[247]; (*2*) reacting Kip3ΔT-AzF-GFP$^{\boldsymbol{M}}$ protomers with two complementary dibenzocyclooctyne (DBCO)-tagged DNA oligos (5'-DBCO OligoA and 3'-DBCO OligoA*) to generate Kip3ΔT-OligoA-GFP$^{\boldsymbol{M}}$ and Kip3ΔT-OligoA*-GFP$^{\boldsymbol{M}}$; and (*3*) hybridizing these two DNA-tagged Kip3 protomers to form the Kip3ΔT-DNA-GFP$^{\boldsymbol{D}}$ dimer (Figure 1b).

To implement this approach, we modified the coding sequence of Kip3ΔT-GFP^{M} to insert an amber codon (TAG) for incorporating AzF to produce Kip3ΔT-AzF-GFP^{M} (Figure 1a)[247]. To verify AzF incorporation and reactivity, Kip3ΔT-AzF-GFP^{M} and Kip3ΔT-GFP^{M} were both incubated to react with DBCO-PEG4-tetramethylrhodamine (DBCO-PEG4-TAMRA). Only the AzF-containing Kip3ΔT-AzF-GFP^{M} was strongly labeled with the TAMRA dye (Supplementary Figure 4.1), which confirmed that AzF can be genetically incorporated into Kip3 and is readily accessible for reacting with DBCO derivatives[66]. We thus proceeded to react Kip3ΔT-AzF-GFP^{M} with two DBCO-tagged complementary DNA oligos separately (DBCO-OligoA and DBCO-OligoA*) to form Kip3ΔT-OligoA-GFP^{M} and Kip3ΔT-OligoA*-GFP^{M}, which were then mixed to form the DNA-based homodimer, Kip3ΔT-DNA-GFP^{D}. Formation of Kip3ΔT-DNA-GFP^{D} was found to be highly specific to DNA hybridization, as stable dimers were only observed in the presence of both Kip3ΔT-OligoA-GFP^{M} and Kip3ΔT-OligoA*-GFP^{M}, but not in the presence of competing DNA oligos (Figure 4.1c).

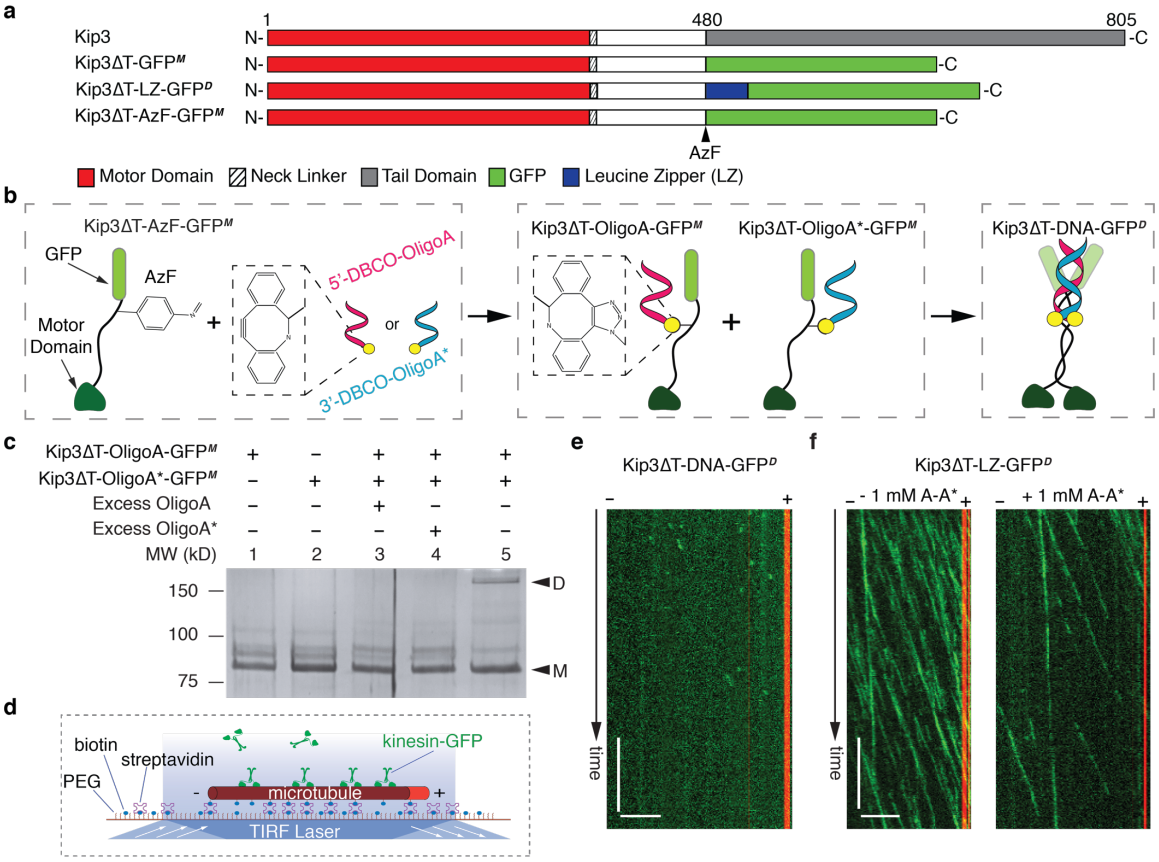

Figure 4.1: The DNA-based homodimer Kip3ΔT-DNA-GFP^{D} fails to exhibit wildtype motility on single microtubules.

(a) Schematic of full-length Kip3, monomeric Kip3ΔT-GFP^{M}, homodimeric Kip3ΔT-LZ-GFP^{D}, and monomeric Kip3ΔT-AzF-GFP^{M} with a genetically incorporated AzF. **(b)** Reaction scheme for making the DNA-based homodimer Kip3ΔT-DNA-GFP^{D}. 5'-DBCO Oligo A and 3'-DBCO Oligo-A* are two complementary DNA oligos (A and A*) that are both functionalized with DBCO (yellow circle). Boxes indicate the structure of DBCO (left) and the ligation product between AzF and DBCO within Kip3ΔT-DNA-GFP^{D} (Center) **(c)** Coomassie-stained SDS-PAGE gel showing that Kip3ΔT-OligoA-GFP^{M} and Kip3ΔT-OligoA*-GFP^{M} react to form Kip3ΔT-DNA-GFP^{D} only in the absence of excess competing DNA oligos (Oligo-A or Oligo-A*). Arrows indicate the expected bands of the monomer (M) and the dimer (D). **(d)** Schematic diagram of the *in vitro* single-molecule motility assay. Microtubules were fluorescently labeled with Hilyte 647, and polarity-marked with a dim minus end and a bright plus end. **(e)** Representative kymograph of Kip3ΔT- DNA-GFP^{D} molecules on a single microtubule. **(f)** Representative kymograph of Kip3ΔT-LZ-GFP^{D} in the presence and absence of 1mM A-A*. Scale bars: 2 min (vertical) and 5 μm (horizontal).

We next performed a single-molecule motility assay to visualize the movement of individual Kip3ΔT-DNA-GFP^{D} molecules on single microtubules (Figure 4.1d). Surprisingly, under the assay condition where the LZ-based homodimer Kip3ΔT-LZ-GFP^{D} clearly displayed processive plus-end-directed motility (Supplementary Figure 4.2), no Kip3ΔT-DNA-GFP^{D} molecules were observed to move processively on the microtubule (Figure 4.1e). Such lack of processive motility was unlikely due to spontaneous disassembly of Kip3ΔT-DNA-GFP^{D} into monomers in the motility experiments, as Kip3ΔT-DNA-GFP^{D} molecules existed predominantly as homodimers (Supplementary Figure 4.3) and displayed processive motility on single microtubules under reduced ionic strength conditions (Supplementary Figure 4.4). Because the duplex DNA (A-A*) in Kip3ΔT-DNA-GFP^{D} is highly negatively charged and in close proximity to the motor domain, we hypothesized that A-A* rendered the DNA-based homodimer nonprocessive by impeding its interaction with microtubules. To test this hypothesis, we analyzed the motility behavior of the processive Kip3ΔT-LZ-GFP^{D} in both the presence and absence of 1 mM A-A*. The results showed that the addition of free A-A* markedly reduced motility events of Kip3ΔT-LZ-GFP^{D} (Figure 4.1d). Such DNA-induced motility "inhibition" appeared to be generic, as the motility of several other processive kinesins was similarly compromised in the presence of either A-A* or other DNA oligos (data not shown). Thus, while stable kinesin dimers can be obtained via the hybridization of complementary DNA oligos, DNA-based kinesin motors may be unsuitable for certain mechanistic studies.

Kip3 dimerized via PEG-based chemical crosslinker exhibits normal microtubule-based motility.

DBCO-PEG4-DBCO is an inert homobifunctional crosslinker that reacts simultaneously with two different AzFs via the DBCO moiety[246]. To further assess the "inhibitory" effect of DNA oligos on kinesin motility, we reacted Kip3ΔT-AzF-GFP^{M} monomers with DBCO-PEG4-DBCO to form an artificial homodimer Kip3ΔT-AzF-GFP^{D} (Figure 4.2a). Formation of Kip3ΔT-AzF-GFP^{D} was confirmed and found to be highly specific to the conjugation between AzF and DBCO-PEG4-DBCO, as no dimer bands were observed for control reactions lacking either Kip3ΔT-AzF-GFP^{M} or DBCO-PEG4-DBCO or both (Figure 4.2b). Like the DNA-based homodimer Kip3ΔT-DNA-GFP^{D} (Supplementary Figure 4.3), Kip3ΔT-AzF-GFP^{M} also exhibited a photobleaching pattern typical of a homodimer (Supplementary Figure 4.5)[248,249]. Our single-molecule motility experiments revealed that unlike motility-deficient Kip3ΔT-DNA-GFP^{D} (Figure 4.1e), Kip3ΔT-AzF-GFP^{D} exhibited processive plus-end-directed motility (Figure 4.2c) with a velocity of 40 ± 9 nm s^{-1} (mean ± s.d., n=297, Figure 4.2d) and a run-length of 1.5 ± 0.1 μm (mean ± s.e.m., n=297, Figure 4.2d). Importantly, these motility parameters (velocity and run-length) of Kip3ΔT-AzF-GFP^{D} were nearly identical to those of the wildtype-like homodimer Kip3ΔT-LZ-GFP^{D} under the same assay conditions (Supplementary Figure 4.2). Thus, crosslinking two identical AzF-containing kinesin monomers via DBCO-PEG4-DBCO does not interfere with their microtubule-based motility. These results provide further evidence that the "inhibitory" effect observed for Kip3ΔT-DNA-GFP^{D} was due to the DNA-based linkage.

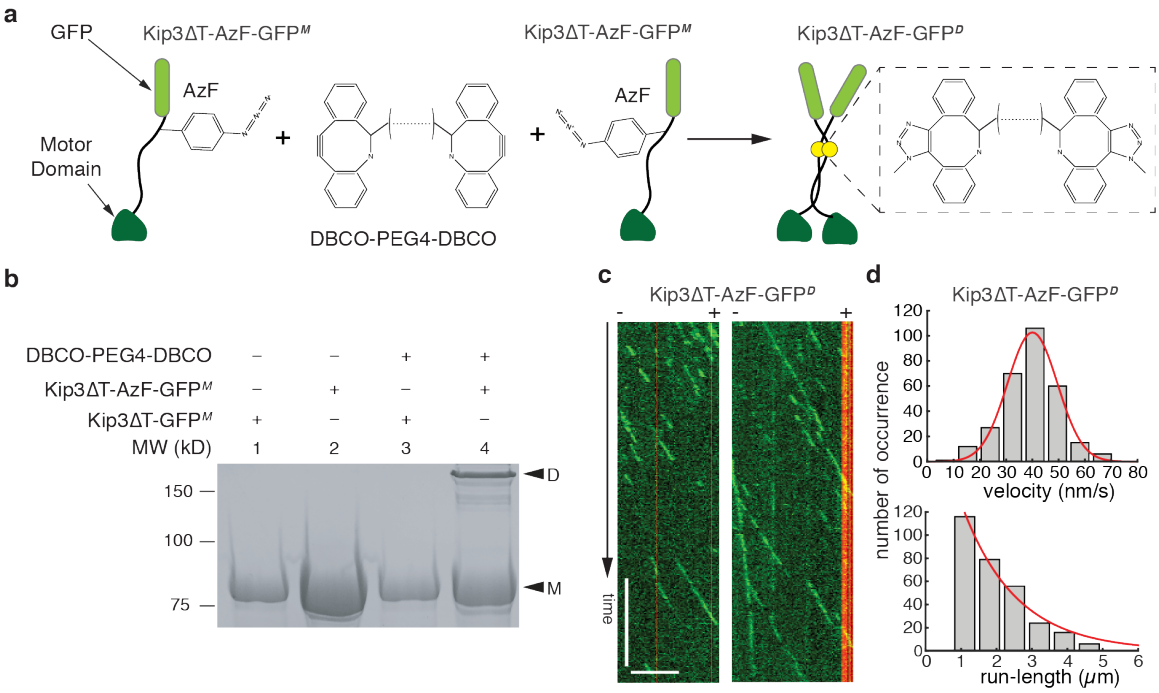

Figure 4.2: The ncAA-based homodimer Kip3ΔT-AzF-GFP^D exhibits wildtype-like motility on single microtubules.

(a) Reaction scheme for forming Kip3ΔT-AzF-GFP^D by crosslinking two AzF-containing Kip3ΔT-AzF-GFP^M via DBCO-PEG4-DBCO (yellow circles). Box shows the structure of the ligation product between AzF and DBCO-PEG4-DBCO within Kip3ΔT-AzF-GFP^D. **(b)** Coomassie-stained SDS-PAGE gel showing that dimerization only occurs in the presence of both Kip3ΔT-AzF-GFP^M and DBCO-PEG4-DBCO. Arrows indicate the expected bands of the monomer (M) and the dimer (D). **(c)** Representative kymographs of Kip3ΔT-AzF-GFP^D molecules on a single microtubule. **(d)** Velocity (Top) and run-length (Bottom) histograms of individual Kip3ΔT-AzF-GFP^D molecules on single microtubules. Red lines indicate a Gaussian fit to the velocity histogram and a single exponential fit to the run-length histogram. Scale bars: 2 minutes (vertical) and 5 μm (horizontal).

Kip3 dimerized via hetero-orthogonal-PEG crosslinker exhibits normal microtubule-based motility.

With a small-molecule PEG-based linker strategy in hand, generation of Kip3-based heterodimers through directional coupling via a covalent PEG heterolinker was evaluated. This directional coupling strategy relies on an orthogonal kinesin protomer pair, where each protomer contains a distinct orthogonal linkage chemistry. To add a second orthogonal chemistry that could be genetically encoded to our existing system, we evaluated the use of a tetrazine-containing ncAA, Tet-v2.0[246]. Tet-v2.0 was an ideal candidate, as the ligation reaction between tetrazines and trans-cyclooctene (TCO) derivatives is highly specific even in the presence AzF and DBCO[250]. We aimed to generate two orthogonal Kip3ΔT protomers, one containing a site-specifically incorporated AzF and the other a Tet-v2.0. In turn, directional coupling via the heterobifunctional crosslinker, DBCO-PEG12-TCO, enables generation of heterodimeric kinesins (Figure 3a). In order to verify Tet-v2.0 incorporation into Kip3ΔT and its accessibility to react with TCO-derivatives, Kip3ΔT-Tet2.0-GFP^{M} was incubated with TCO functionalized TAMRA (sTCO-TAMRA)[251]. Kip3ΔT containing Tet2.0 showed strong specific labeling with sTCO-TAMRA under identical conditions used in Kip3ΔT-AzF-GFP$^{\boldsymbol{M}}$/DBCO-TAMRA labeling assays (Supplemental Figure 6).

To evaluate if the Tet-v2.0 amino acid linkage or the heterolinker interfered with Kip3 motility, the homodimer mimic, Kip3ΔT-AzF/Tet2.0-GFP^{D}, was generated by coupling Kip3ΔT-AzF-GFP$^{\boldsymbol{M}}$ and Kip3ΔT-Tet2.0-GFP^{M} with the heterolinker, DBCO-PEG12-TCO. The coupling reaction was accomplished via a two-step reaction strategy to minimize potential cross-reaction between AzF and TCO[240]. Formation of Kip3ΔT-

AzF/Tet2.0-GFP^{D} was confirmed and found to be highly specific to the crosslinking reaction via DBCO-PEG12-TCO (Figure 3b). Consistent with this observation, microtubule-bound Kip3ΔT-AzF/Tet2.0-GFP^{D} molecules existed primarily as homodimers (Supplementary Figure 7a, b). Single-molecule motility experiments revealed that the heterolinked Kip3ΔT dimer, Kip3ΔT-AzF/Tet2.0-GFP^{D}, moved processively toward the plus ends on single microtubules (Figure 3c) with a velocity of 39 ± 7 nm s^{-1} (mean ± s.d., n=313), and a run-length of 1.6 ± 0.1 μm (mean ± s.e.m., n=313, Supplementary Figure 7c, d). Both motility parameters (velocity and run-length) of the AzF/Tetv2.0-linked Kip3ΔT dimer were nearly identical to those of DBCO-PEG-linked Kip3ΔT homodimers under the same ionic strength and motility conditions (Figure 3d) and therefore also matched those of the leucine zipper-linked Kip3ΔT homodimers. This implies that the heterobifunctional linker DBCO-PEG12-TCO is suitable for making dimeric kinesin motors using AzF and Tet-v2.0 linkages as it did not interfere with Kip3 motility.

Kip3 heterodimer containing rigor mutation remains processive with reduced velocity on microtubules.

To evaluate our ability to generate true kinesin heterodimers using two different ncAA-containing protomers conjugated via a heterolinker, we generated a Kip3ΔT heterodimer containing one motor with a rigor-type mutation (T94N)[237,240] and one wildtype-like kinesin protomer, designated as Kip3ΔT(T94N/WT)-GFP^{D}. Kinesin containing rigor mutations as homodimers have exhibited absolute processive immobility but bind well to microtubules because the mutation compromised the catalytic turnover of

the kinesin motors but not microtubule binding[240]. In order to verify the effects of the rigor mutation on the Kip3ΔT homodimer, the T94N mutation was introduced to the leucine zipper dimerized Kip3 generating the rigor homodimer, Kip3ΔT(T94N)-LZ-GFP^{D} (Supplementary Figure 8). As expected, the single-molecule motility experiments of the impaired, homodimeric rigor Kip3ΔT did not exhibit processive motility and instead remained stationary on single microtubules (Supplementary Figure 8).

To generate a rigor Kip3ΔT heterodimer, the wildtype-like, Tet2.0-containing protomer, Kip3ΔT-Tet2.0-GFP^{M}, was coupled via the hetero-PEG12 linker to the rigor mutant, AzF-containing protomer, Kip3ΔT(T94N)-AzF-GFP^{M} (Figure 3e). Single-molecule motility experiments of the rigor Kip3ΔT heterodimer, Kip3ΔT(T94N/WT)-GFP$^{\boldsymbol{D}}$, showed that a stable dimer was formed (Supplementary Figure 9) and it remained a processive plus-end-directed motor on single microtubules (Figure 3f). The velocity of rigor Kip3ΔT heterodimer was determined to be 16 ± 5 nm s^{-1} (mean ± s.d., n=238, Figure 3g), approximately half that of wildtype-like Kip3ΔT-LZ-GFP$^{\boldsymbol{D}}$ under the same motility conditions (Supplementary Figure 2f). This result demonstrating that kinesin-8 mobility is possible with only a single catalytically functional motor agrees with previous finding on kinesin-1 based rigor mutant[17]. However, unlike previous work on similar kinesin-1 heterodimers, which retained approximately 10% of homodimer velocity[68,236,237,240], a retention of 50% velocity by the Kip3ΔT rigor heterodimer constitutes a far less dramatic reduction in velocity. Furthermore, the run-length of our rigor Kip3ΔT heterodimer was determined to be 1.2 ± 0.1 μm (mean ± s.e.m., n=238, Figure 3g), which was comparable to that of Kip3ΔT-LZ-GFP$^{\boldsymbol{D}}$ (Supplementary Figure 2g). This retention of homodimer run-length by the rigor Kip3ΔT heterodimer was in stark contrast to kinesin-1, where an

equivalent rigor heterodimer impaired run-length by 80%[241]. The ability of Kip3 to retain nearly wildtype-like processivity with a single impaired motor domain implies that multiple levels of regulation could be used to tune kinesin functions *in vivo*.

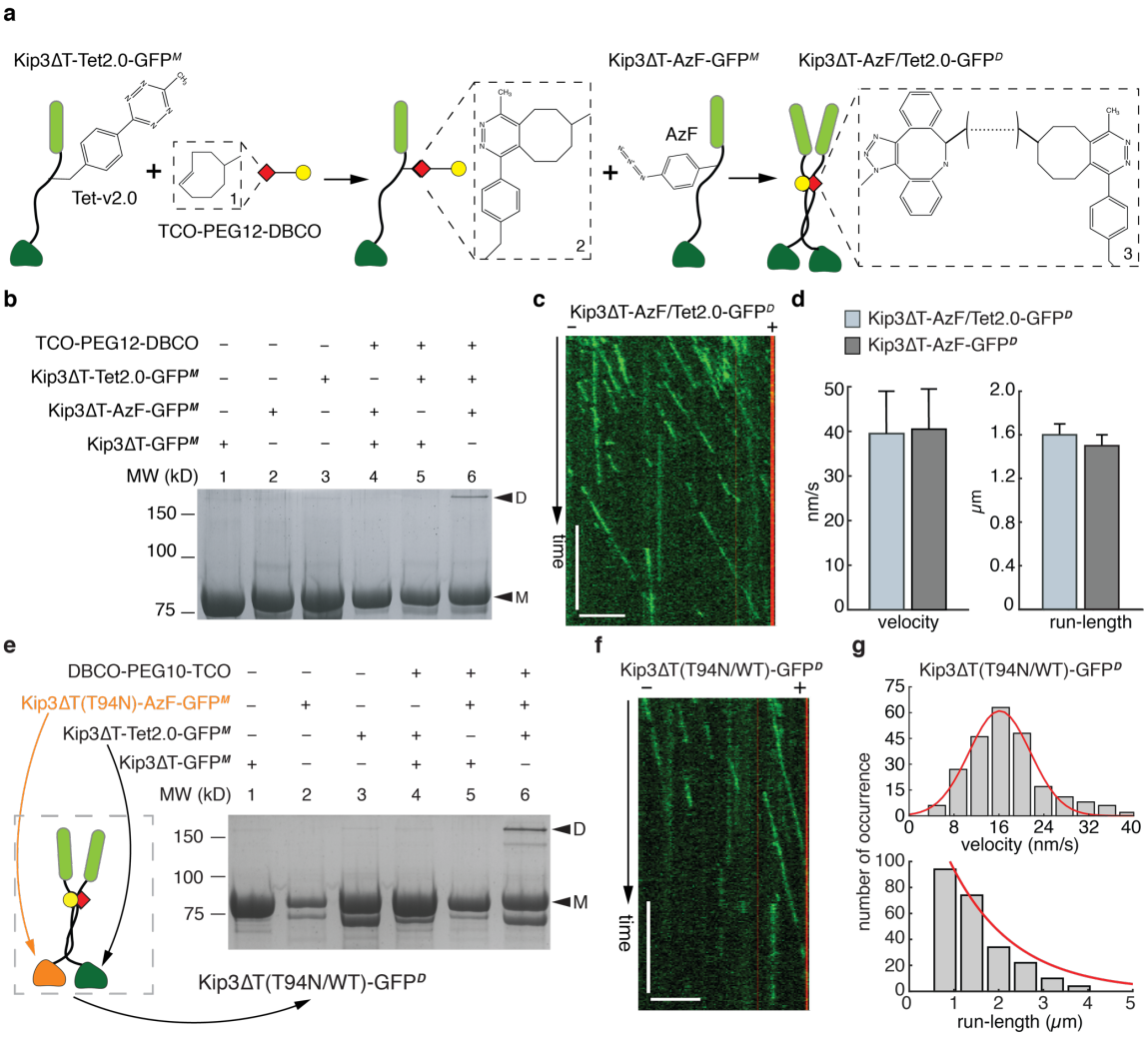

Figure 4.3: The orthogonal ncAA-based homodimer Kip3ΔT-AzF/Tet2.0-GFP^{D} exhibits wildtype-like motility on single microtubules while the heterodimer Kip3ΔT(T94N/WT)-GFP^{D} carrying a single rigor mutant exhibits significant reduction in velocity.

Figure 4.3: The orthogonal ncAA-based homodimer Kip3ΔT-AzF/Tet2.0-GFP^{D} exhibits wildtype-like motility on single microtubules while the heterodimer Kip3ΔT(T94N/WT)-GFP^{D} carrying a single rigor mutant exhibits significant reduction in velocity.

(a) Reaction scheme for forming the homodimer Kip3ΔT-AzF/Tet2.0-GFP^{D} by crosslinking Kip3ΔT-AzF-GFP^{M} and Kip3ΔT-Tet2.0-GFP^{M} via TCO-PEG12-DBCO (yellow circle/red diamond). Boxes indicate the chemical structures of TCO (Box 1), the ligation product between Tet-v2.0 and TCO-PEG12-DBCO (Box 2), and the ligation product between AzF, TCO-PEG12-DBCO and Tet-v2.0 in Kip3ΔT-AzF/Tet2.0-GFP^{D} (Box 3). **(b)** Coomassie-stained SDS-PAGE gel showing that Kip3ΔT-AzF/Tet2.0-GFP^{D} forms only in the presence of Kip3ΔT-AzF-GFP^{M}, Kip3ΔT-Tet2.0-GFP^{M} and TCO-PEG12-DBCO. Arrows indicate the expected bands of the monomer (M) and the dimer (D). **(c)** Representative kymograph of Kip3ΔT-AzF/Tet2.0-GFP^{D} molecules on a single microtubule. **(d)** Comparison of the velocity and run-length between Kip3ΔT-AzF-GFP^{D} and Kip3ΔT-AzF/Tet2.0-GFP^{D}. **(e)** Coomassie-stained SDS-PAGE gel showing that DBCO-PEG10-TCO specifically crosslinks Kip3ΔT-Tet2.0-GFP^{M} and Kip3ΔT(T94N)-AzF-GFP^{M} to form Kip3ΔT(T94N/WT)-GFP^{D}. Arrows indicate the expected bands of the monomer (M) and the dimer (D). **(f)** Representative kymograph of Kip3ΔT(T94N/WT)-GFP^{D} molecules on a single microtubule. **(g)** Velocity (Top) and run-length (Bottom) histograms of individual Kip3ΔT(T94N/WT)-GFP^{D} molecules on a single microtubule. Red lines indicate a Gaussian fit to the velocity histogram and a single exponential fit to the run-length histogram. Scale bars: 2 minutes (vertical) and 5 μm (horizontal).

Conclusion

In summary, we have developed a new method to engineer heterodimeric kinesin motors by combining genetic incorporation of reactive ncAAs and small molecule-based crosslinking. To our knowledge, this is the first report of directional coupling between azide- and tetrazine-containing proteins. This method for generating heterodimers will provide access to essential questions in the kinesin field, as it uses mild reaction conditions to attach an inert chemical linker and overcomes several critical issues in existing approaches, which are based on either tandem purification[10] or DNA hybridization[252-254]. First, our method forms heterodimeric kinesins with high specificity and does not produce homodimer contaminants. Second, our method uses genetic code expansion to site-specifically incorporate a single reactive ncAA, which not only provides exquisite spatial control but also eliminates reliance on cysteine chemistries. Third, by using an inert chemical crosslinker to dimerize distinct protomers, our method does not compromise kinesin motility. It is worth clarifying that our method does not yet allow making full-length kinesin heterodimers, as it requires shortening the central coiled-coil region to disable autonomous dimerization. Nevertheless, one can easily adapt our method to engineer novel heterodimers to gain new insights into the motility mechanisms and functions of different kinesins. For example, a kinesin heterodimer with two nonidentical neck linkers that differ in length and/or amino acid composition would be an extremely useful reagent for dissecting the mechanical role of the neck linker[244]; and crippled kinesin heterodimers can be used to further understand how kinesins coordinate in multi-motor ensembles to achieve optimal efficiency[246]. Due to the advantages of a heterolinker of tunable composition and length, which is reactive towards two different ncAA-containing

proteins, this method should allow exploration of a variety of engineered hetero-protein complexes.

Experimental Section

Molecular cloning of recombinant Kip3 constructs.

cDNA of full-length Kip3 was codon-optimized and synthesized for enhanced protein expression in bacteria (IDT). All recombinant Kip3 constructs were integrated into a modified pBAD vector (Thermo Fisher Scientific) using either isothermal assembly or the Q5 site-directed mutagenesis kit (NEB) and verified by DNA sequencing. All protein constructs contained a C-terminal 6xHis-tag for protein purification.

Protein expression and purification.

Kip3ΔT constructs ncAA incorporation were expressed in BL21-AI cells (Fisher Scientific). Cells were grown at 37 ^{o}C in TPM supplemented with 50 μg ml^{-1} ampicillin until OD_{600} reached 0.8. Expression was then induced with 0.1 mM arabinose for 14-18 hours at 18 ^{o}C. Cells were harvested, flash frozen in liquid nitrogen, and stored at -80 ^{o}C.

For expressing Kip3ΔT containing AzF, the BL21-AI cells contained a pDule plasmid encoding an orthogonal tRNA-synthetase pair genetically incorporating *para*-substituted phenylalanines[218]. Cells were grown at 37 ^{o}C in TPM supplemented with 1mM H-4-Azido-Phe-OH (Bachem), 50 μg ml^{-1} ampicillin and 30 μg ml^{-1} spectinomycin until OD_{600} reached 0.8. Cells were induced with 0.1 mM arabinose for 14-18 hours at 18 ^{o}C and harvested subsequently.

For expressing Kip3ΔT containing Tet-v2.0, the BL21-AI cells contained a pDule plasmid containing an orthogonal tRNA-synthetase pair for genetically incorporating Tet-v2.0[218]. Tet-v2.0 was synthesized using a modified procedure to increase yields (Supplementary Note 4.1). Cells were grown at 37 ^{o}C in TPM supplemented with 1mM Tet-v2.0, 50 μg ml^{-1} ampicillin and 30 μg ml^{-1} spectinomycin until OD_{600} reached 0.8. Cells were induced with 0.1 mM arabinose for 40 hours at 18 ^{o}C, and harvested subsequently.

For protein purification, cell pellets were re-suspended in 50 mM sodium phosphate (NaPi) buffer (pH 7.2) containing 250 mM NaCl, 1 mM $MgCl_2$, 0.5 mM ATP, 10 mM ß-mercaptoethanol, 5% glycerol and 20 mM imidazole in the presence of a protease inhibitor cocktail (Lysis Buffer) and then lysed via sonication. After centrifugation, soluble protein in the supernatant was purified by Talon resin (Clontech) and eluted into 50 mM NaPi buffer (pH 7.2) containing 250 mM NaCl, 1 mM $MgCl_2$, 0.5 mM ATP, 10 mM ß-mercaptoethanol, 5% glycerol and 250 mM imidazole (Elution Buffer). Protein was then flash frozen in liquid nitrogen and stored at -80 ^{o}C.

Kip3ΔT homodimers via two complementary DNA oligos.

Complementary DBCO-tagged DNA oligos DBCO-A (5'-DBCO-GGTAGAGTGGTAAGTAGTGAA) and DBCO-A* (5'-TTCACTACTTACCACTCTACC-DBCO) were designed based on a previous study[218] and synthesized by IDT. Purified Kip3ΔT-AzF-GFP^{M} in Elution Buffer was separately incubated with DBCO-OligoA and DBCO-OligoA* at 4 °C for 3 hours without agitation to Kip3ΔT-OligoA-GFP^{M} and Kip3ΔT-OligoA*-GFP^{M} respectively ([Kip3ΔT-AzF-

GFP^{M}] = 100 μM, [DBCO-OligoA] = [DBCO-OligoA*] = 12.5 μM). Unreacted DBCO-tagged DNA oligos were removed via an affinity purification step using the Talon resin. To form the DNA-based Kip3 dimer, Kip3ΔT-OligoA-GFP^{M} and Kip3ΔT-OligoA*-GFP^{M} were mixed on ice for 30 minutes. For SDS-PAGE analysis, samples were not heated prior to loading.

Kip3ΔT homodimers via the homobifunctional crosslinker DBCO-PEG4-DBCO.

To make the Kip3ΔT-AzF-GFP^{D} homodimer, Kip3ΔT-AzF-GFP^{M} in the Elution Buffer was incubated with DBCO-PEG4-DBCO (Click Chemistry Tools) at 4 °C for 3 hours without agitation ([DBCO-PEG4-DBCO] = 25μM, and [Kip3ΔT-AzF-GFP^{M}] = 100μM). The dimerization reaction was quenched by flash freezing in liquid nitrogen, and proteins were subsequently stored at -80 ºC.

Kip3ΔT dimers via the heterobifunctional crosslinker TCO-PEG12-DBCO.

To form the Kip3ΔT-AzF/Tet2.0-GFP^{D} dimer, Kip3ΔT-Tet2.0-GFP^{M} was first incubated to react with TCO-PEG12-DBCO (Click Chemistry Tools) at 4 °C for 30 minutes without agitation ([Kip3ΔT-Tet2.0-GFP^{M}] = 100μM, and [TCO-PEG12-DBCO] = 25μM). Unreacted TCO-PEG12-DBCO was removed via an affinity purification step using the Talon resin. Eluted protein was incubated with excess Kip3ΔT-AzF-GFP^{M} at 4 °C for 3 hours without agitation. After this step, the reaction mix was flash-frozen in liquid nitrogen and stored at -80 ºC with no additional purification.

Kip3ΔT(T94N)-LZ-GFP^{D} was formed similarly to Kip3ΔT-AzF/Tet2.0-GFP^{D}, with Kip3ΔT(T94N)-AzF-GFP^{M} used in place of Kip3ΔT-AzF-GFP^{M}.

Total internal reflection fluorescence (TIRF) microscopy.

All time-lapse imaging experiments were performed at room temperature using an Axio Observer Z1 objective-type TIRF microscope (Zeiss) equipped with a 100x 1.46 NA oil-immersion objective and a back-thinned electron multiplier CCD camera (Photometrics). All time-lapse imaging experiments used flow chambers that were made by attaching a coverslip to a microscope glass slide via double-sided tape as previously described[255-257]. Functionalized coverslips were used to reduce nonspecific surface absorption of kinesin molecules.

For the single-molecule photobleaching experiments, GFP-tagged kinesin molecules were properly diluted and bound to surface-immobilized HyLite 647-microtubules in a BRB80-based buffer supplemented with 200 mM KCl, 20 μM taxol and 1.3 mg ml^{-1} casein. After extensive washing to remove unbound molecules, time-lapse images were continuously recorded with 200-ms exposure until the field of view was bleached. Photobleaching steps of individual GFP-tagged kinesin motors were obtained by tracking the fluorescence intensity in ImageJ (NIH).

For most *in vitro* single-molecule motility experiments, the motility chamber was perfused with 0.5 mg ml^{-1} streptavidin for immobilizing polarity-marked HyLite 647-microtubules. GFP-tagged kinesin molecules were then diluted in the normal ionic strength motility buffer (BRB80 supplemented with 200 mM KCl, 1 mM ATP, 25 μM taxol, 1.3 mg ml^{-1} casein, and an oxygen scavenger system) and added to the chamber. For low-ionic

strength motility experiments, the motility buffer contained 100 mM KCl instead of 200 mM KCl. Time-lapse images were acquired at 100-ms exposure, 2 frames per second, and between 5 and 10-minute duration to determine the velocity and run-length. Kymographs were generated in ImageJ (NIH) to extract directionality, velocity and run-length information. Velocity and run-length were determined by fitting the histograms to a Gaussian distribution and a single exponential distribution respectively in Matlab (MathWorks)

Acknowledgment

We thank Dr. K.-F. Tseng (Oregon State University) for critical reading of the manuscript, and members of the Mehl and Qiu labs for helpful discussions.

Supplementary Information

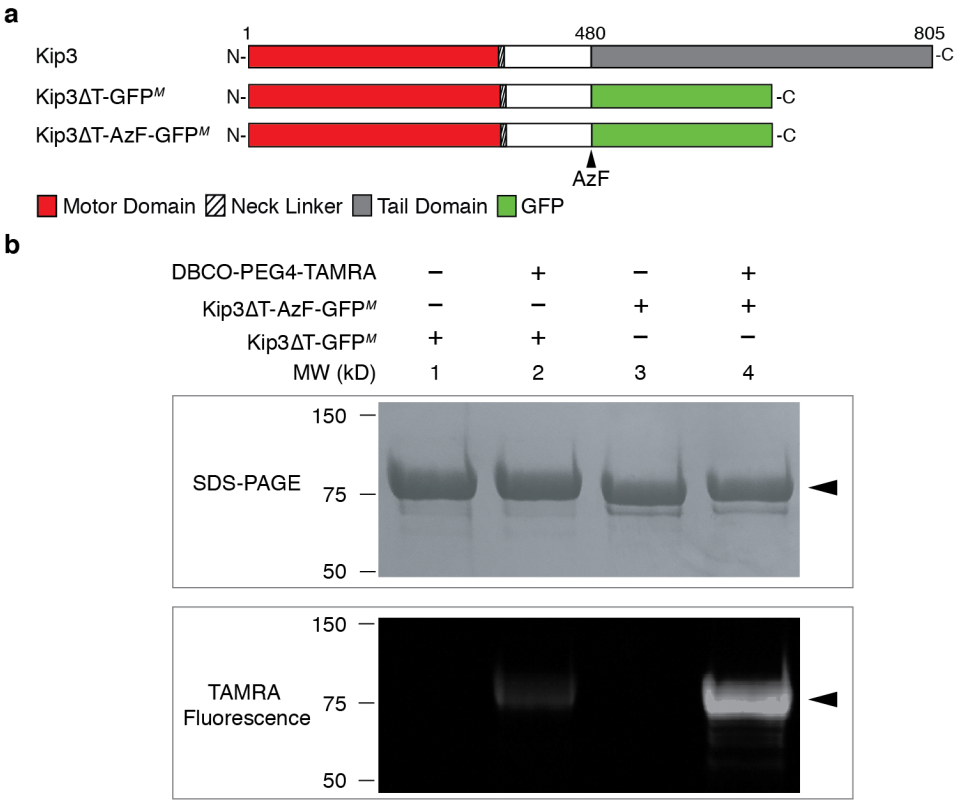

Figure 4.S1: Reactive AzF can be genetically incorporated into Kip3 and readily reacts with DBCO derivatives.

(a) Schematic of the full-length Kip3, Kip3ΔT-GFP^{M}, and Kip3ΔT-AzF-GFP^{M}. **(b)** Analyses of site-specific incorporation of AzF and its reaction with the azide-reactive DBCO-PEG4-TAMRA. Arrows indicate the protein bands of Kip3ΔT-GFP^{M} and Kip3ΔT-AzF-GFP^{M}.

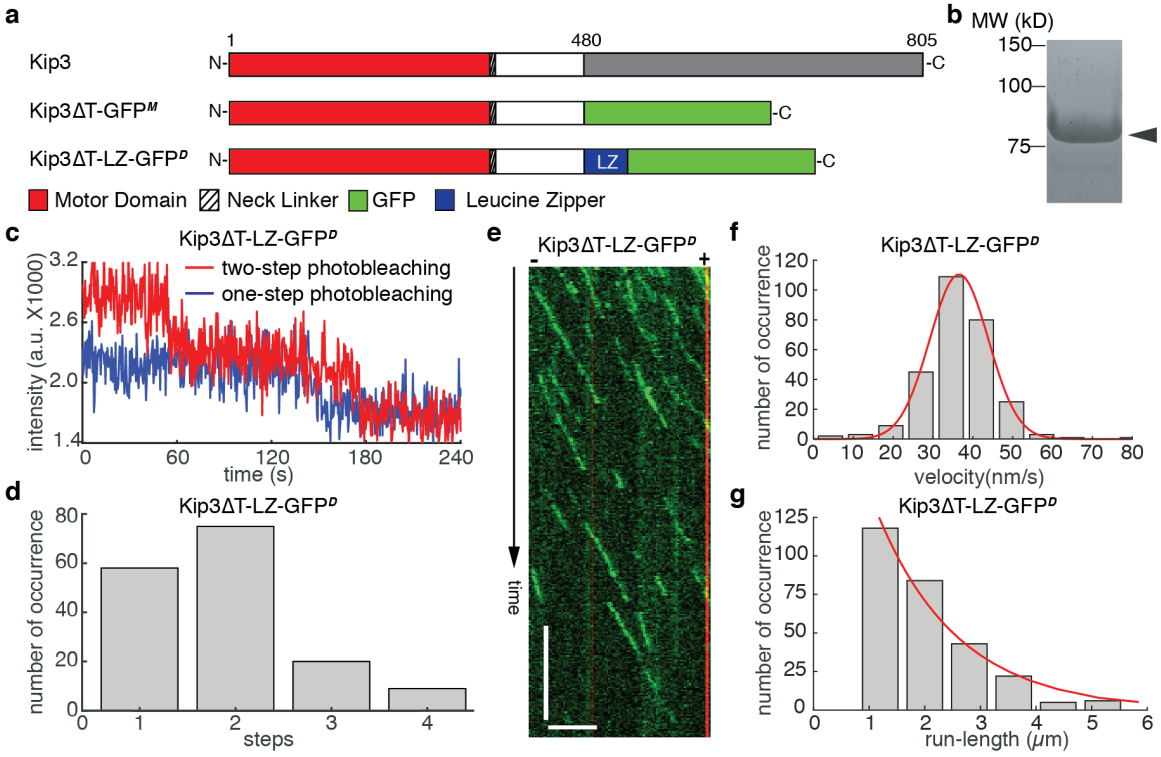

Figure 4.S2: Kip3ΔT-LZ-GFP^{D} forms a homodimer that exhibits processive plus-end-directed motility on single microtubules.

(a) Schematic diagrams of the full-length Kip3, Kip3ΔT-GFP^{M} and Kip3ΔT-LZ-GFP^{D}. **(b)** Coomassie-stained SDS-PAGE of purified Kip3ΔT-LZ-GFP^{D} (arrow). **(c)** Representative photobleaching traces of Kip3ΔT-LZ-GFP^{D} on surface-immobilized microtubules. **(d)** Photobleaching histogram of Kip3ΔT-LZ-GFP^{D} (n = 164). **(e)** Representative kymograph of individual Kip3ΔT-LZ-GFP^{D} molecules moving on a single microtubule. **(f)** Velocity histogram of Kip3ΔT-LZ-GFP^{D} on single microtubules. Red line indicates a Gaussian fit, and the velocity was determined to be 36 ± 7 nm s^{-1} (mean ± s.d., n=279). **(g)** Run-length histogram of Kip3ΔT-LZ-GFP^{D} on single microtubules. Red line indicates a single exponential fit, and the run-length was determined to be 1.5 ± 0.1 μm (mean ± s.e.m., n=279). Scale bars: 2 minutes (vertical) and 5 μm (horizontal).

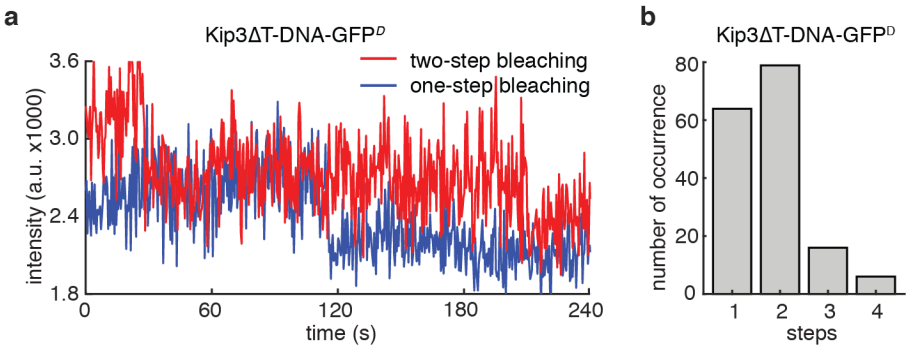

Figure 4.S3: Kip3ΔT-DNA-GFP^D exhibits photobleaching behavior typical of dimeric kinesins.

(a) Representative photobleaching traces of Kip3ΔT-DNA-GFP$^{\boldsymbol{D}}$ on surface-immobilized microtubules. **(b)** Photobleaching histogram of Kip3ΔT-DNA-GFP$^{\boldsymbol{D}}$ (n = 164).

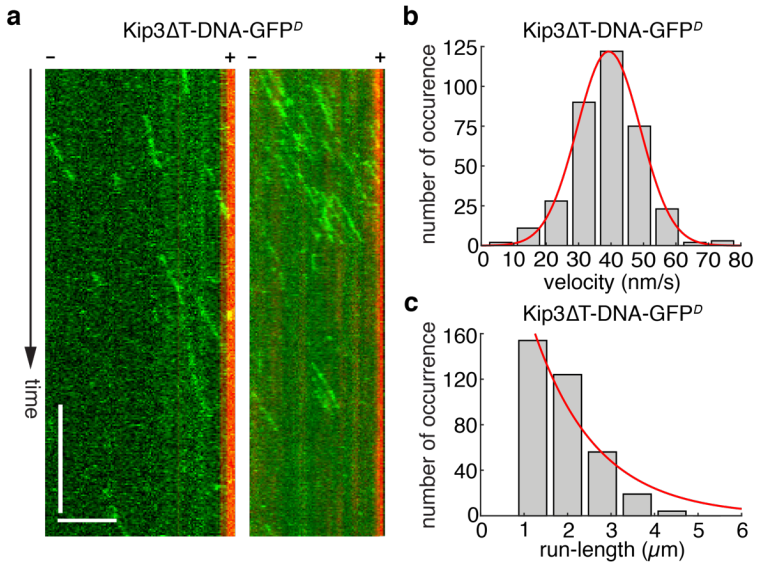

Figure 4.S4: Kip3ΔT-DNA-GFP^D exhibits processive motility on single microtubules in low ionic strength motility buffer.

(a) Representative kymographs of Kip3ΔT-DNA-GFP^D on single microtubules in the low ionic strength motility buffer (BRB80 with 100 mM KCl). **(b)** Velocity histogram of Kip3ΔT-DNA-GFP^D on single microtubules. Red line indicates a Gaussian fit, and the velocity was determined to be 39 ± 10 nm s^{-1} (mean ± s.d., n=358). **(c)** Run-length histogram of Kip3ΔT-DNA-GFP^D on single microtubules. Red line indicates a single exponential fit, and the run-length was determined to be 1.5 ± 0.1 μm (mean ± s.e.m., n=358). Scale bars: 2 minutes (vertical) and 5 μm (horizontal).

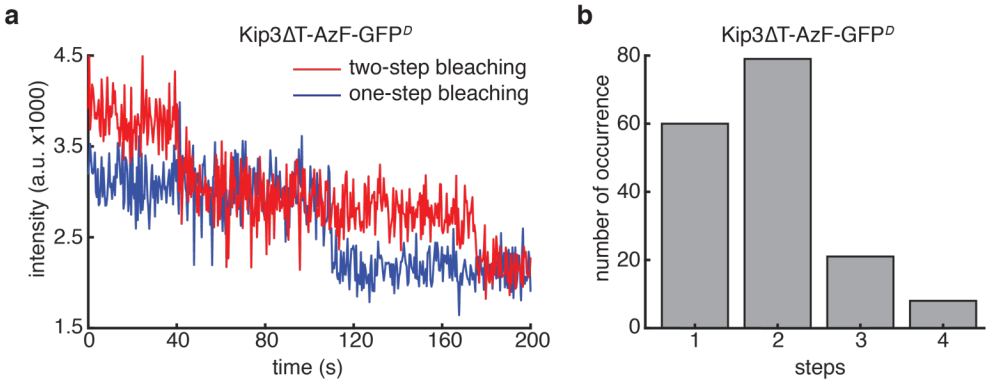

Figure 4.S5: Kip3ΔT-AzF-GFP^D exhibits photobleaching behavior typical of dimeric kinesins.

(a) Representative photobleaching traces of Kip3ΔT-AzF-GFP$^{\boldsymbol{D}}$ on surface-immobilized microtubules. **(b)** Photobleaching histogram of Kip3ΔT-AzF-GFP$^{\boldsymbol{D}}$ (n = 167).

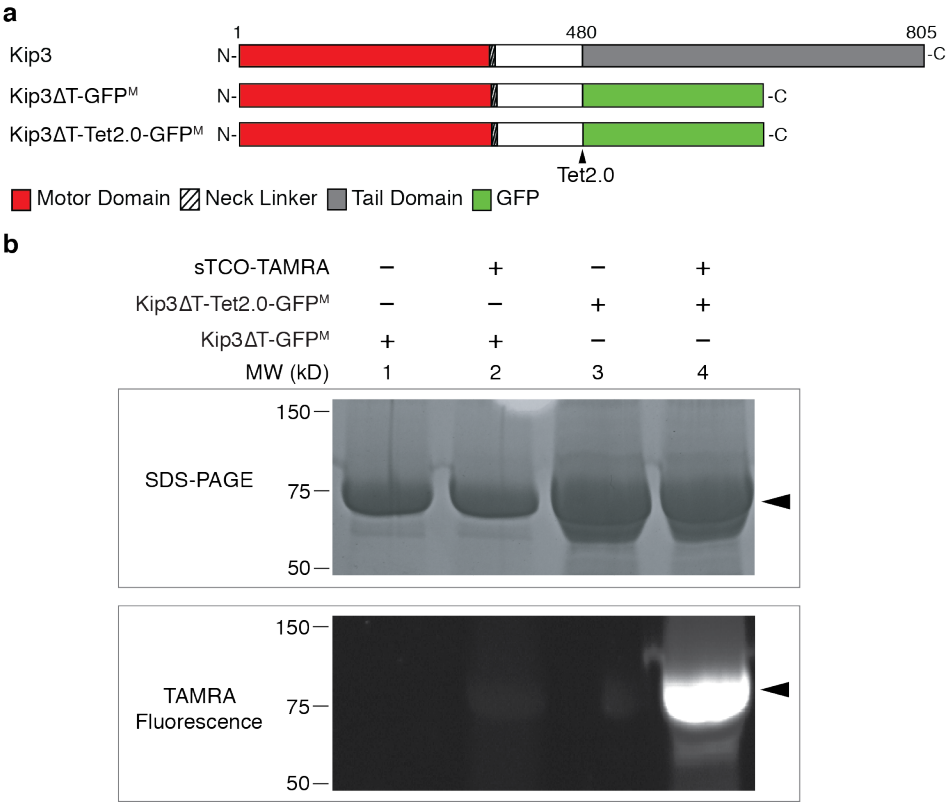

Figure 4.S6: Reactive Tet-v2.0 can be genetically incorporated in Kip3 and readily reacts with TCO derivatives.

(a) Schematic of the full-length Kip3, Kip3ΔT-GFP^{M}, and Kip3ΔT-Tet2.0-GFP^{M}. **(b)** Analyses of site-specific incorporation of Tet-v2.0 and its reaction with the tetrazine-reactive sTCO-TAMRA. Arrows indicate the protein bands of Kip3ΔT-GFP^{M} and Kip3ΔT-Tet2.0-GFP^{M}.

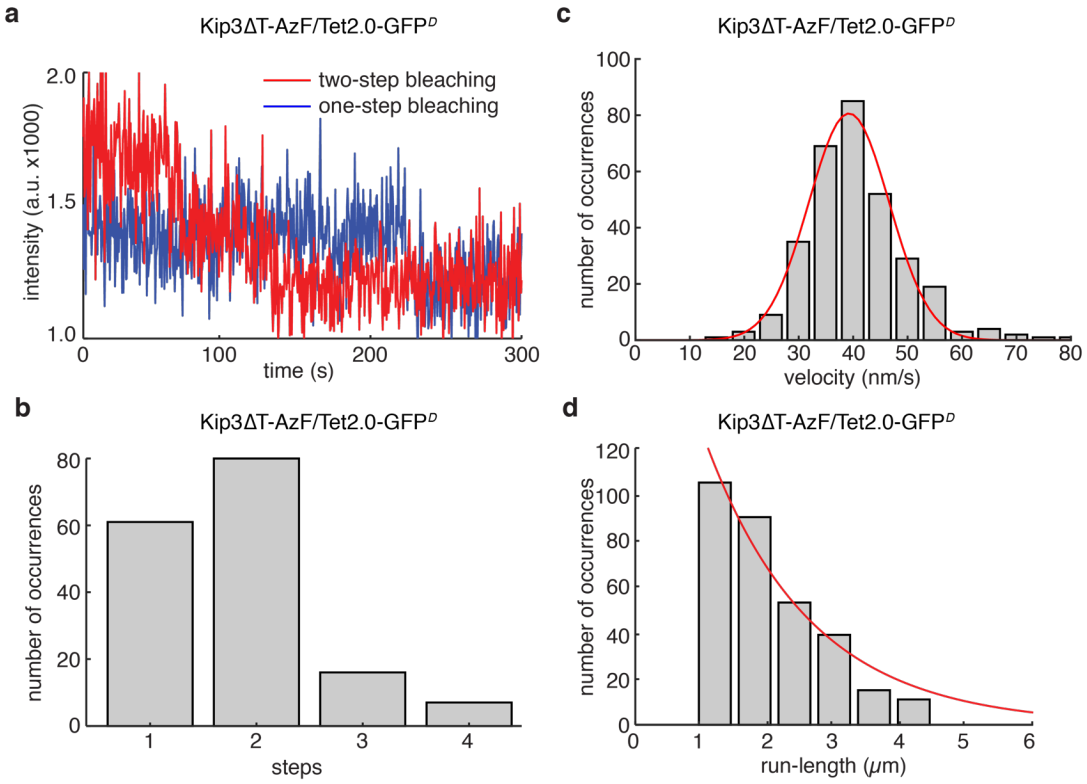

Figure 4.S7: Kip3ΔT-AzF/Tet2.0-GFP^D exhibits processive motility on single microtubules as individual homodimers.

(a) Representative photobleaching traces of Kip3ΔT-AzF/Tet2.0-GFP$^{\boldsymbol{D}}$ on surface-immobilized microtubules. **(b)** Photobleaching histogram of Kip3ΔT-AzF/Tet2.0-GFP$^{\boldsymbol{D}}$ (n = 164). **(c)** Velocity histogram of Kip3ΔT-AzF/Tet2.0-GFP^D on single microtubules. Red line indicates a Gaussian fit to the velocity histogram. **(c)** Run-length histogram of Kip3ΔT-AzF/Tet2.0-GFP$^{\boldsymbol{D}}$ on single microtubules. Red line indicates a single exponential fit to the run-length histogram.

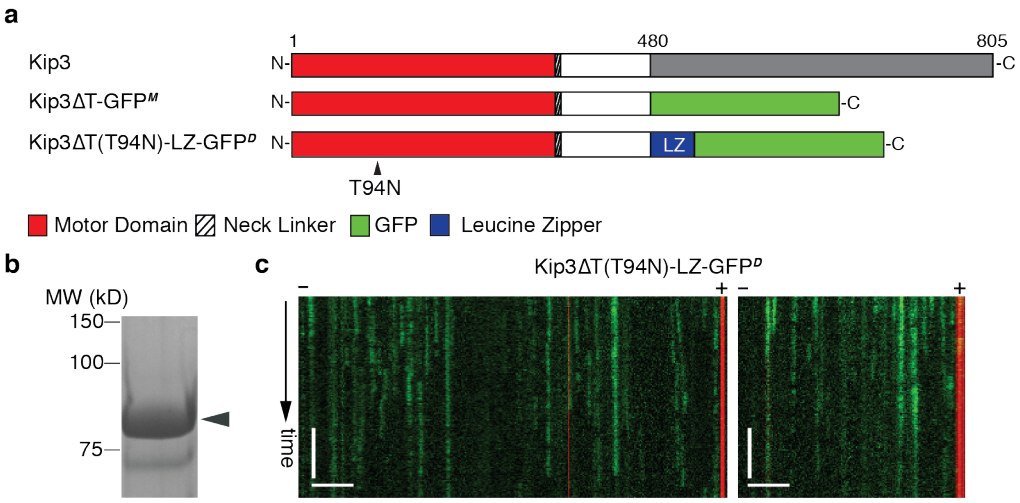

Figure 4.S8: The rigor homodimer Kip3ΔT(T94N)-LZ-GFP^{D} tightly binds to the microtubules and does not exhibit motility.

(a) Schematic diagrams of the full-length Kip3, Kip3ΔT-GFP^{M} and Kip3ΔT(T94N)-LZ-GFP^{D}. **(b)** Coomassie-stained SDS-PAGE gel of Kip3ΔT(T94N)-LZ-GFP^{D} (arrow). **(c)** Representative kymographs showing that Kip3ΔT(T94N)-LZ-GFP^{D} tightly binds to the microtubules and exhibits no motility in the presence of ATP. Scale bars: 1 minute (vertical) and 5 μm (horizontal).

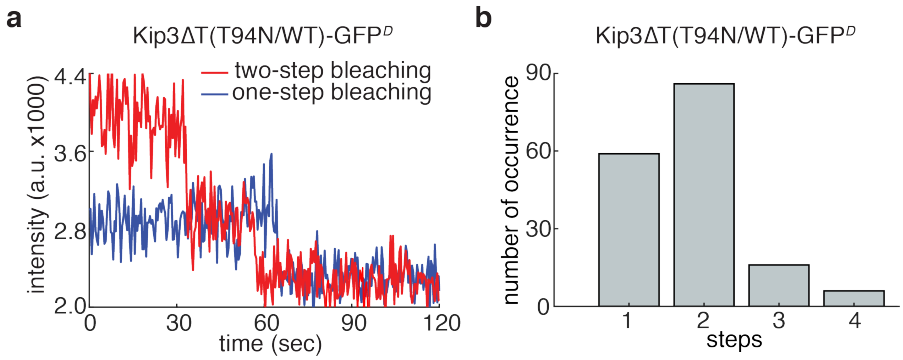

Figure 4.S9: The heterodimer Kip3ΔT(T94N/WT)-GFP^D exhibits photobleaching behavior typical of dimeric kinesins.

(a) Representative photobleaching traces of Kip3ΔT(T94N/WT)-GFP^D on surface-immobilized microtubules. **(b)** Photobleaching histogram of Kip3ΔT(T94N/WT)-GFP^D (n = 167).

Supplementary Note 4.1

High-yield synthesis procedure of Tet-v2.0

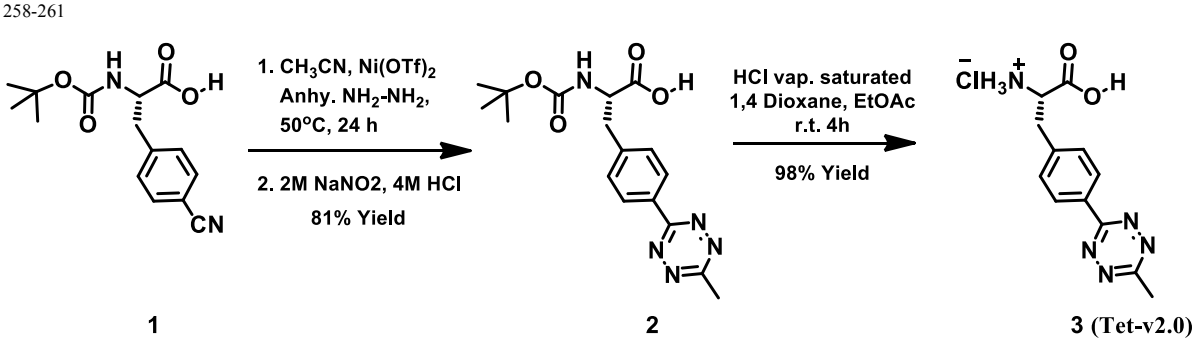

(S)-2-((tert-butoxycarbonyl)amino)-3-(4-(6-methyl-1,2,4,5-tetrazin-3-yl)phenyl)propanoic acid (**2**): In a flame-dried, 48 mL heavy-wall reaction tube with a stir bar, Boc-protected 4-cyano phenylalanine (800 mg, 2.75 mmol) was charged with $Ni(OTf)_2$ (490 mg, 1.38 mmol) and acetonitrile (1.4 mL, 27.5 mmol) under argon atmosphere. Next, anhydrous hydrazine (4.4 mL, 137.5 mmol) was slowly added to the reaction tube. The reaction mixture was then purged with argon for 10 minutes under constant stirring, sealed immediately afterwards, and heated to and kept at 50-55 ^oC for 24 hours. After that the reaction mixture was cooled to room temperature, opened slowly and added 20 eqv. 2 M $NaNO_2$ solution and 5 mL water. Next, the reaction mixture was washed with ethyl acetate (2x 20 ml) to remove the homo-coupling product. The aqueous phase was acidified with 4 M HCl (pH = ~2) under ice cold condition and extracted with ethyl acetate (3x 30 mL). The combined organic layer was washed with brine, dried with anhydrous Na_2SO_4, and concentrated under reduced pressure. Silica gel flash column chromatography (30-35% ethyl acetate with 1% acetic acid in hexanes) yielded 802 mg of Boc-protected Tet-v2.0 amino acid **2** (2.23 mmol, 81 %) in the form of a pinkish red gummy material. ^1H NMR (400MHz, $CDCl_3$) δ 8.54 (d, 2H), 7.44 (d, 2H), 5.06 (d, 1H), 4.71 (bs, 1H), 3.37- 3.19 (dd, 2H), 3.1 (s, 3H), 1.44 (s, 9H). ^{13}C NMR (175MHz, $CDCl_3$) δ 175.3, 167.2, 163.9,155.3, 141.2, 130.4, 128.1, 127.8, 80.4, 54.1, 37.9, 28.3, 21.2.

Chloride salt of (S)-2-amino-3-(4-(6-methyl-1,2,4,5-tetrazin-3-yl)phenyl) propanoic acid (**3**): In a dry round bottom flask, Boc-protected Tet-v2.0 amino acid **2** (800 mg or 2.23 mmol in 5 mL ethyl acetate) was charged with 3 mL HCl gas saturated 1,4 Dioxane under argon atmosphere. The reaction was carried out at room temperature with constant stirring until the starting materials were completely consumed based on the monitoring by thin layer chromatography (normally 3 to 4 h). The reaction mixture was then concentrated under reduced pressure, re-dissolved in ethyl acetate (2x 10 mL), and re-concentrated to remove excess HCl gas and to obtain the final product Tet-v2.0 in the form of a pink solid material (yield = ~98%). ^{1}H NMR (400MHz, CD_3OD) δ 8.56 (d, 2H), 7.60 (d, 2H), 4.39 (t, 1H), 3.48- 3.33 (dd, 2H), 3.1 (s, 3H). ^{13}C NMR (175MHz, CD_3OD) δ 171.2, 169.1, 165.3, 140.7, 133.3, 131.7, 129.6, 55.1, 37.4, 21.3. ESI-MS calculated for $C_{12}H_{14}N_5O_2$ ($[M + H]^+$) 260.114, found 260.1.

Chapter 5

Conclusion

Highlights of Reported Work

In this section, I will highlight some of the major findings of each chapter and their potential impacts. In the remaining sections I will outline ongoing and potential future work that continues the research presented here and will finish with some concluding remarks on the kinesin field and the direction of ongoing research.

In chapter 2, we used single-molecule TIRF microscopy to characterize the mitotic kinesin-14 KlpA. We discovered that KlpA was a novel processive kinesin-14 that exhibited context-dependent bidirectionality. KlpA is the first processive homodimeric kinesin-14 to be discovered. Additionally, KlpA is the first kinesin-14 observed to be plus end-directed, markedly expanding our understanding of the diversity of kinesin-14s. We discovered that the context-dependent directionality of KlpA depends upon its microtubule-binding tail domain, which is the de facto directionality switch. Context-dependent directionality was discovered in mitotic kinsin-5s, kinesin-14s counterpart within the mitotic spindle, and has since been well studied. This work on KlpA provides the first evidence to suggest that context-dependent directional switching may be a unique property of mitotic kinesins, and could also exist among some, if not all, mitotic kinesin-14s. Furthermore, this context-dependent directionality provided a potential model for KlpA function within the mitotic spindle at the spindle midzone. This work has contributed to the growing interest in kinesin-14s, a particularly understudied kinesin subfamily, and has been referenced in work on directionality determinants in kinesins[120] as well as studies on the expanded diversity of kinesin-14 function[262]. The work in chapter 2 is an example of the tremendous amount of information yet to be discovered about the diversity of kinesins outside of conventional kinesin or the kinesin-1 subfamily.

In chapter 3, we followed up on our initial characterization of KlpA presented in chapter 2, which outlined a possible mechanism for KlpA function at spindle midzones, to examine more closely the potential function and regulation of KlpA and its function at spindle poles (an area of opposite microtubule polarity to the spindle midzone). We discovered that these mitotic proteins are able to regulate the activity of KlpA on microtubules: interacting to cause KlpA to change direction and become a minus end-directed motor or forming a ternary complex with KlpA that is anchored on microtubules. To our knowledge this is the first example of an interacting or potential cargo protein (TinA) causing a directional switch of a kinesin motor protein. Additionally, to our knowledge this is the first example of ternary complex formation that locks a kinesin motor protein in a "rigor"-like state on microtubules. After characterization of these regulatory mechanisms, we were able to propose an expanded model of KlpA function within the mitotic spindle. This model accounted for the activity of KlpA at spindle midzones as well as localization and function at the spindle poles. Based on our findings we were able to propose a potential mechanism for kinesin-14-dependent anchoring of spindle microtubules and the resulting "protruding spindle microtubule" phenotype in the absence of kinesin-14 that has been widely observed *in vivo*. While this work is yet to be published, we expect it to have a significant impact as errors in chromosome separation that result from these protruding spindle microtubules have been shown to cause cellular aneuploidy, a hallmark of cancerous cells. Mechanistic understanding of these pathways has been an intense area of research, yet mechanisms responsible for this kinesin-14-based anchoring of spindle microtubules have until know, been largely unknown.

In chapter 4, we developed a new method for generation of kinesin heterodimers. To enable incorporation of unique biorthogonal chemistries into kinesin protomers that could then be linked to form heterodimers, we relied on genetic code expansion and noncanonical amino acid incorporation. After discovering that linkage via complementary DNA oligos interfered with kinesin activity, we developed a method that utilizes a directional small-molecule-based linker that relies on the incorporation of two orthogonal noncanonical amino acids for linkage and subsequent heterodimer formation. This method overcame the significant shortcomings of previously existing methods for kinesin heterodimer formation, and in turn significantly expands our ability to generate tailored kinesin heterodimers. Kinesin heterodimers are important reagents for studying the fundamental mechanisms of coordination that are responsible for regulating kinesin activity and function on microtubules. Our method has significant advantages over others and provides access to previously unexplored kinesin mechanism such as: a kinesin heterodimer with two nonidentical neck linkers that differ in length and/or amino acid composition for dissecting the mechanical role of the neck linker and crippled kinesin heterodimers that can be used to further understand how kinesins coordinate in multi-motor ensembles to achieve optimal efficiency. Furthermore, application towards systems where reaction conditions can be further optimized may enable a simple one-step heterolinking strategy that can more generally provide a level of temporal control not offered by other approaches.

Future Directions

While the work described in chapters 2 and 3 represent a significant advance in our understanding of the mitotic kinesin-14 KlpA, it also provides a strong foundation for future studies. Based on our findings in chapter 2 related to the processivity and context-dependent directionality of KlpA, it was immediately apparent that the mechanisms responsible for this unique motility were particularly significant. To answer these questions and potentially confirm our proposed mechanism, structures of KlpA on microtubules in various contexts is needed. The most obvious way to achieve these structures would be via cryo-EM reconstitution of KlpA on microtubules. While not a trivial task, we are currently working with collaborators to assess if structures of KlpA can be generated. Once a structure of KlpA on microtubules can be generated, changes to its tail domain or potentially the KlpA structure within microtubule overlaps could then be used to probe how structural changes are related to the resulting change in KlpA activity. These findings would potentially provide a detailed structural mechanism for KlpA context-dependent directionality, a mechanism that could have implications for other context-dependent directional motors, or other mitotic kinesins.

The work described in chapter 3 while significant, provides motivation for a multitude of follow-up studies to build upon those initial findings. The most immediately accessible and natural continuation of this work would be to determine if the observed interactions between KlpA and TinA and AnWdr8 are conserved in higher eukaryotes. Because all three of these proteins are highly conserved, study of all three components in other organisms should be relatively straight forward. Of particular interest is whether or not the unique processive motility of KlpA is a required component for the observed

regulatory effects of TinA and AnWdr8. As most kinesin-14s in higher eukaryotes are typical non-processive motors, this question can be explored. The contribution of KlpAs' unique directionality can also be explored, as the kinesin-14 from yeast Kar3 is also a processive kinesin-14, but it maintains minus end-directed motility on microtubules. Kar3 provides a unique opportunity to decouple the directionality and processivity aspects of this potentially conserved mitotic regulation scheme. Because KlpA has been shown to be able to substitute for Kar3 in yeast cells[262], there is some evidence that Kar3 and KlpA can functionally overlap. Study of this conservation is particularly significant in human cells, where this spindle microtubule anchoring mechanism may have implications in cancer development and therefore potential treatment.

Further work is also planned to study the stoichiometry and kinetics of TinA binding to KlpA in both the presence and absence of AnWdr8. This information will provide insight into the TinA-enabled minus end-directed motility of KlpA as well as and potential effect of AnWdr8. One potential method to probe and measure this binding is NMR spectroscopy. We have established that the intrinsically disordered tail domain of KlpA is a suitable candidate for NMR spectroscopy and we aim to use 3D-based methods to make peak assignments for the KlpA tail domain. Once determined, these peak assignments could then be used to identify residues responsible for interaction or binding to TinA or microtubules (tubulin). If TinA/KlpA interacting residue identities are obtained, point-mutations can be made in full-length KlpA to validate in our single-molecule TIRF assays.

Lastly, the work presented in chapter 4 provides the tools necessary for many new and powerful studies. Even though a separate model kinesin was used to develop our

heterodimerization technique, we were originally motivated to develop this approach to use it in studying the unique coordination of KlpA. Now that an effective general approach to heterodimer formation has been established, exploration of the mechanisms that enable KlpA to remain processive on microtubules as well as its directionality determinants are possible. For one, we are interested in the inherent directionality of the motor domain of KlpA. By replacing the motor domain of kinesin-1 with that of KlpA, as well as the interconversion of each motor domain's respective neck linker (or neck mimic in the case of KlpA), the inherent directionality could potentially be determined. Additionally, kinesin-1/KlpA heterodimeric chimeras (either opposing motor domains, opposing neck linkers, or some combination of the two) can be used to probe the directionality determinants of KlpA.

Because our method does not require the coiled-coil domains for dimerization, their contribution to the motility of KlpA can be decoupled. Our working model is that tension provided by the binding of KlpA's tail domain to the microtubule is transmitted via the coiled-coil to the neck-mimic of KlpA and this torque is sufficient to switch its direction of stepping. There is evidence that kinesin-14s are sensitive to external forces, where little force is needed to cause backwards (or plus end-directed) stepping[263,264]. These stepping events behave similarly to "catch bonds", whose interaction is enhanced by mechanical force. This force can be artificially applied to enable kinesin-14 plus end-directed motility on microtubules[239]. In support of our KlpA stalk-dependent plus end-directed motility hypothesis, we have preliminary results suggesting that the rigidity of this stalk is required for plus end-directed motility and introduction of flexibility into the coiled-coil domain yields a minus end-directed processive KlpA motor. By using constructs that lack the

coiled-coil stalk but retain KlpAs' tail domain, the entirety of contribution of the stalk to KlpA motility on microtubules can be determined. Moreover, structural elements of known physical properties (length, rigidity, composition, shape, etc) can be added *in trans* back to KlpA coil-coil-less chimeras to build and expand a simple working model for the contribution of the stalk domain. The contribution of stalk domains to kinesin motility and function on microtubules remains a relatively unexplored area within the kinesin field and we hope that our method for the generation of heterodimers enables researches to uncover the role of these domains among the functionally and structurally diverse subfamilies of kinesin motors.

Another project that I consider well suited to our heterodimerization method would be the study of posttranslational regulation of kinesins. Kinesins are highly regulated by covalent posttranslational modifications, which have been identified in most kinesins and are often found within their motor domains[265]. Recent work has shown one such modification alters the chemomechanical properties of the human mitotic kinesin-5 Eg5, enabling it to function much more efficiently under load and in ensembles which alter its mitotic function[239]. While these findings are particularly impactful, the effect of posttranslational modifications on the mechanics of kinesins remain almost completely unexplored. We feel that our heterodimerization is well suited for further studies as the same genetic code expansion techniques we previously used and can also be used to site-specifically incorporate phospho-amino acids [265]. We are particularly interested in investigating asymmetry of phosphorylation as a means to tune kinesin activity *in vivo*. To our knowledge, this phenomenon has never been explored, and prior to development of the

needed noncanonical amino acids as well as our heterodimerization method, such studies would not have been possible.

Concluding Remarks

As I mentioned in chapter 1, interest in kinesins has grown tremendously since their initial discovery. An enormous amount of work has been done to uncover the diverse composition of the kinesin family and to characterize their functions in cells. As is often the case, further discovery yields new research questions. Many outstanding questions remain including fundamental principles that govern their function. As nanomachines, the mechanics of these highly efficient and versatile motors are truly fascinating. Understanding the fundamental properties that guide their function and diversity may one day enable engineered kinesins that may be used to probe essential cellular processes, are used in industrial bioreactors, or even are capable of targeted drug delivery. While much of the ongoing research focuses on those kinesins of most clinical relevance, it is critical to study these mechanisms in more simple model systems to build the framework of our understanding. To that end, I hope that my work focused on the function of a mitotic kinesin-14 from fungi has helped to both further understanding of kinesin-14 function within mitotic spindles and also to enable future studies in more complex systems. The mitotic spindle represents a robust and intricate machinery, essential to most life, and inherently highly relevant to cancer. A complete understanding of the mitotic spindle and its function is an immense task that will require the contributions of many and require solving many fundamental problems in discrete steps along the way.

Sometimes it can be difficult to decide which problems to tackle first but I do believe that as long as a person lets the science guide and pursues interesting problems, valuable information will be gained in the end. This belief stems from my (albeit limited) experience, where often my growth as a scientist was most stimulated by the challenge and adversity (and also diversity) of failure. We are all aware of the trope that in life, one must be willing to fail in order to accomplish great things. Be that as it may, I truly believe that the exceptional scientists preceding me have simply been more willing to fail and more determined to learn through failure than their peers. Moving forward I hope to do the same (except, of course, in the defense of the thesis presented herein).

References

1. Schliwa, M. & Woehlke, G. Molecular motors. *Nature* **422,** 759–765 (2003).

2. Smith, C. A. & Rayment, I. Biochemistry, I. R.1995. X-ray Structure of the Magnesium (II)-Pyrophosphate Complex of the Truncated Head of Dictyostelium discoideum Myosin to 2.7. ANG. Resolution. *Biochemistry* **34,** 8973-8981 (1995).

3. Smith, C. A. & Rayment, I. X-ray structure of the magnesium(II)-pyrophosphate complex of the truncated head of Dictyostelium discoideum myosin to 2.7 A resolution. *Biochemistry* **34,** 8973–8981 (1995).

4. Kull, F. J., Sablin, E. P., Lau, R., Fletterick, R. J. & Vale, R. D. Crystal structure of the kinesin motor domain reveals a structural similarity to myosin. *Nature* **380,** 550–555 (1996).

5. Sablin, E. P., Kull, F. J., Cooke, R., Vale, R. D. & Fletterick, R. J. Crystal structure of the motor domain of the kinesin-related motor ncd. *Nature* **380,** 555–559 (1996).

6. Vale, R. D. Switches, latches, and amplifiers: common themes of G proteins and molecular motors. *J. Cell Biol.* **135,** 291–302 (1996).

7. Kull, F. J., Vale, R. D. & Fletterick, R. J. The case for a common ancestor: kinesin and myosin motor proteins and G proteins. *J. Muscle Res. Cell Motil.* **19,** 877–886 (1998).

8. Miki, H., Okada, Y. & Hirokawa, N. Analysis of the kinesin superfamily: insights into structure and function. *Trends Cell Biol.* **15,** 467–476 (2005).

9. Mickolajczyk, K. J. *et al.* Kinetics of nucleotide-dependent structural transitions in the kinesin-1 hydrolysis cycle. *Proc. Natl. Acad. Sci. U.S.A.* **112,** E7186–93 (2015).

10. Hariharan, V. & Hancock, W. O. Insights into the mechanical properties of the kinesin neck linker domain from sequence analysis and molecular dynamics simulations. *Cell Mol. Bioeng.* **2,** 177–189 (2009).

11. Liu, H.-L., Pemble, C. W. & Endow, S. A. Neck-motor interactions trigger rotation of the kinesin stalk. *Sci. Rep.* **2,** 236 (2012).

12. Seeger, M. A., Zhang, Y. & Rice, S. E. Kinesin tail domains are intrinsically disordered. *Proteins* **80,** 2437–2446 (2012).

13. Yip, Y. Y. *et al.* The light chains of kinesin-1 are autoinhibited. *Proc. Natl. Acad. Sci. U.S.A.* **113,** 2418–2423 (2016).

14. Pakala, S. B., Nair, V. S., Reddy, S. D. & Kumar, R. Signaling-dependent phosphorylation of mitotic centromere-associated kinesin regulates microtubule depolymerization and its centrosomal localization. *J. Biol. Chem.* **287,** 40560–40569 (2012).

15. Hirokawa, N., Noda, Y., Tanaka, Y. & Niwa, S. Kinesin superfamily motor proteins and intracellular transport. *Nat. Rev. Mol. Cell Biol.* **10,** 682–696 (2009).

16. Hornick, J. E., Karanjeet, K., Collins, E. S. & Hinchcliffe, E. H. Kinesins to the core: The role of microtubule-based motor proteins in building the mitotic spindle midzone. *Semin. Cell Dev. Biol.* **21,** 290–299 (2010).

17. Akhmanova, A. & Steinmetz, M. O. Control of microtubule organization and dynamics: two ends in the limelight. *Nat. Rev. Mol. Cell Biol.* **16,** 711–726 (2015).

18. Sproul, L. R., Anderson, D. J., Mackey, A. T., Saunders, W. S. & Gilbert, S. P. Cik1 targets the minus-end kinesin depolymerase Kar3 to microtubule plus ends. *Curr. Biol.* **15,** 1420–1427 (2005).

19. Marx, A., Müller, J., Mandelkow, E. M., Hoenger, A. & Mandelkow, E. Interaction of kinesin motors, microtubules, and MAPs. *J. Muscle Res. Cell Motil.* **27,** 125–137 (2005).

20. Rath, O. & Kozielski, F. Kinesins and cancer. *Nat. Rev. Cancer* **12,** 527–539 (2012).

21. Madhivanan, K. & Aguilar, R. C. Ciliopathies: the trafficking connection. *Traffic* **15,** 1031–1056 (2014).

22. Millecamps, S. & Julien, J.-P. Axonal transport deficits and neurodegenerative diseases. *Nat. Rev. Neurosci.* **14,** 161–176 (2013).

23. Brady, S. T. A novel brain ATPase with properties expected for the fast axonal transport motor. *Nature* **317,** 73–75 (1985).

24. Hirokawa, N. Kinesin and dynein superfamily proteins and the mechanism of organelle transport. *Science* **279,** 519–526 (1998).

25. Miki, H., Setou, M., Kaneshiro, K. & Hirokawa, N. All kinesin superfamily protein, KIF, genes in mouse and human. *Proc. Natl. Acad. Sci. U.S.A.* **98,** 7004–7011 (2001).

26. Lawrence, C. J. *et al.* A standardized kinesin nomenclature. *J. Cell Biol.* **167,** 19–22 (2004).

27. Vale R., Reese, T. & Sheetz, M. Identification of a novel force-generating protein, kinesin, involved in microtubule-based motility. *Cell* **42,** 39–50 (1985).

28. Dagenbach, E. M. & Endow, S. A. A new kinesin tree. *J. Cell Sci.* **117,** 3–7 (2004).

29. Walczak, C. E., Gayek, S. & Ohi, R. Microtubule-depolymerizing kinesins. *Annu. Rev. Cell Dev. Biol.* **29,** 417–441 (2013).

30. Wordeman, L. Microtubule-depolymerizing kinesins. *Curr. Opin. Cell Biol.* **17,** 82–88 (2005).

31. Ogawa, T., Nitta, R., Okada, Y. & Hirokawa, N. A common mechanism for microtubule destabilizers-M type kinesins stabilize curling of the protofilament using the class-specific neck and loops. *Cell* **116,** 591–602 (2004).

32. Howard, J., Hudspeth, A. J. & Vale, R. D. Movement of microtubules by single kinesin molecules. *Nature* **342,** 154–158 (1989).

33. Svoboda, K., Schmidt, C. F., Schnapp, B. J. & Block, S. M. Direct observation of kinesin stepping by optical trapping interferometry. *Nature* **365,** 721–727 (1993).

34. Hua, W. Distinguishing inchworm and hand-over-hand processive kinesin movement by neck rotation measurements. *Science* **295,** 844–848 (2002).

35. Rice, S. *et al.* A structural change in the kinesin motor protein that drives motility. *Nature* **402,** 778–784 (1999).

36. Asbury, C. L., Fehr, A. N. & Block, S. M. Kinesin moves by an asymmetric hand-over-hand mechanism. *Science* **302,** 2130–2134 (2003).

37. Yildiz, A., Tomishige, M., Vale, R. D. & Selvin, P. R. Kinesin walks hand-over-hand. *Science* **303,** 676–678 (2004).

38. Schnitzer, M. J. & Block, S. M. Kinesin hydrolyses one ATP per 8-nm step. *Nature* **388,** 386–390 (1997).

39. Hua, W., Young, E. C., Fleming, M. L. & Gelles, J. Coupling of kinesin steps to ATP hydrolysis. *Nature* **388,** 390–393 (1997).

40. Coy, D. L., Wagenbach, M. & Howard, J. Kinesin takes one 8-nm step for each ATP that it hydrolyzes. *JBC* **274,** 3667–3671 (1999).

41. Block, S. M. Kinesin motor mechanics: binding, stepping, tracking, gating, and limping. *Biophys. J.* **92,** 2986–2995 (2007).

42. Rosenfeld, S. S., Fordyce, P. M., Jefferson, G. M., King, P. H. & Block, S. M. Stepping and stretching. How kinesin uses internal strain to walk processively. *JBC* **278,** 18550–18556 (2003).

43. Yildiz, A., Tomishige, M., Gennerich, A. & Vale, R. D. Intramolecular strain coordinates kinesin stepping behavior along microtubules. *Cell* **134,** 1030–1041 (2008).

44. Shastry, S. & Hancock, W. O. Interhead tension determines processivity across diverse N-terminal kinesins. *Proc. Natl. Acad. Sci. U.S.A.* **108,** 16253–16258 (2011).

45. Guydosh, N. R. & Block, S. M. Backsteps induced by nucleotide analogs suggest the front head of kinesin is gated by strain. *Proc. Natl. Acad. Sci. U.S.A.* **103,** 8054–8059 (2006).

46. Klumpp, L. M., Hoenger, A. & Gilbert, S. P. Kinesin's second step. *Proc. Natl. Acad. Sci. U.S.A.* **101,** 3444–3449 (2004).

47. Crevel, I. M.-T. *et al.* What kinesin does at roadblocks: the coordination mechanism for molecular walking. *EMBO J.* **23,** 23–32 (2003).

48. Schief, W. R., Clark, R. H., Crevenna, A. H. & Howard, J. Inhibition of kinesin motility by ADP and phosphate supports a hand-over-hand mechanism. *Proc. Natl. Acad. Sci. U.S.A.* **101,** 1183–1188 (2004).

49. Clancy, B. E., Behnke-Parks, W. M., Andreasson, J. O. L., Rosenfeld, S. S. & Block, S. M. A universal pathway for kinesin stepping. *Nat. Struct. Mol. Biol.* **18,** 1020–1027 (2011).

50. Cao, L. *et al.* The structure of apo-kinesin bound to tubulin links the nucleotide cycle to movement. *Nat. Commun.* **5,** 5364 (2014).

51. Kutys, M. L., Fricks, J. & Hancock, W. O. Monte Carlo analysis of neck linker extension in kinesin molecular motors. *PLOS Comput. Biol.* **6,** e1000980 (2010).

52. Shastry, S. & Hancock, W. O. Neck linker length determines the degree of processivity in kinesin-1 and kinesin-2 motors. *Curr. Biol.* **20,** 939–943 (2010).

53. Alonso, M. C. *et al.* An ATP gate controls tubulin binding by the tethered head of kinesin-1. *Science* **316,** 120–123 (2007).

54. Düselder, A., Thiede, C., Schmidt, C. F. & Lakämper, S. Neck-linker length dependence of processive Kinesin-5 motility. *J. Mol. Biol.* **423,** 159–168 (2012).

55. Mickolajczyk, K. J. & Hancock, W. O. Kinesin processivity Is determined by a kinetic race from a vulnerable one-head-bound state. *Biophys. J.* **112,** 2615–2623 (2017).

56. Wollman, A. J. M., Sanchez-Cano, C., Carstairs, H. M. J., Cross, R. A. & Turberfield, A. J. Transport and self-organization across different length scales powered by motor proteins and programmed by DNA. *Nat. Nanotechnol.* **9,** 44–47 (2014).

57. Block, S. M., Goldstein, L. S. & Schnapp, B. J. Bead movement by single kinesin molecules studied with optical tweezers. *Nature* **348,** 348–352 (1990).

58. Wang, W., Cao, L., Wang, C., Gigant, B. & Knossow, M. Kinesin, 30 years later: Recent insights from structural studies. *Protein Sci.* **24,** 1047–1056 (2015).

59. Mieck, C., Molodtsov, M. I., Drzewicka, K. & van der Vaart, B. Non-catalytic motor domains enable processive movement and functional diversification of the kinesin-14 Kar3. *eLife* (2015). doi:10.7554/eLife.04489.001

60. Weinger, J. S., Qiu, M., Yang, G. & Kapoor, T. M. A nonmotor microtubule binding Ssite in kinesin-5 is required for filament crosslinking and sliding. *Curr. Biol.* **21,** 154–160 (2011).

61. Wickstead, B. & Gull, K. A 'holistic' kinesin phylogeny reveals new kinesin families and predicts protein functions. *Mol. Biol. Cell* **17,** 1734–1743 (2006).

62. Sablin, E. P. *et al.* Direction determination in the minus-end-directed kinesin motor ncd. *Nature* **395,** 813–816 (1998).

63. Endow, S. A. & Waligora, K. W. Determinants of kinesin motor polarity. *Science* **281,** 1200–1202 (1998).

64. Endres, N. F., Yoshioka, C., Milligan, R. A. & Vale, R. D. A lever-arm rotation drives motility of the minus-end-directed kinesin Ncd. *Nature* **439,** 875–878 (2006).

65. Zhang, P., Dai, W., Hahn, J. & Gilbert, S. P. Drosophila Ncd reveals an evolutionarily conserved powerstroke mechanism for homodimeric and heterodimeric kinesin-14s. *Proc. Natl. Acad. Sci. U.S.A.* **112,** 6359–6364 (2015).

66. Popchock, A. R. *et al.* The mitotic kinesin-14 KlpA contains a context-dependent directionality switch. *Nat. Commun.* **8,** 13999 (2017).

67. Tseng, K.-F. *et al.* The preprophase band-associated kinesin-14 OsKCH2 is a processive minus-end-directed microtubule motor. *Nat. Commun.* **9,** 1067 (2018).

68. Mieck, C. *et al.* Non-catalytic motor domains enable processive movement and functional diversification of the kinesin-14 Kar3. *eLife* **4,** 1161 (2015).

69. Horio, T. & Murata, T. The role of dynamic instability in microtubule organization. *Front. Plant Sci.* **5,** 511 (2014).

70. McDonald, H. B., Stewart, R. J. & Goldstein, L. S. The kinesin-like ncd protein of Drosophila is a minus end-directed microtubule motor. *Cell* **63,** 1159–1165 (1990).

71. Mountain, V. *et al.* The kinesin-related protein, HSET, opposes the activity of Eg5 and cross-links microtubules in the mammalian mitotic spindle. *J. Cell Biol.* **147,** 351–366 (1999).

72. Furuta, K., Edamatsu, M., Maeda, Y. & Toyoshima, Y. Y. Diffusion and directed movement: in vitro motile properties of fission yeast kinesin-14 Pkl1. *JBC* **283,** 36465–36473 (2008).

73. Walter, W. J., Machens, I., Rafieian, F. & Diez, S. The non-processive rice kinesin-14 OsKCH1 transports actin filaments along microtubules with two distinct velocities. *Nat. Plants* **1,** 15111 (2015).

74. Hentrich, C. & Surrey, T. Microtubule organization by the antagonistic mitotic motors kinesin-5 and kinesin-14. *J. Cell Biol.* **189,** 465–480 (2010).

75. Walczak, C. E., Vernos, I., Mitchison, T. J., Karsenti, E. & Heald, R. A model for the proposed roles of different microtubule-based motor proteins in establishing spindle bipolarity. *Curr. Biol.* **8,** 903–913 (1998).

76. Wordeman, L. How kinesin motor proteins drive mitotic spindle function: Lessons from molecular assays. *Semin. Cell Dev. Biol.* **21,** 260–268 (2010).

77. Cai, S., Weaver, L. N., Ems-McClung, S. C. & Walczak, C. E. Kinesin-14 family proteins HSET/XCTK2 control spindle length by cross-linking and sliding microtubules. *Mol. Biol. Cell* **20,** 1348–1359 (2009).

78. Roostalu, J. *et al.* Directional switching of the kinesin Cin8 through motor coupling. *Science* **332,** 94–99 (2011).

79. Kapitein, L. C. *et al.* The bipolar mitotic kinesin Eg5 moves on both microtubules that it crosslinks. *Nature* **435,** 114–118 (2005).

80. Kapitein, L. C. *et al.* Microtubule cross-linking triggers the directional motility of kinesin-5. *J. Cell Biol.* **182,** 421–428 (2008).

81. Edamatsu, M. Bidirectional motility of the fission yeast kinesin-5, Cut7. *Biochem. Biophys. Res. Commun.* **446,** 231–234 (2014).

82. Winey, M. & Bloom, K. Mitotic spindle form and function. *Genetics* **190,** 1197–1224 (2012).

83. di Pietro, F., Echard, A. & Morin, X. Regulation of mitotic spindle orientation: an integrated view. *EMBO Rep.* **17,** 1106–1130 (2016).

84. Rieder, C. L. & Salmon, E. D. The vertebrate cell kinetochore and its roles during mitosis. *Trends Cell Biol.* **8,** 310–318 (1998).

85. Heald, R. & Khodjakov, A. Thirty years of search and capture: The complex simplicity of mitotic spindle assembly. *J. Cell Biol.* **211,** 1103–1111 (2015).

86. Hyman, A. A. & Mitchison, T. J. Two different microtubule-based motor activities with opposite polarities in kinetochores. *Nature* **351,** 206–211 (1991).

87. Yen, T. J., Li, G., Schaar, B. T., Szilak, I. & Cleveland, D. W. CENP-E is a putative kinetochore motor that accumulates just before mitosis. *Nature* **359,** 536–539 (1992).

88. Steuer, E. R., Wordeman, L., Schroer, T. A. & Sheetz, M. P. Localization of cytoplasmic dynein to mitotic spindles and kinetochores. *Nature* **345,** 266–268 (1990).

89. Pfarr, C. M. *et al.* Cytoplasmic dynein is localized to kinetochores during mitosis. *Nature* **345,** 263–265 (1990).

90. Rieder, C. L. Motile kinetochores and polar ejection forces dictate chromosome position on the vertebrate mitotic spindle. *J. Cell Biol.* **124,** 223–233 (1994).

91. McHugh, T. & Welburn, J. P. I. Dynein at kinetochores: Making the connection. *J. Cell Biol.* **216,** 855–857 (2017).

92. Reddy, A. S. Molecular motors and their functions in plants. *Int. Rev. Cytol.* **204,** 97–178 (2001).

93. Saunders, W. S. & Hoyt, M. A. Kinesin-related proteins required for structural integrity of the mitotic spindle. *Cell* **70,** 451–458 (1992).

94. Sharp, D. J., Yu, K. R., Sisson, J. C., Sullivan, W. & Scholey, J. M. Antagonistic microtubule-sliding motors position mitotic centrosomes in Drosophila early embryos. *Nat. Cell Biol.* **1,** 51–54 (1999).

95. Cassimeris, L. & Skibbens, R. V. Regulated assembly of the mitotic spindle: a perspective from two ends. *CIMB* **5,** 99–112 (2003).

96. Ferenz, N. P., Gable, A. & Wadsworth, P. Mitotic functions of kinesin-5. *Semin. Cell Dev. Biol.* **21,** 255–259 (2010).

97. Olmsted, Z. T., Colliver, A. G., Riehlman, T. D. & Paluh, J. L. Kinesin-14 and kinesin-5 antagonistically regulate microtubule nucleation by γ-TuRC in yeast and human cells. *Nat. Commun.* **5,** 5339–15 (2014).

98. Syrovatkina, V. & Tran, P. T. Loss of kinesin-14 results in aneuploidy via kinesin-5-dependent microtubule protrusions leading to chromosome cut. *Nat. Commun.* **6,** 7322 (2015).

99. Hepperla, A. J. *et al.* Minus-end-directed kinesin-14 motors align antiparallel microtubules to control metaphase spindle length. *Dev. Cell* **31,** 61–72 (2014).

100. Mana-Capelli, S., McLean, J. R., Chen, C.-T., Gould, K. L. & McCollum, D. The kinesin-14 Klp2 is negatively regulated by the SIN for proper spindle elongation and telophase nuclear positioning. *Mol. Biol. Cell* **23,** 4592–4600 (2012).

101. Ambrose, J. C. & Cyr, R. The kinesin ATK5 functions in early spindle assembly in Arabidopsis. *The Plant Cell* **19,** 226–236 (2007).

102. Wang, B. *et al.* The Aspergillus nidulans bimC4 mutation provides an excellent tool for identification of kinesin-14 inhibitors. *Fungal Genet. Biol.* **82,** 51–55 (2015).

103. Yukawa, M., Ikebe, C. & Toda, T. The Msd1-Wdr8-Pkl1 complex anchors microtubule minus ends to fission yeast spindle pole bodies. *J. Cell Biol.* **209,** 549–562 (2015).

104. Roostalu, J. *et al.* Directional switching of the kinesin Cin8 through motor coupling. *Science* **332,** 94–99 (2011).

105. Gerson-Gurwitz, A. *et al.* Directionality of individual kinesin-5 Cin8 motors is modulated by loop 8, ionic strength and microtubule geometry. *EMBO J.* **30,** 4942–4954 (2011).

106. Fridman, V. *et al.* Kinesin-5 Kip1 is a bi-directional motor that stabilizes microtubules and tracks their plus-ends in vivo. *J Cell Sci* **126,** 4147–4159 (2013).

107. Enos, A. P. & Morris, N. R. Mutation of a gene that encodes a kinesin-like protein blocks nuclear division in A. nidulans. *Cell* **60,** 1019–1027 (1990).

108. Hagan, I. & Yanagida, M. Novel potential mitotic motor protein encoded by the fission yeast cut7+ gene. *Nature* **347,** 563–566 (1990).

109. Blangy, A. *et al.* Phosphorylation by p34cdc2 regulates spindle association of human Eg5, a kinesin-related motor essential for bipolar spindle formation in vivo. *Cell* **83,** 1159–1169 (1995).

110. Bannigan, A. *et al.* A conserved role for kinesin-5 in plant mitosis. *J Cell Sci* **120,** 2819–2827 (2007).

111. Heck, M. M. *et al.* The kinesin-like protein KLP61F is essential for mitosis in Drosophila. *J. Cell Biol.* **123,** 665–679 (1993).

112. Hoyt, M. A., He, L., Loo, K. K. & Saunders, W. S. Two Saccharomyces cerevisiae kinesin-related gene products required for mitotic spindle assembly. *J. Cell Biol.* **118,** 109–120 (1992).

113. Roof, D. M., Meluh, P. B. & Rose, M. D. Kinesin-related proteins required for assembly of the mitotic spindle. *J. Cell Biol.* **118,** 95–108 (1992).

114. Sawin, K. E., LeGuellec, K., Philippe, M. & Mitchison, T. J. Mitotic spindle organization by a plus-end-directed microtubule motor. *Nature* **359,** 540–543 (1992).

115. Kaseda, K., McAinsh, A. D. & Cross, R. A. Walking, hopping, diffusing and braking modes of kinesin-5. *Biochem. Soc. Trans.* **37,** 1045–1049 (2009).

116. Ferenz, N. P., Paul, R., Fagerstrom, C., Mogilner, A. & Wadsworth, P. Dynein antagonizes eg5 by crosslinking and sliding antiparallel microtubules. *Curr. Biol.* **19,** 1833–1838 (2009).

117. Gaglio, T. *et al.* Opposing motor activities are required for the organization of the mammalian mitotic spindle pole. *J. Cell Biol.* **135,** 399–414 (1996).

118. Mitchison, T. J. *et al.* Roles of polymerization dynamics, opposed motors, and a tensile element in governing the length of Xenopus extract meiotic spindles. *Mol. Biol. Cell* **16,** 3064–3076 (2005).

119. Tanenbaum, M. E., Macůrek, L., Galjart, N. & Medema, R. H. Dynein, Lis1 and CLIP-170 counteract Eg5-dependent centrosome separation during bipolar spindle assembly. *EMBO J.* **27,** 3235–3245 (2008).

120. O'Connell, M. J., Meluh, P. B., Rose, M. D. & Morris, N. R. Suppression of the bimC4 mitotic spindle defect by deletion of klpA, a gene encoding a KAR3-related kinesin-like protein in Aspergillus nidulans. *J. Cell Biol.* **120,** 153–162 (1993).

121. Pidoux, A. L., LeDizet, M. & Cande, W. Z. Fission yeast pkl1 is a kinesin-related protein involved in mitotic spindle function. *Mol. Biol. Cell* **7,** 1639–1655 (1996).

122. Kim, N. & Song, K. KIFC1 is essential for bipolar spindle formation and genomic stability in the primary human fibroblast IMR-90 cell. *Cell Struct. Funct.* **38,** 21–30 (2013).

123. Civelekoglu-Scholey, G., Tao, L., Brust-Mascher, I., Wollman, R. & Scholey, J. M. Prometaphase spindle maintenance by an antagonistic motor-dependent force balance made robust by a disassembling lamin-B envelope. *J. Cell Biol.* **188,** 49–68 (2010).

124. Brust-Mascher, I., Sommi, P., Cheerambathur, D. K. & Scholey, J. M. Kinesin-5-dependent poleward flux and spindle length control in Drosophila embryo mitosis. *Mol. Biol. Cell* **20,** 1749–1762 (2009).

125. Scheffler, K., Minnes, R., Fraisier, V., Paoletti, A. & Tran, P. T. Microtubule minus end motors kinesin-14 and dynein drive nuclear congression in parallel pathways. *J. Cell Biol.* **209,** 47–58 (2015).

126. Kuriyama, R. *et al.* Characterization of a minus end-directed kinesin-like motor protein from cultured mammalian cells. *J. Cell Biol.* **129,** 1049–1059 (1995).

127. Delorme, C., Joshi, M. & Allingham, J. S. Crystal structure of the Candida albicans Kar3 kinesin motor domain fused to maltose-binding protein. *Biochem. Biophys. Res. Commun.* **428,** 427–432 (2012).

128. Karabay, A. & Walker, R. A. Identification of microtubule binding sites in the Ncd tail domain. *Biochemistry* **38,** 1838–1849 (1999).

129. Fink, G. *et al.* The mitotic kinesin-14 Ncd drives directional microtubule–microtubule sliding. *Nat. Cell Biol.* **11,** 717–723 (2009).

130. Braun, M., Drummond, D. R., Cross, R. A. & McAinsh, A. D. The kinesin-14 Klp2 organizes microtubules into parallel bundles by an ATP-dependent sorting mechanism. *Nat. Cell Biol.* **11,** 724–730 (2009).

131. Chavali, P. L. *et al.* A CEP215-HSET complex links centrosomes with spindle poles and drives centrosome clustering in cancer. *Nat. Commun.* **7,** 11005 (2016).

132. Endow, S. A. & Komma, D. J. Centrosome and spindle function of the Drosophila Ncd microtubule motor visualized in live embryos using Ncd-GFP fusion proteins. *J. Cell Sci.* **109 (Pt 10),** 2429–2442 (1996).

133. Hori, A., Ikebe, C., Tada, M. & Toda, T. Msd1/SSX2IP-dependent microtubule anchorage ensures spindle orientation and primary cilia formation. *EMBO Rep.* **15,** 175–184 (2014).

134. Mountain, V. *et al.* The kinesin-related protein, HSET, opposes the activity of Eg5 and cross-links microtubules in the mammalian mitotic spindle. *J. Cell Biol.* **147,** 351–366 (1999).

135. Walczak, C. E., Verma, S. & Mitchison, T. J. XCTK2: a kinesin-related protein that promotes mitotic spindle assembly in Xenopus laevis egg extracts. *J. Cell Biol.* **136,** 859–870 (1997).

136. Endow, S. A., Chandra, R., Komma, D. J., Yamamoto, A. H. & Salmon, E. D. Mutants of the Drosophila ncd microtubule motor protein cause centrosomal and spindle pole defects in mitosis. *J. Cell Sci.* **107 (Pt 4),** 859–867 (1994).

137. Matthies, H. J., McDonald, H. B., Goldstein, L. S. & Theurkauf, W. E. Anastral meiotic spindle morphogenesis: role of the non-claret disjunctional kinesin-like protein. *J. Cell Biol.* **134,** 455–464 (1996).

138. Surrey, T., Nedelec, F., Leibler, S. & Karsenti, E. Physical properties determining self-organization of motors and microtubules. *Science* **292,** 1167–1171 (2001).

139. Ambrose, J. C., Li, W., Marcus, A., Ma, H. & Cyr, R. A minus-end-directed kinesin with plus-end tracking protein activity is involved in spindle morphogenesis. *Mol. Biol. Cell* **16,** 1584–1592 (2005).

140. Walczak, C. E. & Heald, R. Mechanisms of mitotic spindle assembly and function. *Int. Rev. Cytol.* **265,** 111–158 (2008).

141. Bornens, M. Centrosome composition and microtubule anchoring mechanisms. *Curr. Opin. Cell Biol.* **14,** 25–34 (2002).

142. Cai, S., Weaver, L. N., Ems-McClung, S. C. & Walczak, C. E. Proper organization of microtubule minus ends is needed for midzone stability and cytokinesis. *Curr. Biol.* **20,** 880–885 (2010).

143. Kim, N. & Song, K. KIFC1 Is Essential for Bipolar Spindle Formation and Genomic Stability in the Primary Human Fibroblast IMR-90 Cell. *Cell Struct. Funct.* **38,** 21–30 (2013).

144. Logarinho, E. *et al.* CLASPs prevent irreversible multipolarity by ensuring spindle-pole resistance to traction forces during chromosome alignment. *Nat. Cell Biol.* **14,** 295–303 (2012).

145. Lin, T.-C., Neuner, A. & Schiebel, E. Targeting of γ-tubulin complexes to microtubule organizing centers: conservation and divergence. *Trends Cell Biol.* **25,** 296–307 (2015).

146. Toya, M. *et al.* Gamma-tubulin complex-mediated anchoring of spindle microtubules to spindle-pole bodies requires Msd1 in fission yeast. *Nat. Cell Biol.* **9,** 646–653 (2007).

147. Shen, K.-F. & Osmani, S. A. Regulation of mitosis by the NIMA kinase involves TINA and its newly discovered partner, An-WDR8, at spindle pole bodies. *Mol. Biol. Cell* **24,** 3842–3856 (2013).

148. Osmani, A. H., Davies, J., Oakley, C. E., Oakley, B. R. & Osmani, S. A. TINA interacts with the NIMA kinase in Aspergillus nidulans and negatively regulates astral microtubules during metaphase arrest. *Mol. Biol. Cell* **14,** 3169–3179 (2003).

149. Potapova, T. A., Zhu, J. & Li, R. Aneuploidy and chromosomal instability: a vicious cycle driving cellular evolution and cancer genome chaos. *Cancer Metastasis Rev.* **32,** 377–389 (2013).

150. Fang, X. & Zhang, P. Aneuploidy and tumorigenesis. *Semin. Cell Dev. Biol.* **22,** 595–601 (2011).

151. Gordon, D. J., Resio, B. & Pellman, D. Causes and consequences of aneuploidy in cancer. *Nat. Rev. Genet.* **13,** 189–203 (2012).

152. Nicholson, J. M. & Cimini, D. How mitotic errors contribute to karyotypic diversity in cancer. *Adv. Cancer Res.* **112,** 43–75 (2011).

153. Kleylein-Sohn, J. *et al.* Acentrosomal spindle organization renders cancer cells dependent on the kinesin HSET. *J. Cell Sci.* **125,** 5391–5402 (2012).

154. Pannu, V. *et al.* HSET overexpression fuels tumor progression via centrosome clustering-independent mechanisms in breast cancer patients. *Oncotarget* **6,** 6076–6091 (2015).

155. Good, J. A. D., Skoufias, D. A. & Kozielski, F. Elucidating the functionality of kinesins: an overview of small molecule inhibitors. *Semin. Cell Dev. Biol.* **22,** 935–945 (2011).

156. Kwok, B. H., Yang, J. G. & Kapoor, T. M. The rate of bipolar spindle assembly depends on the microtubule-gliding velocity of the mitotic kinesin Eg5. *Curr. Biol.* **14,** 1783–1788 (2004).

157. Miyamoto, D. T., Perlman, Z. E., Burbank, K. S., Groen, A. C. & Mitchison, T. J. The kinesin Eg5 drives poleward microtubule flux in Xenopus laevis egg extract spindles. *J. Cell Biol.* **167,** 813–818 (2004).

158. Cahu, J. *et al.* Phosphorylation by Cdk1 increases the binding of Eg5 to microtubules in vitro and in Xenopus egg extract spindles. *PLoS ONE* **3,** e3936 (2008).

159. El-Nassan, H. B. Advances in the discovery of kinesin spindle protein (Eg5) inhibitors as antitumor agents. *Eur. J. Med. Chem.* **62,** 614–631 (2013).

160. Huszar, D., Theoclitou, M.-E., Skolnik, J. & Herbst, R. Kinesin motor proteins as targets for cancer therapy. *Cancer Metastasis Rev.* **28,** 197–208 (2009).

161. Hansen, G. M. & Justice, M. J. Activation of Hex and mEg5 by retroviral insertion may contribute to mouse B-cell leukemia. *Oncogene* **18,** 6531–6539 (1999).

162. Carter, B. Z. *et al.* Regulation and targeting of Eg5, a mitotic motor protein in blast crisis CML: overcoming imatinib resistance. *Cell Cycle* **5,** 2223–2229 (2006).

163. Ding, S. *et al.* Overexpression of Eg5 predicts unfavorable prognosis in non-muscle invasive bladder urothelial carcinoma. *Int. J. Urol.* **18,** 432–438 (2011).

164. Liu, M. *et al.* Ectopic expression of the microtubule-dependent motor protein Eg5 promotes pancreatic tumourigenesis. *J. Pathol.* **221,** 221–228 (2010).

165. Purcell, J. W. *et al.* Activity of the kinesin spindle protein inhibitor ispinesib (SB-715992) in models of breast cancer. *Clin. Cancer Res.* **16,** 566–576 (2010).

166. Castillo, A., Morse, H. C., Godfrey, V. L., Naeem, R. & Justice, M. J. Overexpression of Eg5 causes genomic instability and tumor formation in mice. *Cancer Res.* **67,** 10138–10147 (2007).

167. Kapoor, T. M., Mayer, T. U., Coughlin, M. L. & Mitchison, T. J. Probing spindle assembly mechanisms with monastrol, a small molecule inhibitor of the mitotic kinesin, Eg5. *J. Cell Biol.* **150,** 975–988 (2000).

168. Mayer, T. U. *et al.* Small molecule inhibitor of mitotic spindle bipolarity identified in a phenotype-based screen. *Science* **286,** 971–974 (1999).

169. Masuda, A., Maeno, K., Nakagawa, T., Saito, H. & Takahashi, T. Association between mitotic spindle checkpoint impairment and susceptibility to the induction of apoptosis by anti-microtubule agents in human lung cancers. *Am. J. Pathol.* **163,** 1109–1116 (2003).

170. Sarli, V. & Giannis, A. Inhibitors of mitotic kinesins: next-generation antimitotics. *ChemMedChem* **1,** 293–298 (2006).

171. Hayashi, N., Koller, E., Fazli, L. & Gleave, M. E. Effects of Eg5 knockdown on human prostate cancer xenograft growth and chemosensitivity. *Prostate* **68,** 1283–1295 (2008).

172. Liu, M. *et al.* Validating the mitotic kinesin Eg5 as a therapeutic target in pancreatic cancer cells and tumor xenografts using a specific inhibitor. *Biochem. Pharmacol.* **76,** 169–178 (2008).

173. Nakai, R. *et al.* K858, a novel inhibitor of mitotic kinesin Eg5 and antitumor agent, induces cell death in cancer cells. *Cancer Res.* **69,** 3901–3909 (2009).

174. DeBonis, S. *et al.* In vitro screening for inhibitors of the human mitotic kinesin Eg5 with antimitotic and antitumor activities. *Mol. Cancer Ther.* **3,** 1079–1090 (2004).

175. Sakowicz, R. *et al.* Antitumor activity of a kinesin inhibitor. *Cancer Res.* **64,** 3276–3280 (2004).

176. Chin, G. M. & Herbst, R. Induction of apoptosis by monastrol, an inhibitor of the mitotic kinesin Eg5, is independent of the spindle checkpoint. *Mol. Cancer Ther.* **5,** 2580–2591 (2006).

177. Turner, J. *et al.* Crystal structure of the mitotic spindle kinesin Eg5 reveals a novel conformation of the neck-linker. *JBC* **276,** 25496–25502 (2001).

178. Maliga, Z., Kapoor, T. M. & Mitchison, T. J. Evidence that monastrol is an allosteric inhibitor of the mitotic kinesin Eg5. *Chem. Biol.* **9,** 989–996 (2002).

179. Maliga, Z. & Mitchison, T. J. Small-molecule and mutational analysis of allosteric Eg5 inhibition by monastrol. *BMC Chem. Biol.* **6,** 2 (2006).

180. Maliga, Z. *et al.* A pathway of structural changes produced by monastrol binding to Eg5. *JBC* **281,** 7977–7982 (2006).

181. Lad, L. *et al.* Mechanism of inhibition of human KSP by ispinesib. *Biochemistry* **47,** 3576–3585 (2008).

182. Zhang, B., Liu, J.-F., Xu, Y. & Ng, S.-C. Crystal structure of HsEg5 in complex with clinical candidate CK0238273 provides insight into inhibitory mechanism, potency, and specificity. *Biochem. Biophys. Res. Commun.* **372,** 565–570 (2008).

183. Grinberg-Rashi, H. *et al.* The expression of three genes in primary non-small cell lung cancer is associated with metastatic spread to the brain. *Clin. Cancer Res.* **15,** 1755–1761 (2009).

184. De, S., Cipriano, R., Jackson, M. W. & Stark, G. R. Overexpression of kinesins mediates docetaxel resistance in breast cancer cells. *Cancer Res.* **69,** 8035–8042 (2009).

185. Kwon, M. *et al.* Mechanisms to suppress multipolar divisions in cancer cells with extra centrosomes. *Genes Dev.* **22,** 2189–2203 (2008).

186. Wu, J. *et al.* Discovery and mechanistic study of a small molecule inhibitor for motor protein KIFC1. *ACS Chem. Biol.* **8,** 2201–2208 (2013).

187. Lingle, W. L. *et al.* Centrosome amplification drives chromosomal instability in breast tumor development. *Proc. Natl. Acad. Sci. U.S.A.* **99,** 1978–1983 (2002).

188. Holland, A. J. & Cleveland, D. W. Boveri revisited: chromosomal instability, aneuploidy and tumorigenesis. *Nat. Rev. Mol. Cell Biol.* **10,** 478–487 (2009).

189. Chen, S. *et al.* Transient endoreplication down-regulates the kinesin-14 HSET and contributes to genomic instability. *Mol. Biol. Cell* **27,** 2911–2923 (2016).

190. Watts, C. A. *et al.* Design, synthesis, and biological evaluation of an allosteric inhibitor of HSET that targets cancer cells with supernumerary centrosomes. *Chem. Biol.* **20,** 1399–1410 (2013).

191. Zhang, W. *et al.* Discovery of a novel inhibitor of kinesin-like protein KIFC1. *Biochem. J.* **473,** 1027–1035 (2016).

192. Park, H.-W. *et al.* Structural basis of small molecule ATPase inhibition of a human mitotic kinesin motor protein. *Nat. Rev. Mol. Cell Biol.* **7,** 15121 (2017).

193. Karsenti, E. & Vernos, I. The mitotic spindle: a self-made machine. *Science* **294,** 543–547 (2001).

194. Marcus, A. I., Li, W., Ma, H. & Cyr, R. J. A kinesin mutant with an atypical bipolar spindle undergoes normal mitosis. *Mol. Biol. Cell* **14,** 1717–1726 (2003).

195. Endow, S. A. & Higuchi, H. A mutant of the motor protein kinesin that moves in both directions on microtubules. *Nature* **406,** 913–916 (2000).

196. Hatsumi, M. & Endow, S. A. The Drosophila ncd microtubule motor protein is spindle-associated in meiotic and mitotic cells. *J. Cell Sci.* **103,** 1013–1020 (1992).

197. Goshima, G., Nédélec, F. & Vale, R. D. Mechanisms for focusing mitotic spindle poles by minus end–directed motor proteins. *J. Cell Biol.* **171,** 229–240 (2005).

198. Matuliene, J. *et al.* Function of a minus-end-directed kinesin-like motor protein in mammalian cells. *J. Cell Sci.* **112,** 4041–4050 (1999).

199. Endow, S. A., Henikoff, S. & Soler-Niedziela, L. Mediation of meiotic and early mitotic chromosome segregation in Drosophila by a protein related to kinesin. *Nature* **345,** 81–83 (1990).

200. Gordon, M. B., Howard, L. & Compton, D. A. Chromosome movement in mitosis requires microtubule anchorage at spindle poles. *J. Cell Biol.* **152,** 425–434 (2001).

201. McDonald, H. B. & Goldstein, L. S. Identification and characterization of a gene encoding a kinesin-like protein in Drosophila. *Cell* **61,** 991–1000 (1990).

202. Prigozhina, N. L., Walker, R. A., Oakley, C. E. & Oakley, B. R. γ-Tubulin and the C-terminal motor domain kinesin-like protein, KLPA, function in the establishment of spindle bipolarity in Aspergillus nidulans. *Mol. Biol. Cell* **12,** 3161–3174 (2001).

203. Jonsson, E., Yamada, M., Vale, R. D. & Goshima, G. Clustering of a kinesin-14 motor enables processive retrograde microtubule-based transport in plants. *Nat. Plants* **1,** 15087–6 (2015).

204. Case, R. B., Pierce, D. W., Hom-Booher, N., Hart, C. L. & Vale, R. D. The directional preference of kinesin motors is specified by an element outside of the motor catalytic domain. *Cell* **90,** 959–966 (1997).

205. Furuta, K. *et al.* Measuring collective transport by defined numbers of processive and nonprocessive kinesin motors. *Proc. Natl. Acad. Sci. U.S.A.* **110,** 501–506 (2013).

206. Fink, G. *et al.* The mitotic kinesin-14 Ncd drives directional microtubule–microtubule sliding. *Nat. Cell Biol.* **11,** 717–723 (2009).

207. Walker, R. A., Salmon, E. D. & Endow, S. A. The Drosophila claret segregation protein is a minus-end directed motor molecule. *Nature* **347,** 780–782 (1990).

208. Marcus, A. I., Ambrose, J. C., Blickley, L., Hancock, W. O. & Cyr, R. J. Arabidopsis thaliana protein, ATK1, is a minus-end directed kinesin that exhibits non-processive movement. *Cell Motil. Cytoskeleton* **52,** 144–150 (2002).

209. Endow, S. A. *et al.* Yeast Kar3 is a minus-end microtubule motor protein that destabilizes microtubules preferentially at the minus ends. *EMBO J.* **13,** 2708–2713 (1994).

210. Henningsen, U. & Schliwa, M. Reversal in the direction of movement of a molecular motor. *Nature* **389,** 93–96 (1997).

211. Yun, M. *et al.* Rotation of the stalk/neck and one head in a new crystal structure of the kinesin motor protein, Ncd. *EMBO J.* **22,** 5382–5389 (2003).

212. Wendt, T. G. *et al.* Microscopic evidence for a minus-end-directed power stroke in the kinesin motor ncd. *EMBO J.* **21,** 5969–5978 (2002).

213. Su, X. *et al.* Mechanisms underlying the dual-mode regulation of microtubule dynamics by Kip3/kinesin-8. *Mol. Cell* **43,** 751–763 (2011).

214. Endow, S. A. Microtubule motors in spindle and chromosome motility. *Eur. J. Biochem.* **262,** 12–18 (1999).

215. Erickson, H. P. Size and shape of protein molecules at the nanometer level determined by sedimentation, gel filtration, and electron microscopy. *Biol. Proced. Online* **11,** 32–51 (2009).

216. Howard, J. & Hyman, A. A. Preparation of marked microtubules for the assay of the polarity of microtubule-based motors by fluorescence microscopy. *Methods Cell Biol.* **39,** 105–113 (1993).

217. Roberts, A. J., Goodman, B. S. & Reck-Peterson, S. L. Reconstitution of dynein transport to the microtubule plus end by kinesin. *eLife* **3,** e02641 (2014).

218. Qiu, W. *et al.* Dynein achieves processive motion using both stochastic and coordinated stepping. *Nat. Struct. Mol. Biol.* **19,** 193–200 (2012).

219. Lu, H., Ali, M. Y., Bookwalter, C. S., Warshaw, D. M. & Trybus, K. M. Diffusive movement of processive kinesin-1 on microtubules. *Traffic* **10,** 1429–1438 (2009).

220. Dammermann, A., Desai, A. & Oegema, K. The minus end in sight. *Curr. Biol.* **13,** R614–24 (2003).

221. Hori, A. *et al.* The conserved Wdr8-hMsd1/SSX2IP complex localises to the centrosome and ensures proper spindle length and orientation. *Biochem. Biophys. Re.s Commun.* **468,** 39–45 (2015).

222. Chavali, P. L. *et al.* A CEP215-HSET complex links centrosomes with spindle poles and drives centrosome clustering in cancer. *Nat. Commun.* **7,** 11005 (2016).

223. Braun, M. *et al.* The human kinesin-14 HSET tracks the tips of growing microtubules in vitro. *Cytoskeleton* **70,** 515–521 (2013).

224. Aldaz, H., Rice, L. M., Stearns, T. & Agard, D. A. Insights into microtubule nucleation from the crystal structure of human gamma-tubulin. *Nature* **435,** 523–527 (2005).

225. Oakley, B. R., Paolillo, V. & Zheng, Y. γ-Tubulin complexes in microtubule nucleation and beyond. *Mol. Biol. Cell* **26,** 2957–2962 (2015).

226. Subramanian, R. *et al.* Insights into antiparallel microtubule crosslinking by PRC1, a conserved nonmotor microtubule binding protein. *Cell* **142,** 433–443 (2010).

227. Clark, S. A. *et al.* Multivalency regulates activity in an intrinsically disordered transcription factor. *eLife* **7,** e36258 (2018).

228. Hwang, T. L., van Zijl, P. C. & Mori, S. Accurate quantitation of water-amide proton exchange rates using the phase-modulated CLEAN chemical EXchange (CLEANEX-PM) approach with a Fast-HSQC (FHSQC) detection scheme. *J. Biomol. NMR* **11,** 221–226 (1998).

229. Verhey, K. J. & Hammond, J. W. Traffic control: regulation of kinesin motors. *Nat. Rev. Mol. Cell Biol.* **10,** 765–777 (2009).

230. Drummond, D. R. Regulation of microtubule dynamics by kinesins. *Semin. Cell Dev. Biol.* **22,** 927–934 (2011).

231. Vicente, J. J. & Wordeman, L. Mitosis, microtubule dynamics and the evolution of kinesins. *Exp. Cell Res.* **334,** 61–69 (2015).

232. Sharp, D. J., Rogers, G. C. & Scholey, J. M. Microtubule motors in mitosis. *Nature* **407,** 41–47 (2000).

233. Chang, Q., Nitta, R., Inoue, S. & Hirokawa, N. Structural basis for the ATP-induced isomerization of kinesin. *J. Mol. Biol.* **425,** 1869–1880 (2013).

234. Gigant, B. *et al.* Structure of a kinesin-tubulin complex and implications for kinesin motility. *Nat. Struct. Mol. Biol.* **20,** 1001–1007 (2013).

235. Andreasson, J. O. L. *et al.* Examining kinesin processivity within a general gating framework. *eLife* **4,** 1166 (2015).

236. Kaseda, K., Higuchi, H. & Hirose, K. Coordination of kinesin's two heads studied with mutant heterodimers. *Proc. Natl. Acad. Sci. U.S.A.* **99,** 16058–16063 (2002).

237. Kaseda, K., Higuchi, H. & Hirose, K. Alternate fast and slow stepping of a heterodimeric kinesin molecule. *Nat. Cell Biol.* **5,** 1079–1082 (2003).

238. Dogan, M. Y., Can, S., Cleary, F. B., Purde, V. & Yildiz, A. Kinesin's front head is gated by the backward orientation of its neck linker. *Cell Rep.* **10,** 1967–1973 (2015).

239. Muretta, J. M. *et al.* A posttranslational modification of the mitotic kinesin Eg5 that enhances its mechanochemical coupling and alters its mitotic function. *Proc. Natl. Acad. Sci. U.S.A.* **115,** E1779–E1788 (2018).

240. Thoresen, T. & Gelles, J. Processive movement by a kinesin heterodimer with an inactivating mutation in one head. *Biochemistry* **47,** 9514–9521 (2008).

241. Miyazono, Y., Hayashi, M., Karagiannis, P., Harada, Y. & Tadakuma, H. Strain through the neck linker ensures processive runs: a DNA-kinesin hybrid nanomachine study. *EMBO J.* **29,** 93–106 (2010).

242. Gardner, M. K., Zanic, M., Gell, C., Bormuth, V. & Howard, J. Depolymerizing kinesins Kip3 and MCAK shape cellular microtubule architecture by differential control of catastrophe. *Cell* **147,** 1092–1103 (2011).

243. Rizk, R. S. & Gupta, M. L. Kip3 clusters kinetochores. *Cell Cycle* **9,** 2491–2501 (2014).

244. Chin, J. W. *et al.* Addition of p-azido-L-phenylalanine to the genetic code of Escherichia coli. *J. Am. Chem. Soc.* **124,** 9026–9027 (2002).

245. Peeler, J. C. & Mehl, R. A. Site-specific incorporation of unnatural amino acids as probes for protein conformational changes. *Methods Mol. Biol.* **794,** 125–134 (2012).

246. Blizzard, R. J. *et al.* Ideal bioorthogonal reactions using a site-specifically encoded tetrazine amino acid. *J. Am. Chem. Soc.* **137,** 10044–10047 (2015).

247. Jewett, J. C. & Bertozzi, C. R. Cu-free click cycloaddition reactions in chemical biology. *Chem. Soc. Rev.* **39,** 1272–1279 (2010).

248. Patterson, D. M., Nazarova, L. A. & Prescher, J. A. Finding the right (bioorthogonal) chemistry. *ACS Chem. Biol.* **9,** 592–605 (2014).

249. Lang, K. & Chin, J. W. Bioorthogonal reactions for labeling proteins. *ACS Chem. Biol.* **9,** 16–20 (2014).

250. Matikonda, S. S. *et al.* Bioorthogonal prodrug activation driven by a strain-promoted 1,3-dipolar cycloaddition. *Chem. Sci.* **6,** 1212–1218 (2015).

251. Nakata, T. & Hirokawa, N. Point mutation of adenosine triphosphate-binding motif generated rigor kinesin that selectively blocks anterograde lysosome membrane transport. *J. Cell Biol.* **131,** 1039–1053 (1995).

252. Bhaban, S., Materassi, D., Li, M., Hays, T. & Salapaka, M. Interrogating emergent transport properties for molecular motor ensembles: a semi-analytical approach. *PLOS Comput. Biol.* **12,** e1005152 (2016).

253. McLaughlin, R. T., Diehl, M. R. & Kolomeisky, A. B. Collective dynamics of processive cytoskeletal motors. *Soft Matter* **12,** 14–21 (2016).

254. Uppulury, K. *et al.* Analysis of cooperative behavior in multiple kinesins motor protein transport by varying structural and chemical properties. *Cell Mol. Bioeng.* **6,** 38–47 (2013).

255. Saito, N. & Kaneko, K. Embedding dual function into molecular motors through collective motion. *Nat. Rev. Mol. Cell Biol.* **7,** 44288 (2017).

256. Yajima, J., M. Yamagishi. Plus-end directionality is present in the catalytic core of kinesin-14 minus-end directed motors. *biorxiv.org* (2018). doi:10.1101/292375

257. Singh, S. K., Pandey, H., Al-Bassam, J. & Gheber, L. Bidirectional motility of kinesin-5 motor proteins: structural determinants, cumulative functions and physiological roles. *Cell. Mol. Life Sci.* **75,** 1757–1771 (2018).

258. Dawe, R. K. *et al.* A Kinesin-14 motor activates neocentromeres to promote meiotic drive in maize. *Cell* **173,** 839–850.e18 (2018).

259. Braun, M. *et al.* Changes in microtubule overlap length regulate kinesin-14-driven microtubule sliding. *Nat. Chem. Biol.* **13,** 1245–1252 (2017).

260. Kato, Y., Miyakawa, T. & Tanokura, M. Overview of the mechanism of cytoskeletal motors based on structure. *Biophys. Rev.* **10,** 571–581 (2018).

261. Gicking, A. M., Qiu, W. & Hancock, W. O. Mitotic kinesins in action: diffusive searching, directional switching, and ensemble coordination. *Mol. Biol. Cell* **29,** 1153–1156 (2018).

262. Molodtsov, M. I. *et al.* A force-induced directional awitch of a molecular motor enables parallel microtubule bundle formation. *Cell* **167,** 539–552.e14 (2016).

263. Hornbeck, P. V. *et al.* PhosphoSitePlus, 2014: mutations, PTMs and recalibrations. *Nucleic Acids Res.* **43,** D512–20 (2015).

264. Liu, Z. *et al.* CPLM: a database of protein lysine modifications. *Nucleic Acids Res.* **42,** D531–6 (2014).

265. Rogerson, D. T. *et al.* Efficient genetic encoding of phosphoserine and its nonhydrolyzable analog. *Nat. Chem. Biol.* **11,** 496–503 (2015).205.